Title

MODELING HEAT AND MASS TRANSFER AT THE MESA GEOTHERMAL ANOMALY, IMPERIAL VALLEY, CALIFORNIA

Authors

Kassoy, D.R.
Goyal, K.P.

Publication Date

1979-02-01

LBL-8784
GREMP-3
UC-66a

Modeling Heat and Mass Transfer at the Mesa Geothermal Anomaly, Imperial Valley, California

D.R. Kassoy and K.P. Goyal
Mechanical Engineering Dept.
University of Colorado
Boulder, Colorado

FEBRUARY 1979

Geothermal Reservoir Engineering Management Program

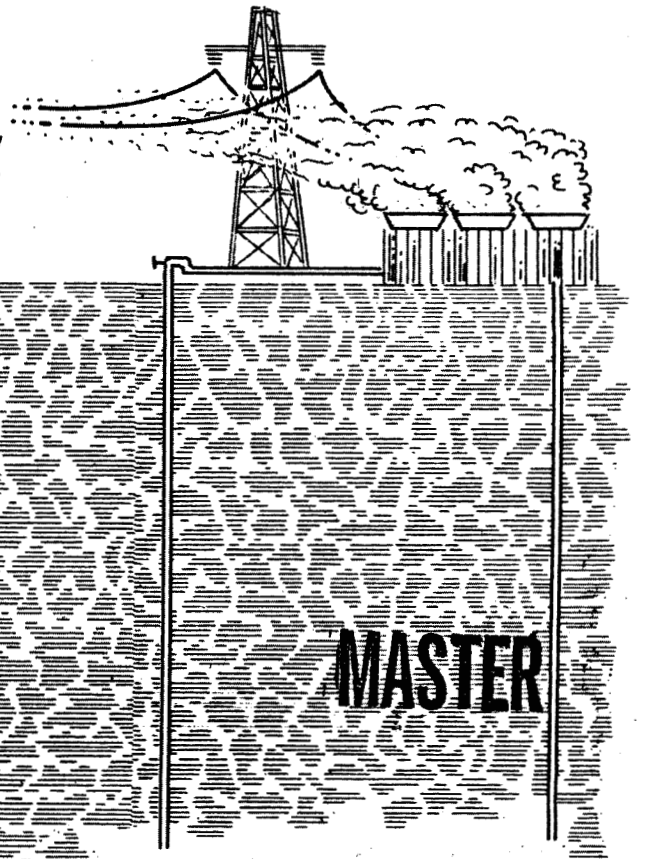

Lawrence Berkeley Laboratory
University of California, Berkeley

Prepared for U.S. Department of Energy under Contract W-7405-ENG-48

DISCLAIMER

Printed in the United States of America
Available from
National Technical Information Service
U.S. Department of Commerce
5285 Port Royal Road
Springfield, VA 22161
Price Code: A09

FINAL PROJECT REPORT

Modeling Heat and Mass Transfer at the Mesa Geothermal Anomaly, Imperial Valley, California

D.R. Kassoy - Project Director
K.P. Goyal - Research Assistant*
Mechanical Engineering Department
University of Colorado
Boulder, Colorado 80309

10 January 1979

*Present address: Earth Sciences Division, Lawrence Berkeley Laboratory, University of California, Berkeley, California 94720

TABLE OF CONTENTS

ACKNOWLEDGEMENTS

This work was performed for the Lawrence Berkeley Laboratory under Purchase Order Number 3166902 sponsored by the United States Department of Energy, Division of Geothermal Energy. We wish to acknowledge the support, guidance and cooperation of Dr. John H. Howard, manager of Reservoir Engineering Group and Werner J. Schwarz, program manager, Geothermal Reservoir Engineering Management Program Earth Sciences Division, Lawrence Berkeley Laboratory, Berkeley, California.

Abstract

The geothermal reservoir modeling effort at the University of Colorado is reviewed briefly. Technical accomplishments during the final funding period 1 April 1978 to 30 November 1978 are described. It is concluded that a physically viable mathematical model of an unexploited geothermal system can be constructed in terms of the fault zone controlled charging of the thermally active section of a reservoir.

NOMENCLATURE

Dimensional quantities carry a prime while non-dimensional quantities do not. Superscript 'f' stands for fluid.

a_1: Constant = $\dfrac{M + \cosh 1/\sqrt{d}}{\sqrt{d}\ \sinh 1/\sqrt{d}}$

a_2: Constant = $\dfrac{M + \frac{\lambda}{\lambda+\ell} \cosh 1/\sqrt{d}}{\sqrt{d}\ \sinh 1/\sqrt{d}}$

b_1: Constant = $1/\sqrt{d}$

b_2: Constant = $\dfrac{\lambda}{\sqrt{d}\ (\lambda+\ell)}$

$C_p(C_v)$: Specific heat at constant pressure (volume)

^oC_p: Reference specific heat at constant pressure and T_o

^oC_v: Specific heat at constant volume and T_o

d: Order one constant

D_a: Darcy number = K_o/L^2

e_i: (i=x,y,z) Unit vectors in x,y,z directions

$\underset{\sim}{g}$: Gravity vector

G_r: Grashof number = $L^3\Delta T g^o\alpha_e/\nu^2_o$

h: Step size

H: Length of the Aquifer.

K_i: (i=x,y,z) Permeability of the medium in the e_i- direction

K_o: Reference permeability of the medium

$K^{y(z)}$: Permeability of the medium in y(z) direction

ℓ: Thickness of the clay cap, ratio of the cap thickness to the depth of the aquifer

L: Characteristic length, depth of the aquifer

M: Mass flow rate

M'_o: Reference mass flow rate per unit width

p: Isotropic pressure, aquifer over pressure

P: Fault over pressure

P_{atm}: Atmospheric pressure

p_H: Hydrostatic pressure corresponding to the density ρ_o

p_{HH}: Hot hydrostatic pressure

p_o: Reference pressure = $\rho_o g L^o \alpha_e \Delta T$

P_{rm}: Prandtl number = ${}^oC_p \mu_o / \lambda^o_m$

q_o: Fault reference velocity = ${}^o\alpha_e \Delta T g K_o / \nu_o$

q_r: Aquifer reference velocity = ye q_o

R: Rayleigh number = $G_r D_a P_{rm}$

T: Temperature at any point in the fault. Ratio of fault temperature to the ambient temperature = T'/T'_o

T_{max}: Maximum temperature in the system

T_o: Reference or ambient temperature

v: Horizontal velocity in the aquifer (= ρ,x horizontal volumetric flux)

$\underline{V}$: A variable = Density times Darcy velocity vector.

V: Horizontal velocity in the fault = $\underline{V} \cdot \underline{e}_y$

W: Vertical velocity in the fault = $\underline{V} \cdot \underline{e}_z$

w: Vertical velocity in the aquifer = ρ x vertical volumetric flux

x: Length variable in x-direction

ye: Half fault width, ratio of fault half width to depth of the aquifer

$\bar{y}$: Horizontal length variable in the fault as well as in the aquifer = y'/ye'

y: Horizontal length variable in the aquifer = y'/L'

$\hat{y}$: Horizontal length variable in the aquifer = y'/H'

$\bar{z}$: Vertical length variable used in the fault as well as in the aquifer = z'/ye'

z^*: Vertical length variable in the aquifer = $\dfrac{z'}{\sqrt{ye'L'}}$

z: Vertical length variable used in the fault as well as in the aquifer = z'/L'

Greek Letters

α_e: Coefficient of thermal expansion

$^o\alpha_e$: Coefficient of thermal expansion at T_o

γ: O(1) number = $\sqrt{Rye^2}$

ΔT: Overall temperature difference across the system = $T_{max} - T_o$

ϵ: A small number

η: Similarity variable = $z^*/y^{1/2} = z/\hat{y}^{1/2}$

θ: Temperature in the aquifer.

θ^c: Temperature in the clay cap

θ_M: Interface temperature between cap and the aquifer

λ: Thermal conductivity, ratio of the thermal conductivities of the clay cap and the aquifer

λ_m: Thermal conductivity of the medium

$\lambda^o m$: Reference thermal conductivity of the medium

μ: Viscosity of the fluid

μ_o: Viscosity of the fluid at temperature T_o

ν: Kinematic viscosity = μ/ρ

ν_o: Reference kinematic viscosity at T_o

ρ: Density

ρ_o Density at T_o

τ: Overheat ratio = $\Delta T/T_o$

ϕ: Porosity = volume of fluid/volume of porous matrix

ω: A variable = $O(\varepsilon^{\frac{1}{2}})$

I. Introduction

During the period 4/1/78 to 11/30/78 the geothermal research project emphasized the completion of a mathematical model of a liquid-dominated resource with characteristic features reminiscent of the Mesa Anomaly, Imperial Valley, California. This modelling effort was a natural outgrowth of an extensive, systematic investigation of liquid-dominated geothermal systems supported initially by the RANN-program of the National Science Foundation and subsequently by the Energy Research and Development Administration and the Department of Energy through Lawrence Berkeley Laboratory.

A comprehensive field data analysis was used to develop an understanding of the significant physical processes occurring in the geothermal reservoir. The Mesa Anomaly, a typical moderate temperature system sited in sediments was chosen for detailed consideration because the ensemble of data was the most complete available to the public. In addition, drilling activity by three operators implied the availability of additional information. Results of the analysis are presented in Black (1975), Bailey (1977) and Goyal (1978).

As the data analysis proceeded and conclusions were digested a conceptual model of the Mesa system began to emerge. We inferred from the available evidence that water heated at depth, perhaps below the sediment-basement rock interface, rises by natural convection in extensively fractured zones associated with faulting. Reservoir charging occurs when the upwelling region is intersected by horizontal sediments with relatively large permeability. The driving force for the convection process arises from the hydrostatic pressure difference existing between the bottom of the hot (light) water column below the upwelling region and the cold (heavy) water far from the anomaly. Reservoir cooling occurs

as the hot water, flowing basically horizontally in various aquifers, transfers heat to the colder surface.

The modelling of heat and mass transfer in the conceptualized geothermal system was found to be carried out most efficaciously in terms of fluid flow in a thermally active, saturated porous medium. Describing equations for such modelling were developed for the project by Morland (1976) and Koeller and Zebib (1977). It was envisioned that material property input(e.g., porosity, permeability, conductivity) would be obtained from the aforementioned field data analysis. Similar considerations apply to the geometrical configuration used in the mathematical analysis and to the boundary conditions applied. Finally we planned to compare the output of the mathematical model (e.g., surface heat flux, temperature and pressure variation with depth) with the available field data in order to validate, and when necessary to alter the model.

The culmination of our efforts is described in the technical section of this report which is, in essense, the third chapter of a Ph.D. thesis by K.P. Goyal. In that work Goyal, with the guidance and assistance of the Project Director, Prof. D.R. Kassoy, has attempted to incorporate the information and ideas made available in earlier phases of the research program into a comprehensive, physically plausible analysis of a fault zone controlled goethermal system. Since there is extensive evidence (Kassoy and Zebib, 1978) that faulting is present in the majority of geothermal systems, it is likely that the concepts developed and approach used to model the resource will have relevance to reservoirs other than the Mesa Anomaly.

II. Technical Summary

a. Conceptualized Model

A pictorial conceptualization of a fault zone controlled geothermal system, shown in a plane transverse to the fault plane, is given in Fig.1. A near-vertical strike-slip fault zone, characterized by relatively high vertical permeability extends through the reservoir sediments of depth ℓ_R and into the basement for a vertical distance ℓ_B. The associated near-vertical fracture system is assumed to be closed by clays in the cap of thickness ℓ_C and deep in the basement by creep deformation of the hot rock system associated with a localized heat source. The transverse width $h<<\ell_R$ represents the extent of the region of vertically oriented fracture distribution associated with the faulting processes.

The local deep thermal source at the Mesa is unknown, as is the specific mechanism for charging the fault with water at depth. Several plausible, but unproven, processes for charging are possible. Since the basement rock is relatively brittle, given the seismic velocity data of Combs and Hadley (1977) it is possible that an extensive generalized fracture system has been created by continual tectonic and periodic intrusive activity in the area. If this is

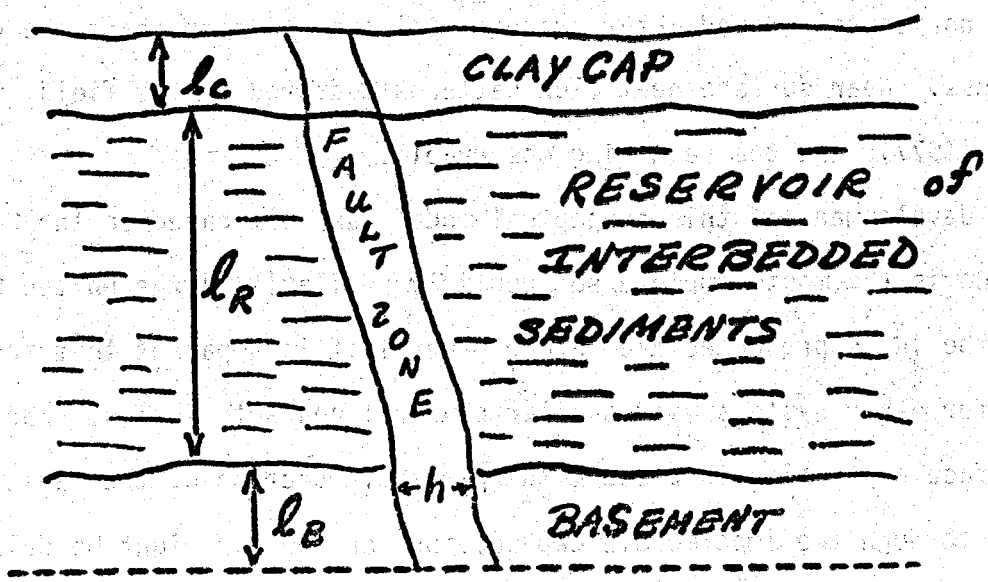

Fig. 1 - Conceptual Model-Transverse View

the case, then water may percolate downward into the hot basement very slowly over an area which is enormous compared to the fault zone itself. The water will flow horizontally toward the fault, driven by the hydrostatic pressure imbalance between the extended "cold" recharge region and the hot upflow column in the fault zone [Donaldson (1970)]. Once the water enters the fault, natural convection processes move the water upward in the narrow fault at a velocity significantly larger than any horizontal velocity in the system.

The liquid rising in the fault zone can charge an intersecting aquifer of reasonable permeability due to the convection-induced artesian over-pressure existing there. There is little communication between the upflow in the fault and the ground water system in the cap due to the significant shale deposits in the latter. The complex interbedding in the reservoir also reduces communication between aquifers to a minimum [Coplen (1976)]. In-the-large, the reservoir flow is basically horizontal in nature due to the large number of discrete shaley layers observed.

The reservoir liquid loses heat to the surface through the sediments and the cap. Heat transfer in the latter is primarily by conduction [Swanberg (1974)] although horizontal ground water systems will tend to complicate the details of the process. Near surface heat flux patterns measured in the field, Combs and Swanberg (1977), are the resulting observable.

The development of this conceptual model has been based on the Mesa field data which is the most complete set publicly available in the United States. Because the ideas presented are rather general it is apparent that the model can be used for other systems with similar physical characteristics. For instance, when surface expression is present the permeable section of the fault could be extended through the impermeable cap section, or the cap might be deleted entirely. More extensive vertical motion in the aquifer might be considered.

It should be noted that Hoagland (1976) and Hoagland and Elders (1977) have conceptualized a similar model for the historical functioning of the Mesa Anomaly. However, they conclude that in the more recent past the system was altered sufficiently by deposition to render the upflow process ineffective. On the basis of geochemical interpretation they indicate that the entire system is presently being cooled by a horizontal flush of cool water which deposits carbonates as it is heated. The plausibility of this model should be tested in the future by an approrpiate heat transfer calculation.

We consider liquid convection in a rigid porous matrix. A single-phase is considered because there is little evidence of preexploitation in-situ boiling in most moderate temperature systems. The known isotherm distribution is such that the boiling point curve is never approached. Pressure distributions associated with natural convection processes are sufficiently small to preclude the possibility of matrix deformation due to the liquid flow itself. The matrix may, however, have a variable distribution of permeability and porosity as is observed from well-log data [Black, (1975)]. These variations are caused by specific structural features, compaction, hydrothermal alteration and the complex stratigraphy present.

We consider first the nature of reservoir charging by upflow in a fault zone for the configuration shown in Fig. 1. When large Rayleigh number (R) flows are considered it is possible to develop semi-analytical solutions. Here R is defined by

$$R = \frac{gk\alpha\ell_R\Delta T}{\nu^2} Pr_m$$

where g is the gravity constant, k is a characteristic permeability, α is a characteristic thermal expansion coefficient for water, ℓ_R is the reservoir depth, ΔT is the characteristic temperature difference through the reservoir, ν is the characteristic kinematic viscosity of water and Pr_m is the Prandtl

number for water based on the thermal conductivity of the staturated porous medium. For typical high temperature thermodynamic values, $\alpha = 5 \times 10^{-4}/°K$, $\nu = 2 \times 10^{-3}$ cm^2/s, a permeability $k = 10^{-9}$ cm^2 and typical (minimal) reservoir values ℓ_R = 1.5 km and ΔT = 50°C, then $R \approx 940$. Of course, sensitivity to the value of k, which is a bit speculative, is noted. For deeper, hotter systems, (Combs' (1977) prediction of the depth of the basement interface at the Mesa is ℓ_R = 3 km and ΔT 200°C) R = 6000. Even if the value of k is reduced considerably it is clear that Rayleigh numbers of 500 should be viable. [Kassoy and Zebib (1975)].

Natural convection theory [Kassoy and Zebib (1975, 1978)] can be used to show that the vertical convection velocity in the fault zone is characterized by

$$v_V = g\, k\alpha\Delta T/\nu$$

For the first set of values used above, $v_V \approx 1$ cm/day. Assuming an average temperature of about 175°C in the convection-active section of the fault, one finds that 1.75×10^7 cal/s km^2 is convected upward. This is about 3 orders of magnitude larger than the purely conductive flux. If a substantial fraction* of this energy is lost to the clay cap and conducted to the surface where Combs [in Rex (1971)] measured 4.88×10^6 cal/s crossing about 110 km^2, then the horizontal area of the fault zone is about 2.9 km^2. Since thermal activity of the Mesa extends along the primary fault for about 16 kms., a fault (fracture-zone) width $h \approx 180$m is suggested. One should recognize that this is an order of magnitude estimate. Given the variable nature of the input a range $100\text{m} \leq h \leq 300\text{m}$ might be appropriate. If k were far smaller than 10^{-9}cm^2 the fault zone area estimate would be far larger, and thus not representative of the relatively

*In the calculation I assumed a 10% loss. The value is based on the temperature difference between well-bores 5-1 and 6-2 in the convective zone.

localized anomalous heat flux properties at the Mesa field.

Convection theory [Kassoy and Zebib, (1975)] can also be used to show that the artesian over-pressure magnitude is given by

$$\Delta P_A = \rho g \ell_R \alpha \Delta T$$

where ρ is the characteristic liquid density. ΔP_A is of the magnitude of 10 bars for the parameters given above. Coplen (1976) has noted that shut-in pressures for Mesa 6-2 have ranged from 3.5 to 8.2 bars, which indicates that there is reasonable agreement between field data and theoretical assessment for the selected parameter values.

The full theoretical calculation emphasizes the mass transfer process in the fault and adjacent aquifer and the heat transfer process in and beneath the clay cap. Full convection equations are used in the fault and aquifer, while the heat transfer in the cap is modeled by the conduction equation. The temperature is assumed constant (at the average annual value) at the surface and at the basement interface. The latter condition is a meaningful representation of the actual physical situation if the effective basement thermal conductivity is larger than that in the aquifers. The precise conditions at depth are, of course, not known. In general, however, crystalline basement rocks can be expected to have larger thermal conductivity values than the neighboring sedimentary material.

The condition far from the fault is assumed to be a conduction-controlled temperature gradient such that the surface heat flux is at the measured background value of about 1.5 HFU. Given that vertical velocities in the far field are small (due to barriers associated with interbedding and clay strata), the pressure distribution with depth at the far boundary can be assumed to be hydrostatic. Horizontal through-flow across the boundary is permitted.

Insofar as the Mesa system is concerned, a basic research goal is to predict surface heat flux and compare with Combs' field data [Rex (1971)]. The solution values depend upon the input mass flux into the fault, which is initially unknown. A parametric variation of the solution with the mass flux to find the heat flux distribution which best resembles the data can be used to ascertain the mass flux. Other formal comparisons involve bore-hole temperature and pressure distributions with depth and aerial isotherm patterns.

Some recognition must be given to the difficulty of interpreting the near-surface heat flux distributions, which in some cases appear to the affected by shallow ground-water motions. Known bore-hole temperature-distributions with depth are less ambiguous, because it is clear that shut-in times were sufficient to obtain thermal equilibrium with formations, and vertical temperature gradients were small enough to preclude large-scale circulation of liquid within the bores.

The conceptual and mathematical models have been used to consider heat and mass transfer in systems reminiscent of the Mesa Anomaly. First we consider heat and mass transfer in a fault and adjacent aquifer when the latter extends to the surface. Liquid enters the fault at a prescribed high temperature and rises isothermally because the Rayleigh number is large. Overpressure in the fault drives hot liquid into the aquifer. Only in a thin layer adjacent to the cool upper impermeable surface is the fault liquid cooled. This thermal boundary layer thickens in the upper portion of the adjacent aquifer as fluid flows horizontally away from the fault. The high Rayleigh number boundary layer theory fails at a specified large distance from the fault, because the cooled thermal layer encompasses a significant fraction of the vertical extent of the aquifer. Thereafter, the heat transfer process is described by a parabolic differential equation which is solved with traditional numerical methods. It

is found that, over a horizontal distance in the aquifer equivalent to several fault depths, the temperature distribution with depth includes a rapidly increasing section (in the thin thermal boundary layer) followed by a larger vertical extent of zero gradient (due to the high Rayleigh number approximation). Thus it is clear that the absence of a temperature gradient need not imply vertical upflow. Given the structural situation specified, zero gradient conditions are found in the fault (strong upflow) and in an extensive portion of the neighboring aquifer, where only horizontal flow exists. Further from the fault, where the aquifer is fully cooled by the cold upper boundary, a nonzero temperature gradient exists throughout the vertical extent of the system.

The surface heat flux above the fault is found to be 30-40 times larger than the conduction-controlled background value, when parameters derived from Mesa data are used . Such large heat transfer rates are not usually observed in systems without surface expression, because the geothermal waters are separated from the surface by a variety of structural effects and groundwater systems. For instance, at the Mesa, the upper 800m of sediments contain a clay content sufficient to preclude the possibility of significant vertical water motion. The effect of this kind of layer on the heat transfer process is considered next. Conduction heat transfer alone in the "cap" rock is coupled with the processes in the aquifer below to find the temperature distributions and surface heat flux. The vertical temperature profiles are found to vary with distance from the fault in a way quite reminiscent of analogous variations in Mesa borehole data.

This may be seen by a qualitative comparison of the borehole temperature variations in Fig. 2 and theoretical predictions in Fig. 3.41 of the technical report. In the former figure, the bores 6-1, 6-2, 8-1, 44-7 and 48-7 are thought to be close to fracture zones while the remainder are further away. In particular 18-28 is farthest from any known fault zone.

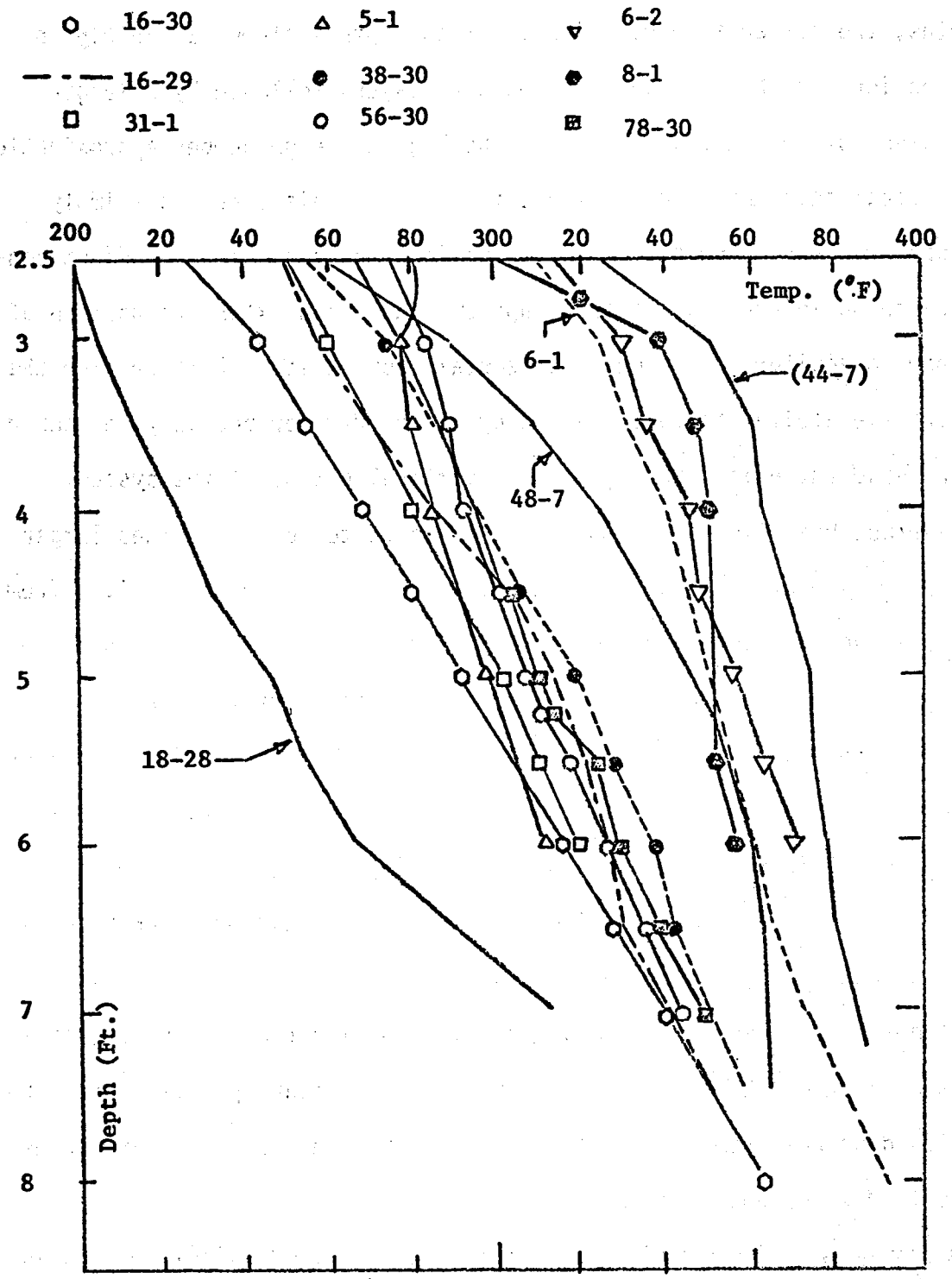

Fig. 2 Temperature (°F) vs. Depth (10^3 ft.) in East Mesa Wells.

The maximum surface heat flux is 3-5 times larger than the background value, for parameter ranges typical of the Mesa. In Fig. 3 we compare surface heat flux data and the theoretical distribution. The qualitative agreement implies that fault zone controlled charging of a geothermal aquifer represents a physically viable mechanism of maintenance of a liquid dominated system. Quantitative differences suggest that further refinements of the model are necessary.

It is to be emphasized that the modeling described has been carried out in order to develop an understanding of heat and mass transfer in systems prior to exploitation. Appropriate characterization of physical processes will improve resource exploration techniques, evaluation and assessment. The conceptual ideas and the mathematical approach used here are quite unlike the more traditional approach to geothermal reservoir engineering, where primary interest focuses on consequences of production. Excellent examples of the latter are the simulation models of Mercer, Pinder and Donaldson (1975), Mercer and Faust (1977), Pritchett et al (1978) and other work by Riney at Systems, Science and Software.

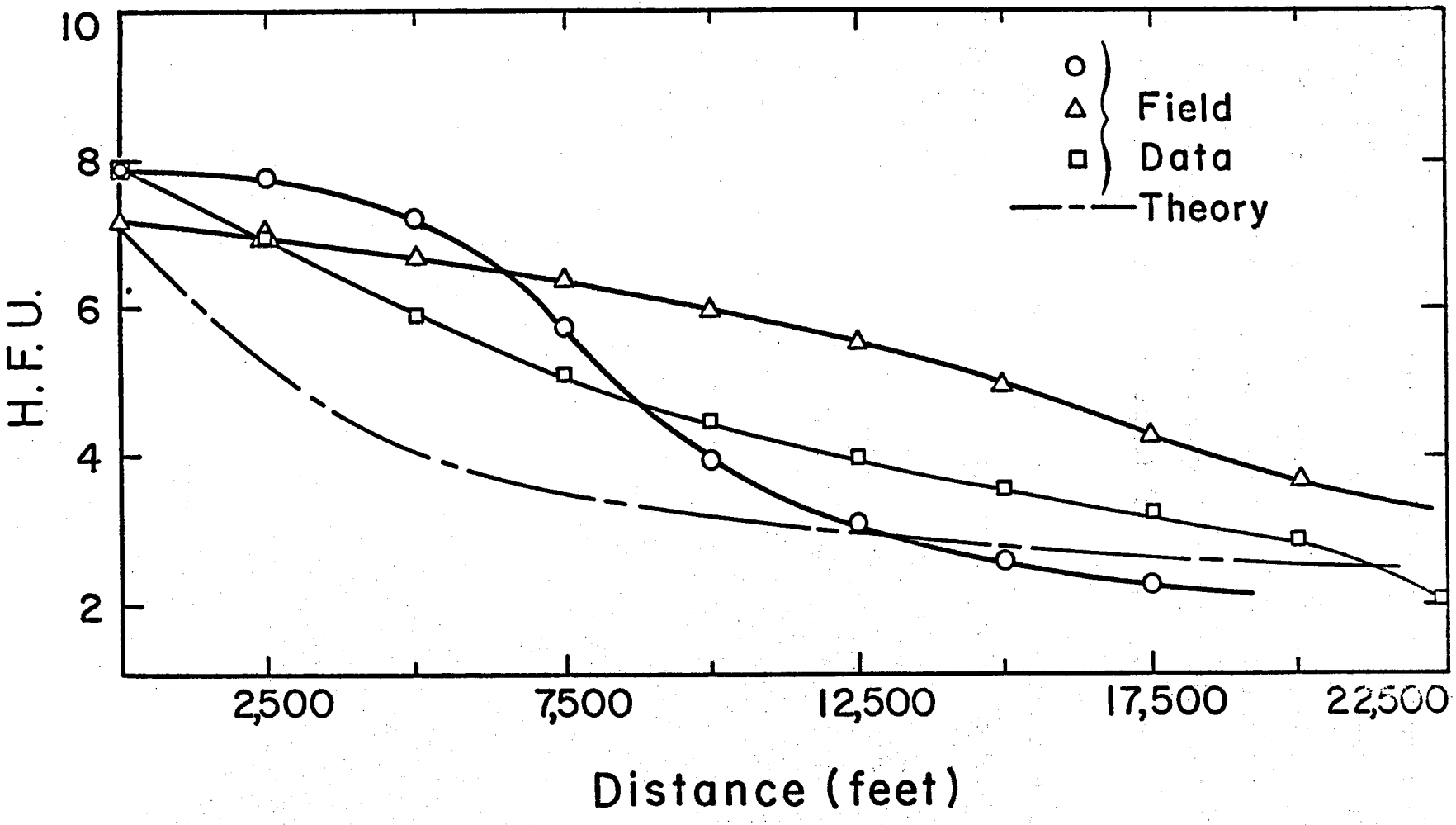

Fig. 3. Comparison of measured near-surface heat flux and theoretical prediction. Field data taken along three different rays outward from the Mesa fault near 6-1 and 6-2.

Bibliography

Baily, T. (1977), CUMER-77-6, Mechanical Engineering Department, University of Colorado, Boulder, Colorado.

Black, H. (1975), CUMER 75-4, Mechanical Engineering Department, University of Colorado, Boulder, Colorado.

Combs, J., and Swanberg, C. (1977) (to appear).

Coplen, T.B. (1976), Cooperative Geothermal Resource Assessment at the Mesa-Geothermal System, I.G.P.P., University of California, Riverside, California.

Donaldson, I. G. (1970), Geothermics 2, 649.

Goyal, K. P. (1978) Ph.D. Thesis, Mechanical Engineering Department, University of Colorado, Boulder, Colorado.

Hoagland, J. R. (1976), Ph.D. Thesis, University of California, Riverside, California.

Hoagland, J.R., and Elders, W.A. (1977), The Evolution of the East Mesa Hydrothermal System, California, U.S.A., IGPP-UCR-77-2, University of California, Riverside, California.

Kassoy, D. R., and Zebib, A. (1975), Phys. of Fluids 18, 375.

Kassoy, D. R., and Zebib, A. (1978), J. Fluid Mechanics 88, 769.

Koeller, R.C. and Zebib, A. (1977), CUMER 77-8, Mechanical Engineering Department, University of Colorado, Boulder, Colorado.

Mercer, J. W., Faust, C. (1977), U.S.G.S. Report 77-234.

Mercer, J. W., Pinder, G.F., and Donaldson, I.G. (1975), J. Geophys. Res. 80, 2608.

Morland, L. W. (1976), CUMER 76-6, Mechanical Engineering Department, University of Colorado,

Pritchett, J. W., Garg, S.K., Brownell, D.H., and Levine, H.B. (1975), Geohydrological Environment Effects of Geothermal Power Production Phase I Systems, Science & Software, La Jolla, California.

Rex, R. W. (1971), Cooperative geological-geophysical-geochemical investigations at geothermal resources in the Imperial Valley area of California, University of California, Riverside, California.

Swanberg, C. (1974), Proc. Conf. on Res. for the Develop. of Geothermal Energy Resources, Pasadena, California, 85.

III. Technical Report

FAULT ZONE CONTROLLED CHARGING OF A GEOTHERMAL RESERVOIR

3.1 Introduction

Over the past three decades much work has been done on convective heat transfer in a porous medium. Horton and Rogers (1945) studied the criterion for the onset of free convection in a porous medium. This was followed by a series of papers by Lapwood (1948), Wooding (1960) and Katto and Masuoka (1967) on the same topics. Combarnous and Bories (1975) have summarized the classical work related to the natural convection in porous media.

For the large temperature differences occurring across many permeable geothermal layers the variation of fluid properties with temperature is significant. Many authors, notably Kassoy and Zebib (1975), Morland, Zebib and Kassoy (1976) and Straus and Schubert (1976) have examined the effect of variable properties on the convection in a uniform porous medium.

Kassoy and Zebib (1975) studied the effect of variable viscosity on the onset of convection in porous media and have found that the critical Rayleigh number is dramatically reduced as compared with the constant viscosity case. Morland, et al.

(1976) found that a further reduction occurred when a constant thermal expansion coefficient, representative of the density variation across the system, was used in the definition of the Rayleigh number.

Straus and Schubert (1976) have studied natural convection of water in thick geothermal layers with temperature differences as large as 345°K and pressure differences as great as 1 k bar. They have included the effect of all variable water properties and found that a lower temperature gradient is needed to start convection as compared with the constant property fluid in a rock of given permeability.

Convection modelling in a slab of homogeneous porous media is too abstract for geothermal applications because realistic internal geologic structure, geometrical boundary configuration and thermal boundary conditions cannot be considered.

Convection processes related to geophysical and geothermal environment have been studied with great interest. Wooding (1957) examined the convection flow in a saturated porous medium with non-isothermal boundary conditions. He applied his method to the geothermal area at Wairakel, New Zealand. Predicted isotherm locations were in fair agreement with temperature measurements made in that area.

Donaldson (1962) studied the temperatures and flow patterns that would be set up in a single permeable layer bounded above and below by impervious conducting sheets and in a two layer system consisting of an upper saturated permeable layer and an underlying layer of impermeable basement rock. He found that the volume flow rates of up to 2×10^{-7} cm^3/cm^2 sec may occur in a 3000 meter thick layer for a Rayleigh number of 165 and that surface heat flux differs by a factor of 9 between regions of upflow and downflow.

The effects of a nonisothermal wall on free convection were studied by Elder (1967a,b). In the first paper he examined the flow in a system, uniformly heated from below and found that above a critical Rayleigh number of about 40, heat transfer is proportional to the square of the temperature difference across the layer and is independent of the thermal conductivity of the medium or the depth of the layer. In the second paper he compared numerical and experimental results for two types of nonsteady convection flows. The first one developed when a blob of hot fluid was released at the base of a porous slab and the second flow developed when a portion of the base of a porous slab was suddenly heated. The agreement between the theory and the experiment in the two cases was good.

Cheng and Lau (1974) have investigated the problem of steady state free convection in an unconfined aquifer bounded by ocean on the sides, with geothermal heating from below. Numerical results of elliptic equations accurate to the first order approximations are obtained for temperature, pressure and stream function as well as for the shape of the water table.

Norton (1975) developed heat transfer computer models to account for variations in fluid properties, conductive and convective heat transfer, and time space variations in the permeability. Fluids were subjected to the ranges of temperatures (ambient - 800°C), pressures (1-1000 bars) and velocities (1-100 m/year). According to his studies convective heat transfer predominates over the conductive heat transfer in the upper 10-15 km of the crust.

Minkowycz and Cheng (1976) studied the free convection about a vertical cylinder embedded in a porous medium, where the vertical surface temperature of the cylinder varies as a power function of the distance from the leading edge. They obtained exact solution for the special case where surface temperature varies linearly with the distance from the leading edge. This analysis may be applied to a cylindrical magma intrusive trapped in an aquifer. The resulting free convective flows induced in the adjacent ground waters can then be studied.

Cheng and Chang (1976) obtained similarity solutions for the convective flow above a heated horizontal surface or below a cooled surface, where wall temperature is a power function of distance from the origin. This analysis has important applications to convective flow above the heated bedrock or below the cooled caprock in a liquid dominated geothermal reservoir.

Kassoy and Zebib (1978) have studied the cooling of fluid rising in a vertical porous channel with impermeable walls whose temperature increases linearly with depth. They have found entry and subsequently fully developed solutions for large Rayleigh numbers. For certain ranges of Rayleigh number and channel width, two-dimensional flow was not found to be possible.

Cheng (1977) studied the effect of lateral injection or withdrawal of fluid along a vertical plane source or sink on free convection boundary layers in a porous medium at high Rayleigh numbers, where both the temperature distribution of the fluid along the plane source or sink and its velocity distribution are prescribed as power functions of the distance. This analysis may be applied to the injection wells where the residual warm water discharged from a geothermal power plant is injected. The resulting convective flow in the adjacent ground water, can, therefore, be studied. This analysis can also be useful when geothermal reservoirs are charged through faults or cracks.

Lau and Cheng (1977) have studied the effect of dike intrusion on free convection in conduction dominated geothermal reservoirs.

Stream lines, temperature distributions and the shape of water table in a two-dimensional volcanic island aquifer are presented.

Recent studies of liquid dominated systems like Wairakei (Grindley, 1965), Broadlands (Grindley, 1970), Long Valley (Rinehart and Ross, 1964), Ahuachapan (Ward and Jacobs, 1971) suggest that geothermal anomalies are intimately associated with specific patterns of faulting.

In the Imperial Valley, California, there are several geothermal anomalies which are close to or intersected by active faults (Elders, et al., 1972). The basic field data for these systems are described by Babcock, Combs and Biehler in Rex (1971), Helgeson (1968), Meidav and Furgerson (1971), Göforth, et al. (1972), Douze and Sorrells (1972), Combs and Swanberg (1977), Combs and Hadley (1975, 1977), Loeltz, et al. (1975), Dutcher, et al. (1972), Elders, et al. (1972), Swanberg (1974,1975), Elders and Bird (1974), Coplen, et al. (1975) and Coplen (1976). Some of the information is surveyed in Kruger and Otte (1973) and in a series of Bureau of Reclamation reports.

3.2 East Mesa Field Data

Black (1975) and Bailey (1977) have considered a large spectrum of the available geological, geophysical, geochemical, hydrological, heat flux and bore hole logging data for the purpose of synthesizing a composite conceptual model of the Mesa system. A summary discussion of the physical nature of the East Mesa field follows.

Location and Setting

The Imperial Valley is a major rift valley, characterized by high heat flow and large quantities of water in storage in the thick fill of alluvium provided by the sediments of the delta of the Colorado River. It occupies part of a deep sediment filled structural basin that extends south from the Coachella Valley to the Gulf of California (Figure 3.1). It is bordered on the west by peninsular ranges, which are mostly granitic rocks of probable Mesozoic age. On the east are the Chocolate Mountains, which in the northern part are principally plutonic and metamorphic rocks of pre-Tertiary age, and to the south are extensive volcanic rocks of Tertiary age.

Stratigraphy

The basin contains three main rock groups. A lower sequence of mainly nonmarine sedimentary rocks of early to middle Tertiary age dominate the basal unit which unconformably overlies pre-Tertiary metamorphic and igneous rocks. However, this basal unit also includes volcanics and small amounts of marine sedimentary rocks. The marine Imperial formation of Pliocene age comprises the beds of the middle sequence. The upper sequence consists predominantly of non-marine deposits of late Tertiary and Quaternary age derived mainly from the Colorado River drainage area. This upper sequence accounts for most of the valley fill in the central part of the trough.

According to the seismic refraction studies of Biehler (1964) maximum sediment thickness in the central part of the trough is

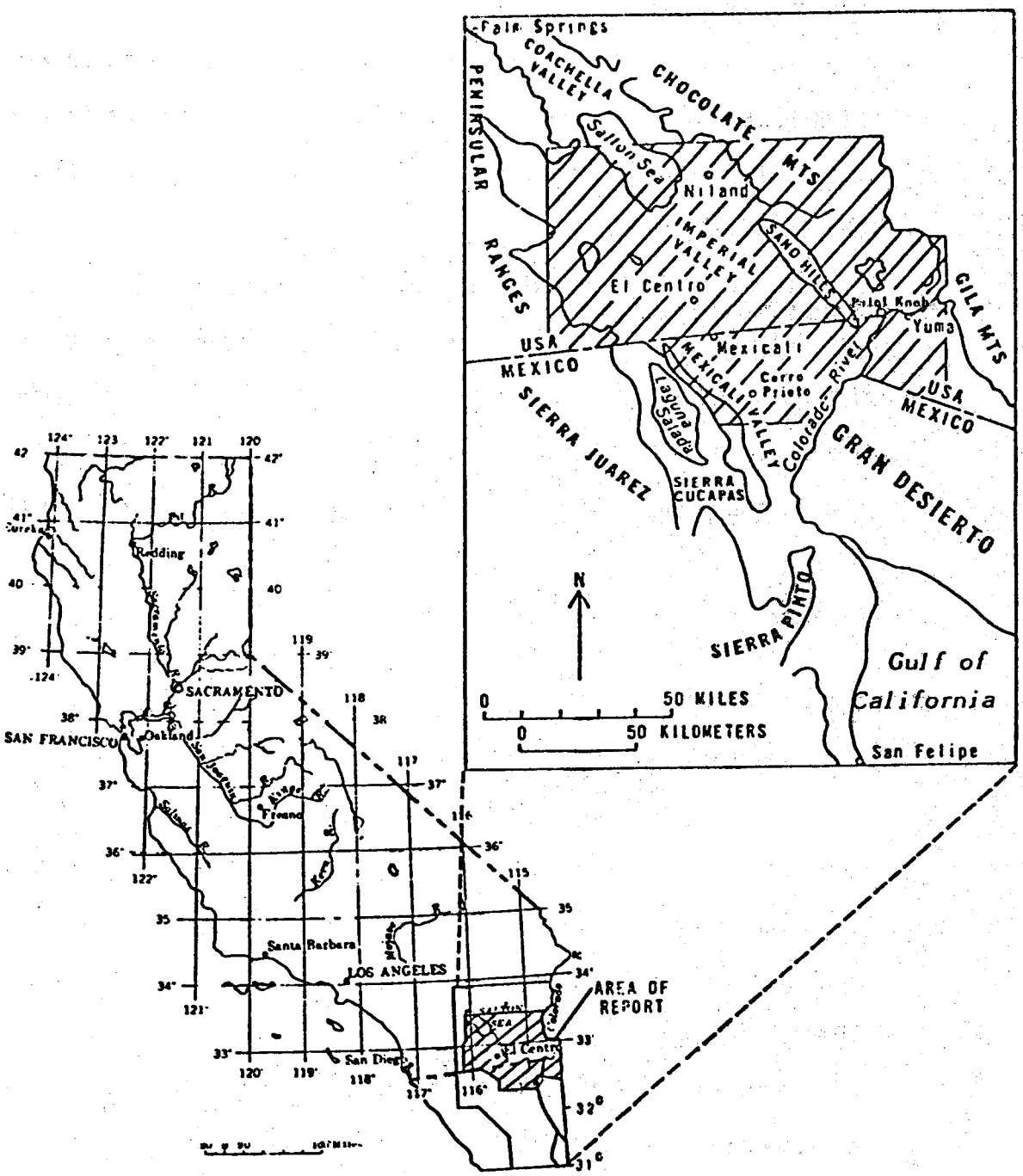

Figure 3.1 Index Map. (Adapted from U.S.G.S. Circular 649)

approximately 6.1 km. The depth to the basement under Mesa anomaly is about 4 km (Combs, Hadley; 1977). This depth reflects the fact that the basin becomes gradually more shallow towards its margins.

Hydrology

Within its thick accumulations of the young valley fill, the sediments of the Imperial Valley comprise a vast water reservoir. In general, horizontal permeability of these sediments is much greater than the vertical permeability. It is true because: (i) platey and ellipsoidal grains are often aligned during sedimentation, and (ii) the lenticular nature of clays in the sediments restricts vertical permeability.

The young alluvial deposits of eastern Imperial Valley contain more sand and gravel than those in the western Imperial Valley. Water table data presented by Dutcher, et al. (1972) show that the regional ground water flow in the Imperial Valley is from the southeast corner to the northwest, i.e., towards the Salton Sea. Recharge to the Imperial Valley is provided by underflow from the Colorado River and precipitation on the uplands bordering the Imperial Valley.

Structure

The Gulf of California coincides with the intersection of East Pacific Rise and the North American continent. The general positive heat flow anomaly of the East Pacific rise extends north at least to the full length of the Salton trough. The structure

of the Imperial Valley is controlled by numerous strike-slip faults of the San Andreas and San Jacinto fault system.

Three faults with no surface expressions, (Rex, 1970; Babcock, 1971; and Combs-Hadley, 1973) have been inferred at the Mesa anomaly by indirect means such as resistivity surveys, microseismic activity and oblique aerial infrared photography (Figure 3.2). Based on microearthquake studies, Combs and Hadley (1977) defined the Mesa fault (also known as the Combs Hadley fault), which functions as a conduit for the rising geothermal fluids of the Mesa geothermal anomaly. In the upper 600 to 800 meters clayey sediments, it is unlikely that significant vertical water motion can occur. Vertically oriented fractures would be filled with clay gouges. However, the presence of slickensides and calcite filled fractures at a depth of 2134 meters in Mesa Well 6-1 appears to support the concept of a fracture zone associated with faulting.

Strata in the central part of the Imperial Valley are essentially horizontal, although dips may occur in the faulted areas. The steepest dips occur at the Valley margins. Stereonet plots of dip directions (Swanberg, 1975), suggest that strata at Mesa 5-1 and 31-1 dip less than 10° to the west. Strata penetrated by Mesa 6-2 and 8-1 show the same tendency above 600 meters.

Using the three point method, Bailey (1977) found the dip of 2° in the Mesa Well 6-1 at the depth of 920 meters. Dip direction for this bed is N48°E. The correlating unit, found at 930

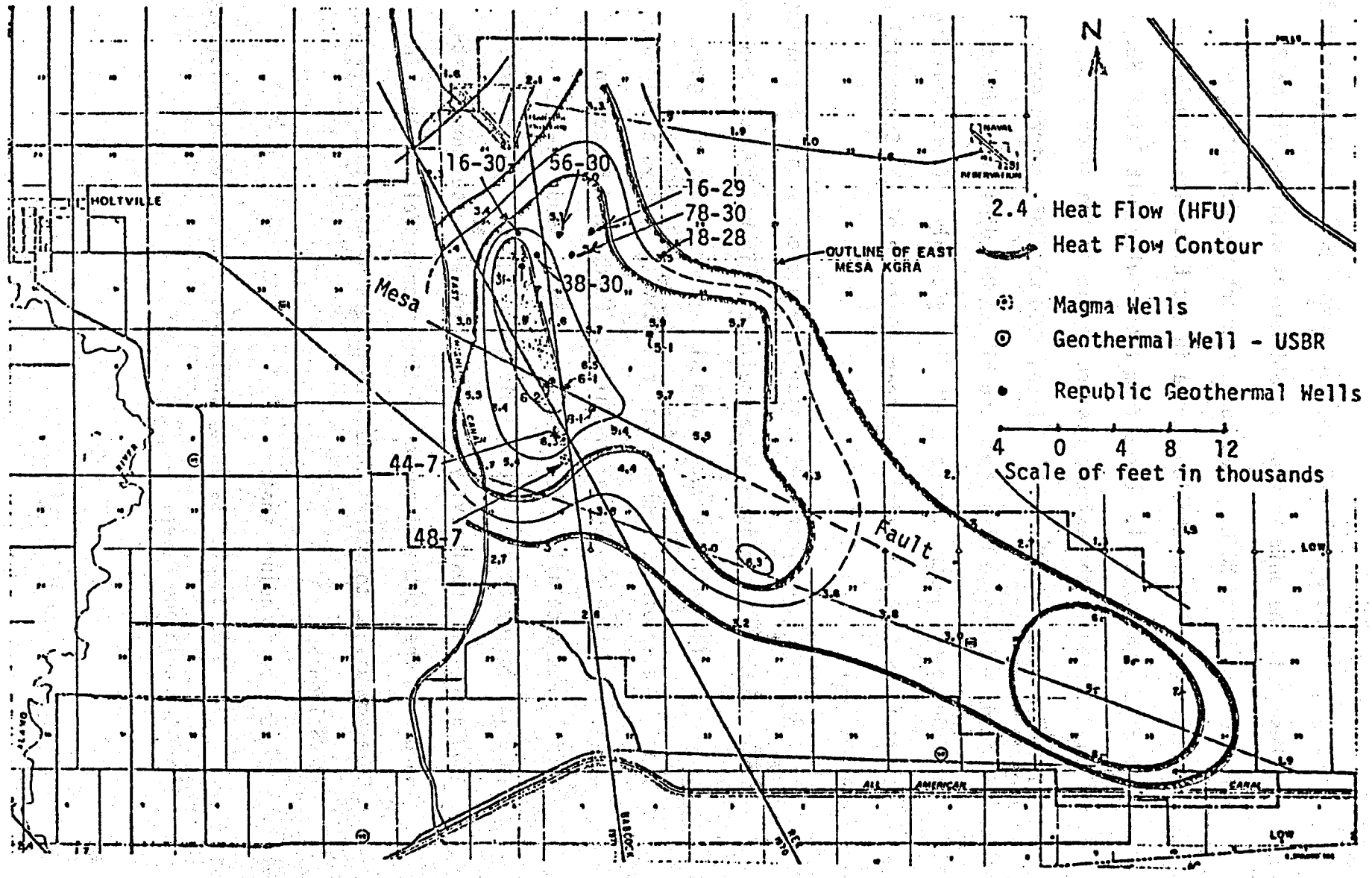

Figure 3.2 East Mesa KGRA Heat Flow (Adapted from USBR, November 1974).

meters at the Mesa Well 6-2, appears to dip N53°E at an angle of 2°. At Mesa 5-1, the unit is found at 851 meters with the dip of 3° in a direction of N8°E. These data support the deductions of Swanberg (1975) that shallow strata in the East Mesa anomaly are essentially horizontal. Cores from the Brawley Unit Stipek No. 1 well, located at the extreme western margin of the study area, displayed dips of 40° to 50° between 1220 and 1830 meters depth. These dips increase with depth and 81° to 84° dips were recorded at 2590 meters depth. These steep dips probably reflect faulting since the Stipek well lies very near the trace of the Superstition Hills fault.

Resistivity--Electrical resistivity decreases with increasing temperature and increasing water salinity. Therefore, the combined effect of high salinity waters and high temperatures in a geothermal reservoir make electrical resistivity surveys a valuable tool in locating geothermal anomalies. Meidav and Furgerson (1971) made a detailed electrical resistivity study of the Imperial Valley at 305, 610 and 915 meters depth. Their results show a regional resistivity gradient which decreases northwestward from the southeast corner of the Imperial Valley, near the Colorado River, to values about two orders of magnitude lower at the Salton Sea.

One may conclude that:

(i) Ground water salinity increases with increasing distance from the Colorado River.

(ii) Many of the faults in the Imperial Valley act as aquitards and restrict horizontal water movement.

(iii) Resistivity lows are found at the East Mesa, Salton Sea, Heber, Brawley and Dunes geothermal anomalies.

Gravity--Gravity studies (Biehler, 1971) revealed the presence of a broad positive gravity anomaly throughout the Imperial Valley. Possible explanations are:

(a) Emplacement of high density crustal material beneath the trough because of:

(i) Clay Diagenesis: This is temperature dependent rather than depth (pressure) dependent (Burst, 1969). Significant dehydration (about 10% to 15% of compacted bulk volume) occurs between temperatures of 100°C and 135°C, rendering a density increase of about .3 g/cm^3. In East Mesa, clay diagenesis would occur at a depth of about 350 to 600 meters.

(ii) Cementation: Calcite filled fractures found in Mesa Well 6-1 at 2134 meters depth may contribute to the density contrast. Deposition of silica and calcite in pores and fractures will raise the density of sandstones.

(iii) Thermal Metamorphism: The gravity high associated with Salton Sea anomaly appears to be mainly due to density increase by metamorphism resulting from high temperatures encountered there. However, a low grade metamorphism, below 2.4 km, may also be contributing to the density contrast in East Mesa area. Samples taken above 2.4 km depth do not show any metamorphism there.

(b) Seismic investigations by Biehler (1964) revealed that the crust is thinner than average beneath the Imperial Valley.

Magnetic--No magnetic anomaly is present at the East Mesa area, as there is at the Buttes area near the Saltan Sea (Black, 1975). Possible explanations are (Bailey, 1977): (i) No buried mass of high magnetic susceptibility exists, (ii) The anomalous mass is buried at a depth at which the magnetic field is too weak to detect.

Microseismic--East Mesa is an active microseismic area. Combs and Hadley (1977) recorded microearthquakes associated with the Mesa geothermal anomaly for five weeks during the summer of 1973 and determined the locations for 36 microearthquakes having epicenters situated in the 150 km^2 areal extent. Focal depths ranged from near surface to about 8 km. More than half of the located events have hypocenters greater than the 4 km which is approximately the depth to crystalline basement. Based on the results of this study, a new right lateral strike slip fault, Mesa fault, was defined (Figure 3.2). Depths to the hypocenters show that the fault is active both above and below the basement.

Heat Flux--Areas of high, near surface heat flow are generally associated with the areas of active volcanism or geothermal areas (Bailey, 1977). Figure 3.2 shows the heat flow contours and the locations of the test wells drilled in East Mesa area by Republic Geothermal Company, United States Bureau of Reclamation (USBR) and Magma Power Company.

Republic Geothermal Company has drilled six wells so far, ranging in depth from 2.25 km to 2.77 km. Towards the south, the

geothermal anomaly is being explored and assessed by U.S.B.R. (five wells) and the Magma Power Company (three wells). Heat flux contours of Figure 3.2 confirm the hypothesis of Combs and Hadley (1977) that Mesa fault acts as a conduit for rising geothermal fluids of the Mesa geothermal anomaly.

Near surface heat flow values for the anomaly itself are as high as 7.9 hfu, with the highest values located near gravity and seismic noise maxima and electrical resistivity minima (Swanberg, 1975). The 3 hfu contour roughly outlines the extent of anomalously high heat flow. Areas outside this contour are only marginally above the regional background and such areas can not be expected to yield a successful production well, although such areas might well prove ideal for disposal of geothermal brine. The area within the 5 hfu contour can be considered the production area. For the Mesa anomaly, over 40 km^2 of land fall within this contour (Swanberg, 1975). It can also be noted from Figure 3.2, that the heat flow values decrease with distance very rapidly west of the zone of maximum heat flow but decrease very slowly to the east. Leakage of cold water, from East Highline Canal into the first 400-500 m of sediments causes the rapid decrease of surface heat flux towards the west, conforming with the strata dip direction there (Swanberg, 1975). There might be some contribution from Alamo River which flows to the west of the East Mesa test site. Positions of the heat flow contours relative to the Mesa fault show the upwelling of the hot brine in the fault and the direction of the flow (northeast and southwest) away from the fault.

Permeability: The thicknesses and depth of sand and sandstone beds having permeabilities greater than 99 millidarcys are plotted in Figure 3.3 for Mesa Well 6-1. It can be seen that permeabilities are lower in the upper 600-700 meters. Middle zone up to 2-2.1 km appears to be a permeable zone containing large percentage of sands and sandstones. Lower zone beyond 2.1 km shows a decrease in permeability. Similar plots for other Mesa wells are available in the report of Black (1975). Figure 3.4 clearly shows the different zones encountered in Mesa Well 6-1 and the relative percentage of sands or sandstones and shales in these zones.

Porosity: The average porosity of the sandstones in the fifty foot intervals and the average porosity of each fifty foot interval (according to the formula: $\frac{\text{porosity of sand x feet of sand}}{50 \text{ ft}}$) are plotted vs. depth for Mesa Well 6-1 in Figure 3.5. Sands in the upper 700-850 meters have the highest porosities in each well, but the porosities of the fifty foot interval are quite low. The large separation between two values indicates the presence of a large amount of shale in upper 700-850 meters (porosity of shale is taken as zero), which is interbedded with porous sands. The report of Black (1975) contains similar plots for other U.S.B.R. wells.

Geochemistry: Bailey (1977) has summarized the available chemical composition of the waters in the Imperial Valley. His conclusions are:

(i) Two different types of waters are present in the East Mesa anomaly. Waters collected between about 1400 and 2200 meters

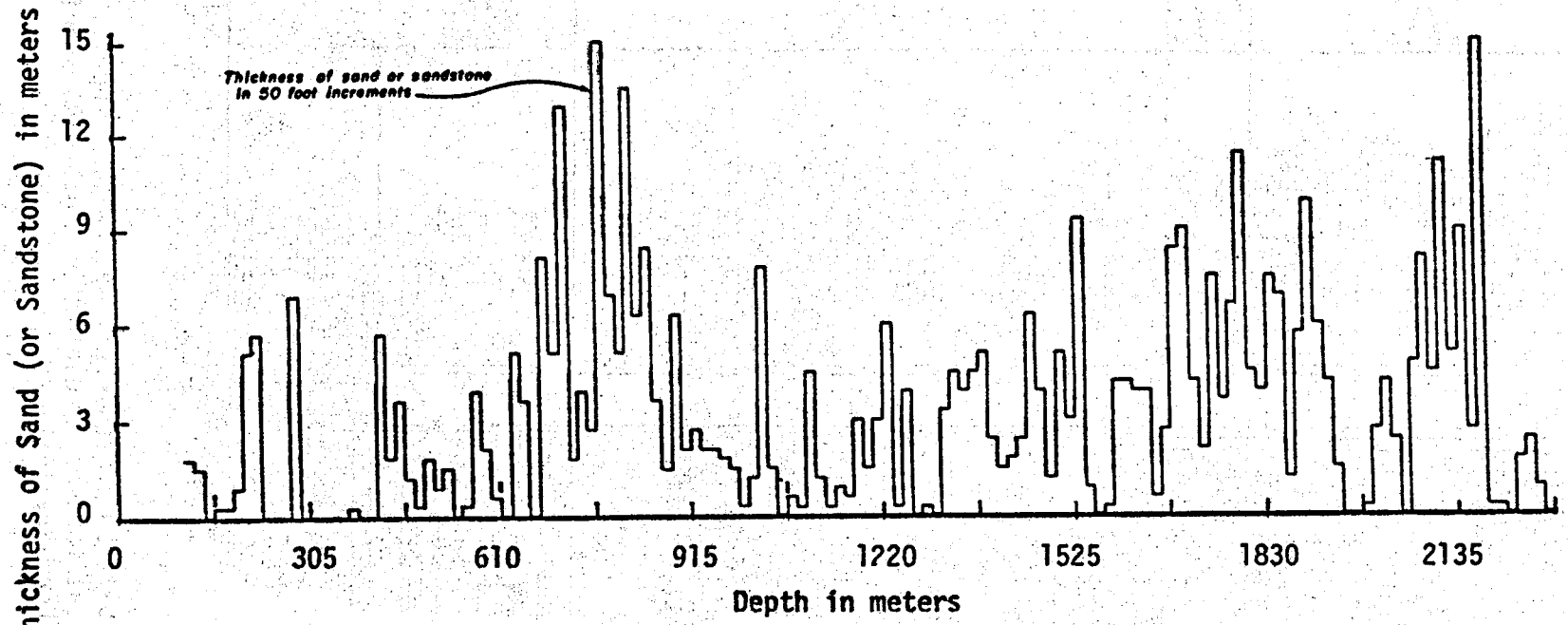

Figure 3.3 Distribution of Sand and Sandstone Having Intergranular Permeabilities and Greater than 99 Millidarcys. Test Well Mesa 6-1, Imperial Valley, California (Adapted from U.S.B.R. Special Report February 1973)

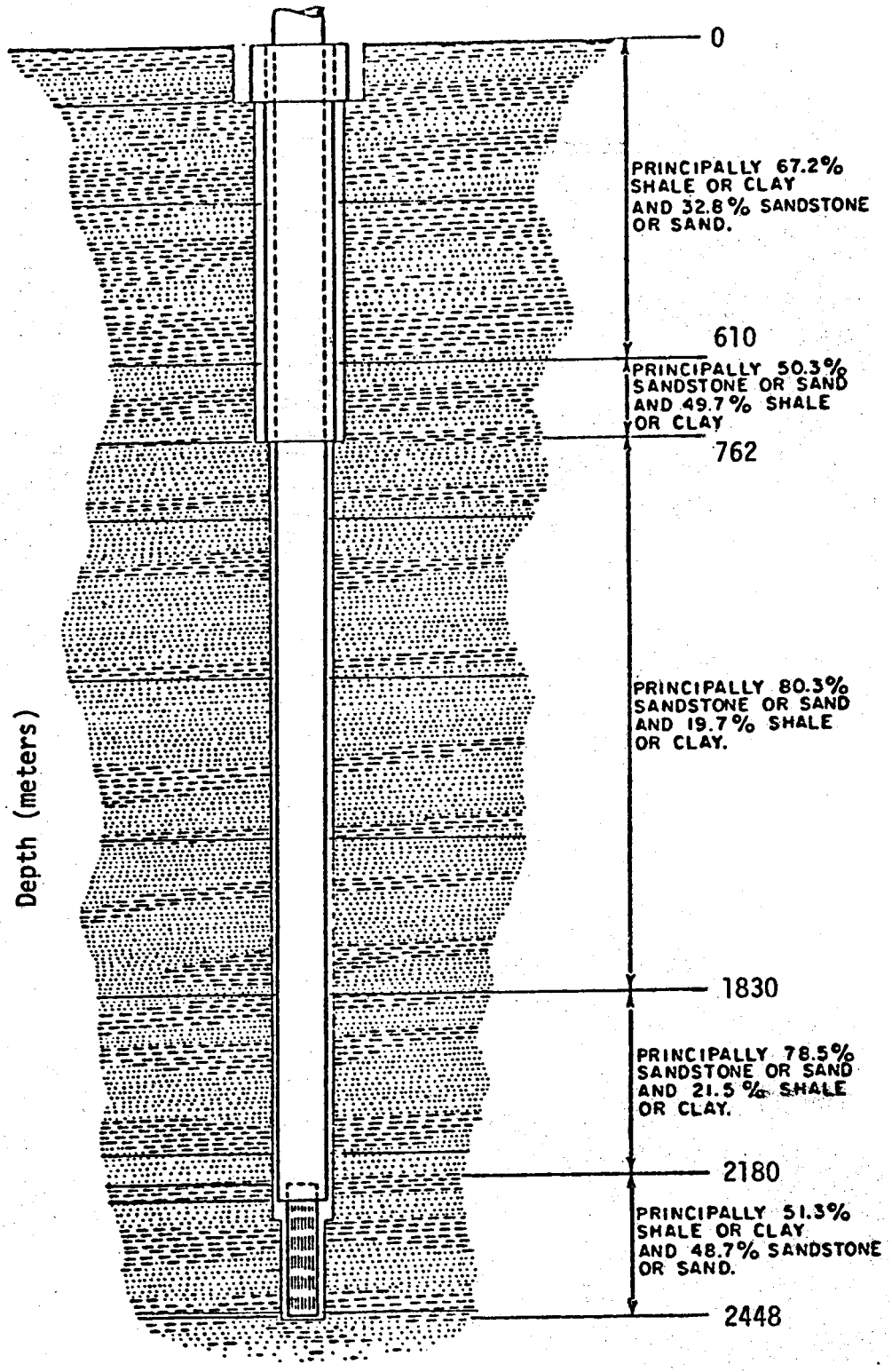

Figure 3.4 Diagram of Test Well Mesa 6-1. Imperial Valley, California. (Adapted from U.S.B.R. Special Report, February 1973)

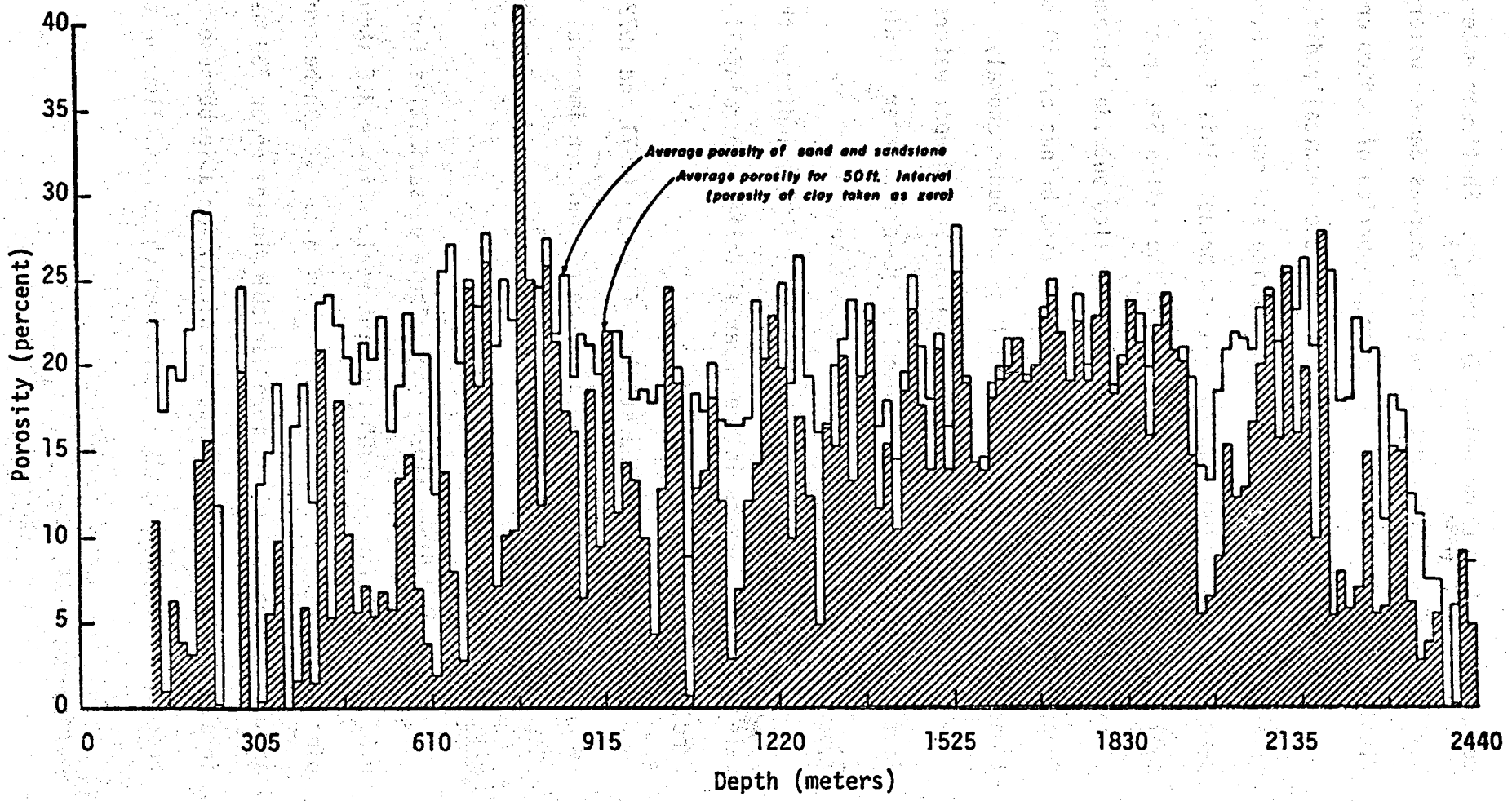

Figure 3.5 Distribution of Porosity Values in Sand and Sandstone in Test Well Mesa 6-1, Imperial Valley California.

depth differ from those below 2200 meters. Shallower waters are similar to those nearby ground waters, whereas deeper waters display high salinity and a greater proportion of sodium chloride.

(ii) Salton Sea anomaly possesses two chemically different brines. Deeper brine is much more saline and contain a higher percentage of calcium than the shallow brine. This deeper hypersaline water appears to be limited to the Salton Sea area, as no evidence of it is found in the wells drilled outside the anomaly. Concentrations of solids in the hypersaline brines are 50 to 100 times those in the waters of East Mesa and Dunes anomaly.

(iii) Shallow waters at the Salton Sea, deeper waters at East Mesa and Dunes anomaly resemble the ocean water, indicating that these waters may all have the same source.

(iv) Chloride/bromide ratio of Rex (1972) indicate that the main sources of waters in the Imperial Valley are rainfall and precipitation runoff.

(v) According to the studies of Coplen (1971 and 1972), the Colorado River is the probable source of southern Imperial Valley geothermal waters while local precipitation provides for the waters of Salton Sea area.

Salinity: Black (1975) has calculated salinities for all U.S.B.R. wells for each 100 foot interval. Figure 3.6 shows the plot of salinity vs depth in Mesa Well 6-1. It can be seen that salinities are higher and more variable in the upper 750 meters in all the wells. Salinities are highly variable because of interbedded, unfractured sands and clays which do not allow vertical

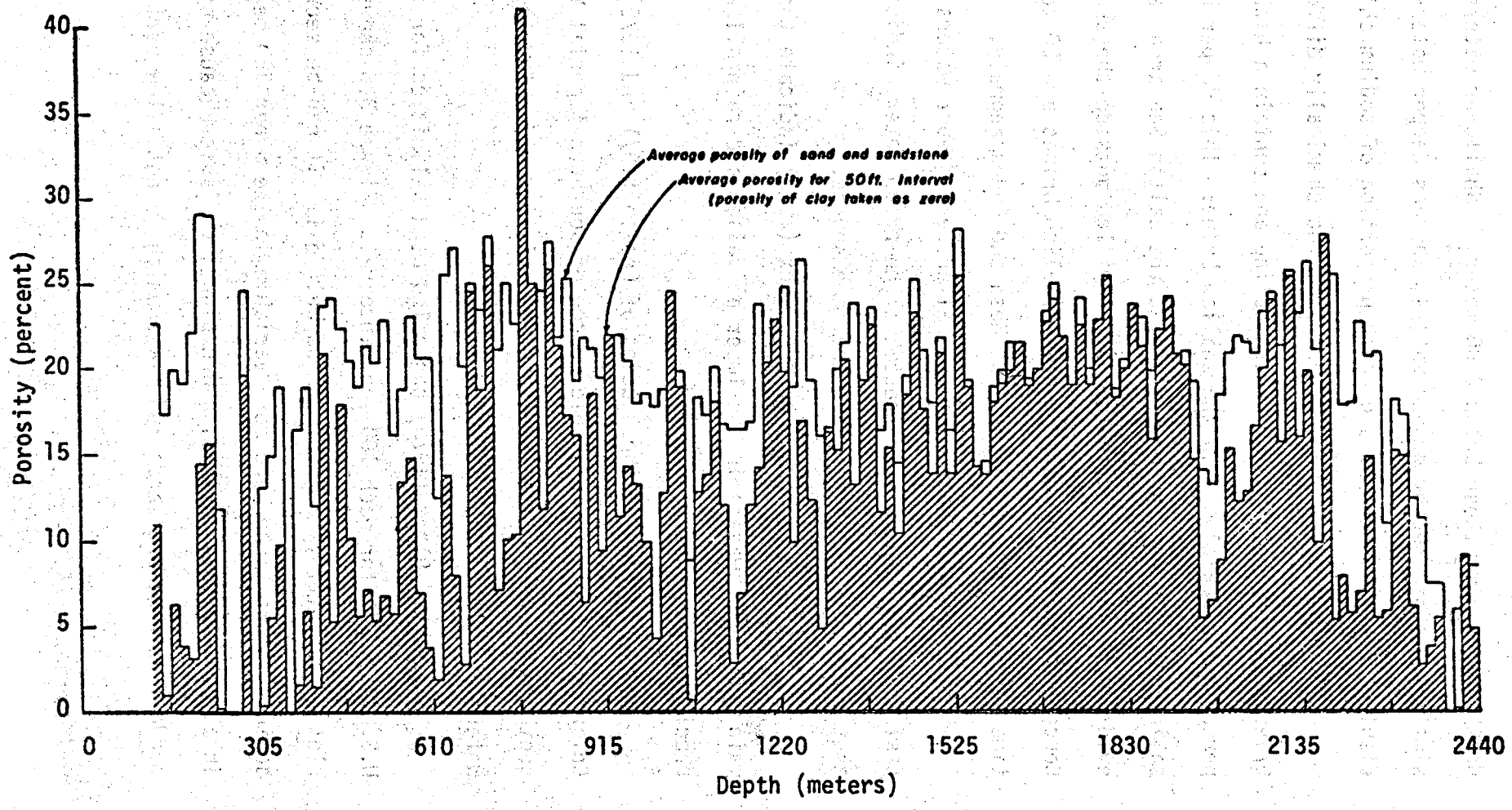

Figure 3.5 Distribution of Porosity Values in Sand and Sandstone in Test Well Mesa 6-1, Imperial Valley California.

depth differ from those below 2200 meters. Shallower waters are similar to those nearby ground waters, whereas deeper waters display high salinity and a greater proportion of sodium chloride.

(ii) Salton Sea anomaly possesses two chemically different brines. Deeper brine is much more saline and contain a higher percentage of calcium than the shallow brine. This deeper hypersaline water appears to be limited to the Salton Sea area, as no evidence of it is found in the wells drilled outside the anomaly. Concentrations of solids in the hypersaline brines are 50 to 100 times those in the waters of East Mesa and Dunes anomaly.

(iii) Shallow waters at the Salton Sea, deeper waters at East Mesa and Dunes anomaly resemble the ocean water, indicating that these waters may all have the same source.

(iv) Chloride/bromide ratio of Rex (1972) indicate that the main sources of waters in the Imperial Valley are rainfall and precipitation runoff.

(v) According to the studies of Coplen (1971 and 1972), the Colorado River is the probable source of southern Imperial Valley geothermal waters while local precipitation provides for the waters of Salton Sea area.

Salinity: Black (1975) has calculated salinities for all U.S.B.R. wells for each 100 foot interval. Figure 3.6 shows the plot of salinity vs depth in Mesa Well 6-1. It can be seen that salinities are higher and more variable in the upper 750 meters in all the wells. Salinities are highly variable because of interbedded, unfractured sands and clays which do not allow vertical

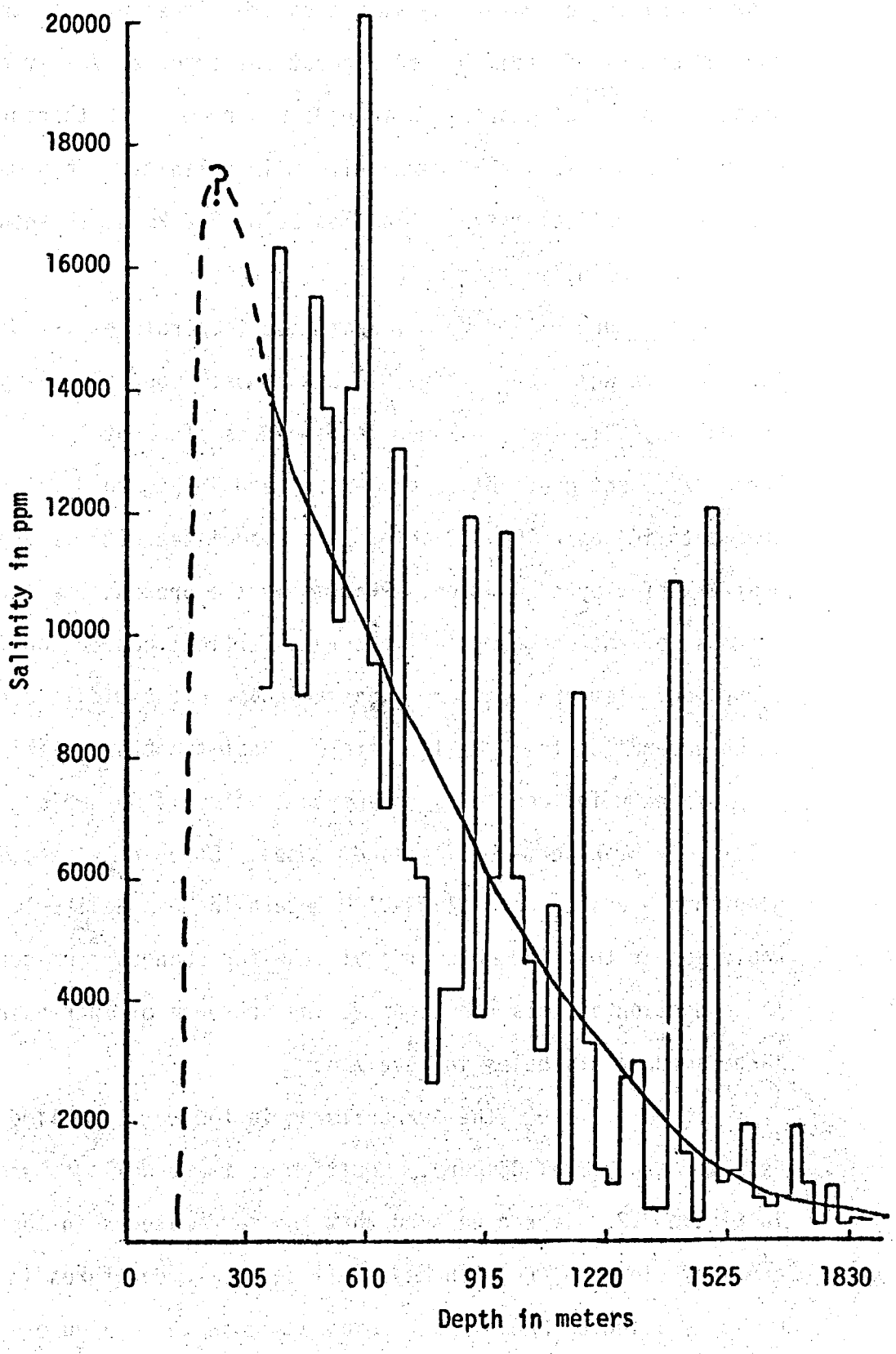

Figure 3.6 Salinity vs. Depth for East Mesa Test Well 6-1. (Adapted from the Report of Black 1975).

flow and mixing of waters. Salinities are higher because the upper 750-900 meters of sediments throughout the Imperial Valley contain greater amounts of evaporites than deeper rocks. Furthermore, water below 900 meters is more uniform in salinity. This may be because of vertical mixing. Samples below 2.2 km depth show increasing salinity with depth.

Temperatures: Figure 3.7 shows the temperatures vs. depth for the five wells drilled by U.S.B.R. Most Imperial Valley geothermal anomalies have maximum temperatures of about 150°C-200°C Three different gradient zones can be seen in Figure 3.7. Steep gradients in upper 700-900 meters are associated with vertical heat transfer by conduction. Presumably the presence of large amounts of interbedded clays prevents vertical convection from occurring. Temperatures are less variable in the middle zone which extends up to 1900-2100 meters. Heat transfer in this zone is profoundly influenced by convection, which is possible in relatively high permeability sandy zones. Steeper temperature gradients are seen below 1900-2100 meters in Mesa Well 6-1. It would appear that the mode of heat transfer changes from convection to conduction at this depth due to the presence of increasingly large amounts of shales in this zone.

Figure 3.8 shows the temperatures in the wells drilled by Republic Geothermal Company. Location of these wells is shown in Figure 3.2. It can be seen that the temperatures in these wells are very close to those in Mesa Well 31-1. Temperatures in the wells, drilled by Magma Power Company are shown in Figure 3.9 and

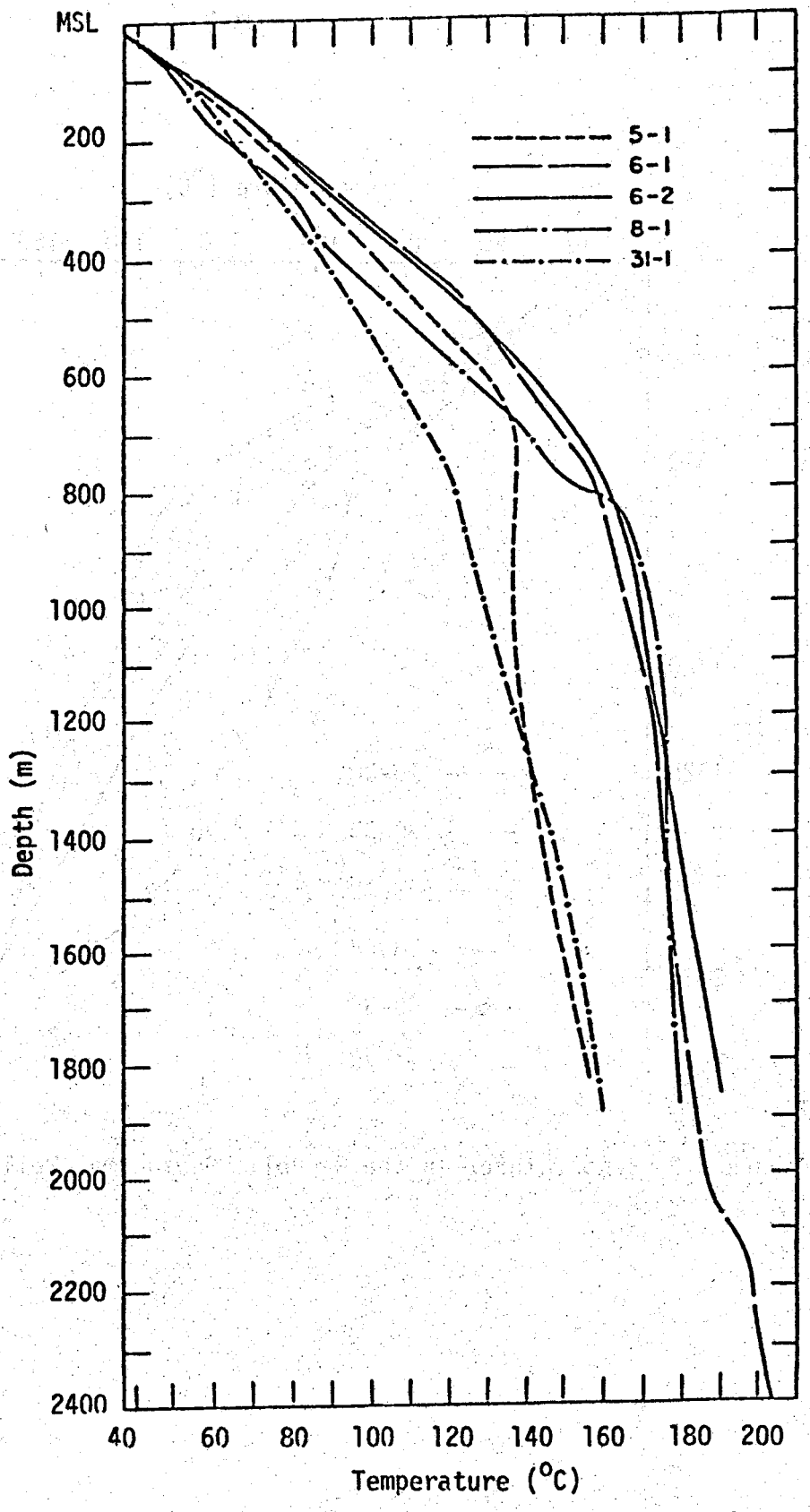

Figure 3.7 Temperatures in U.S.B.R. Wells East Mesa Geothermal Anomaly (Adapted from the report of Bailey 1977).

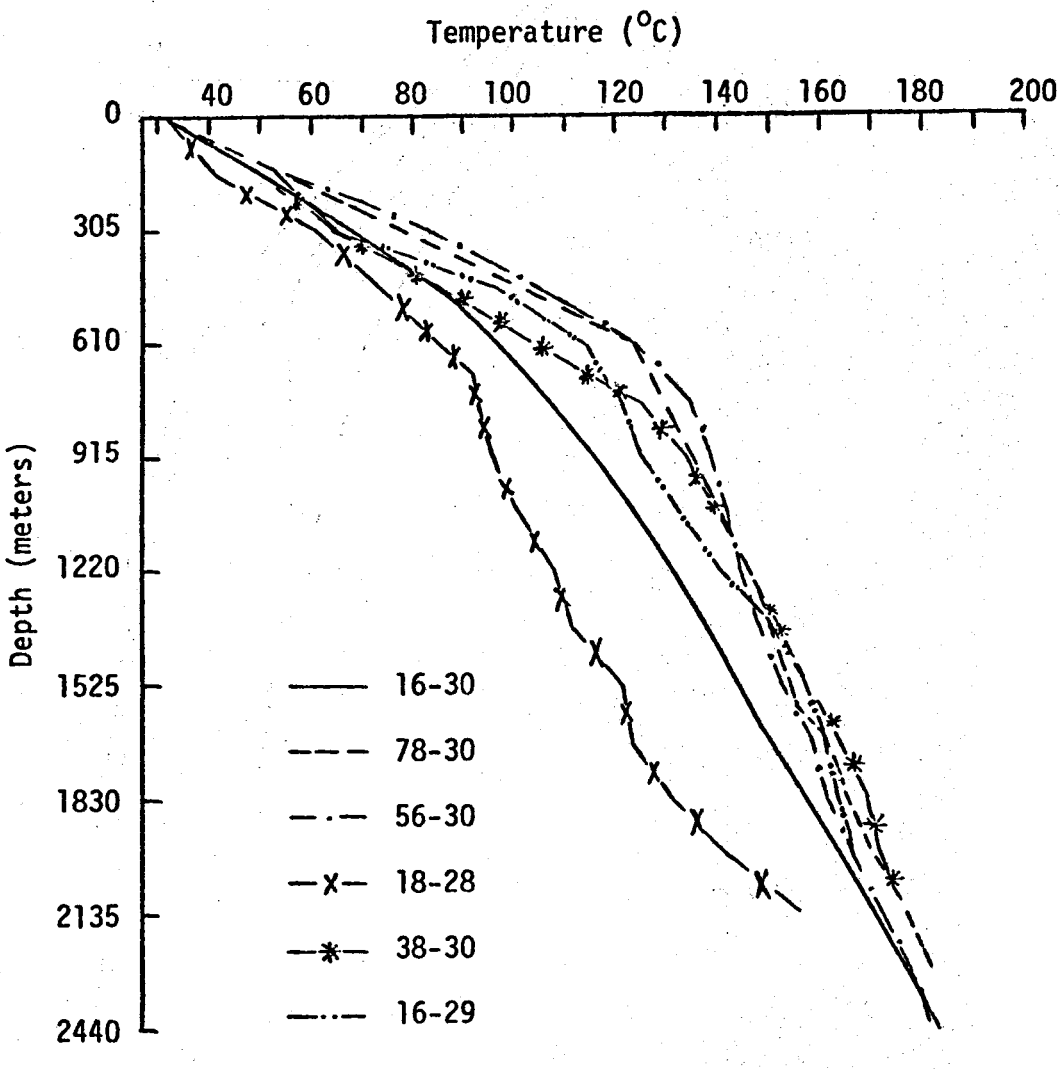

Figure 3.8 Temperatures in the Republic Geothermal Wells

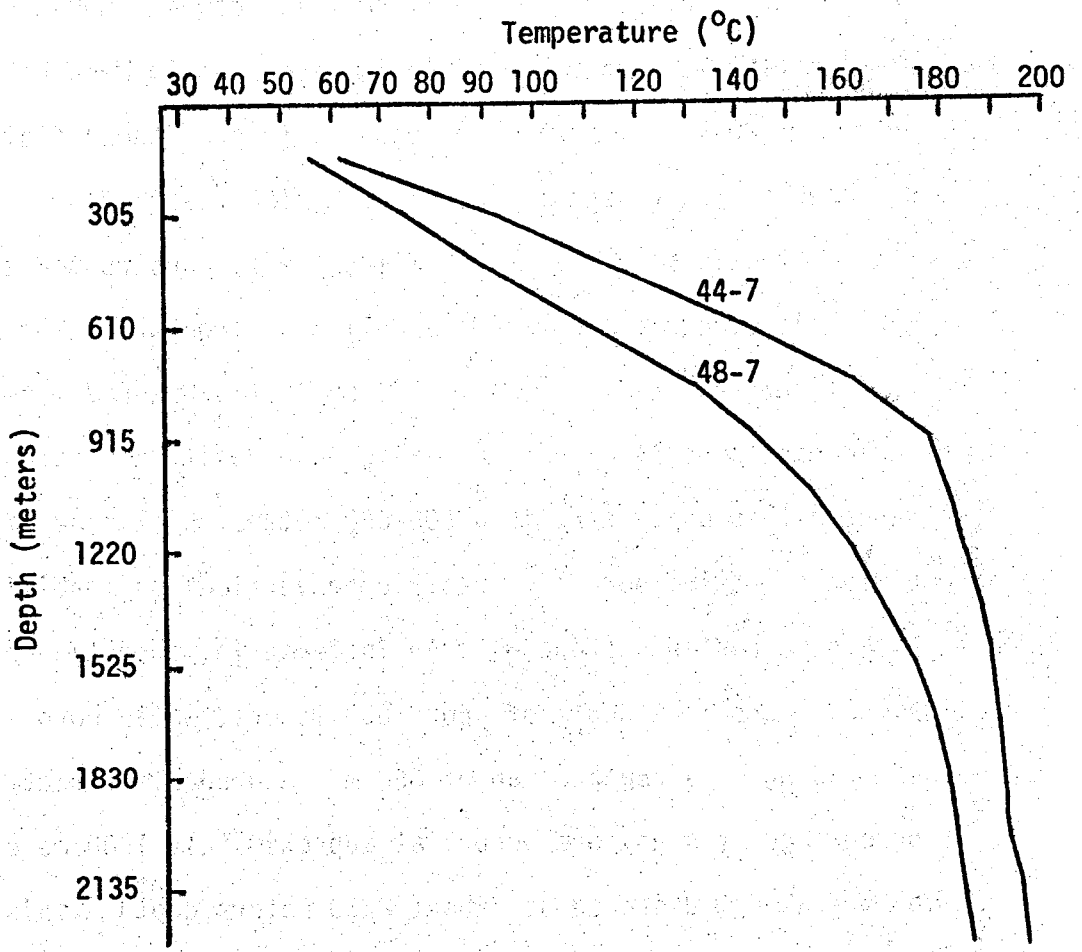

Figure 3.9 Temperatures in the Wells Drilled by Magma Power Company

their relative position is shown in Figure 3.2. Temperatures in these wells are very close to those in Mesa Well 6-1, 6-2, and 8-1. It can be noted that Mesa Well 44-7 is very hot and is hotter than Mesa Well 6-1, 6-2 and 8-1 below 750 meters. Temperature profile of this well is very flat between 1500-1850 meters. The flat temperature profile of Mesa Well 48-7 is between 1800-2100 meters. Similar flat temperature profile is also seen in Mesa Well 8-1 between 1200-1800 meters. One could interpret these flat portions as zones that are strongly affected by fault zone flow.

Synthetic Electric Log: Bailey (1977) constructed the synthetic electric log for Mesa Well 6-1, from which the following conclusions can be derived. The upper few hundred meters of sediments (zone A) appear to have good porosity and sand contents. Beneath this upper zone is a 500-600 meters thick zone of sediments of low effective porosity, restricted vertical permeability and high clay contents (zone B). An increase in percentage of sandstone occurs at a depth of about 650 meters, while porosity starts increasing at a depth of about 850 m. A gradual decrease in percentage of sandstone occurs at approximately 1900 meters and a more abrupt decrease at about 2250 meters depth. This lower clay rich sedimentary sequence is referred to as zone D, while the sand dominated sediments above (which constitute geothermal reservoir) are called zone C.

3.3 Conceptual Model

Figure 3.10 shows the conceptual model of the East Mesa geothermal system. Basement complex of granite-metamorphic rocks is at a depth of about 4 km from the surface (Combs Hadley, 1977). The basement complex is subjected to failure under adequate stress. Fractures, once formed, would tend to be preserved in this high strength rock. Nearly vertical tension fractures probably were the first fractures to form during evolution of the Salton trough. These fractures would increase the vertical permeability much more than the horizontal permeability.

Overlying the basement is zone D, dominated by shale. It is characterized by (1) steepening of the temperature profile in Mesa Well 6-1 below about 2100 meters depth, (2) an increase in percentage of shale and corresponding decrease in sands below 2200 meters depth, and (3) marked change in salinities below 2200 meters depth.

This layer extends from the basement complex to about 1900-2200 meters from the surface. Here the sediments are indurated by overburden and heat, they probably fracture, given any movement on the basement faults. The vertical permeability of these sediments is expected to be good near the fracture zones, but quite low away from the fracture zones. Horizontal permeability in this layer is also thought to be only moderate because of the presence of clay and dirty sands.

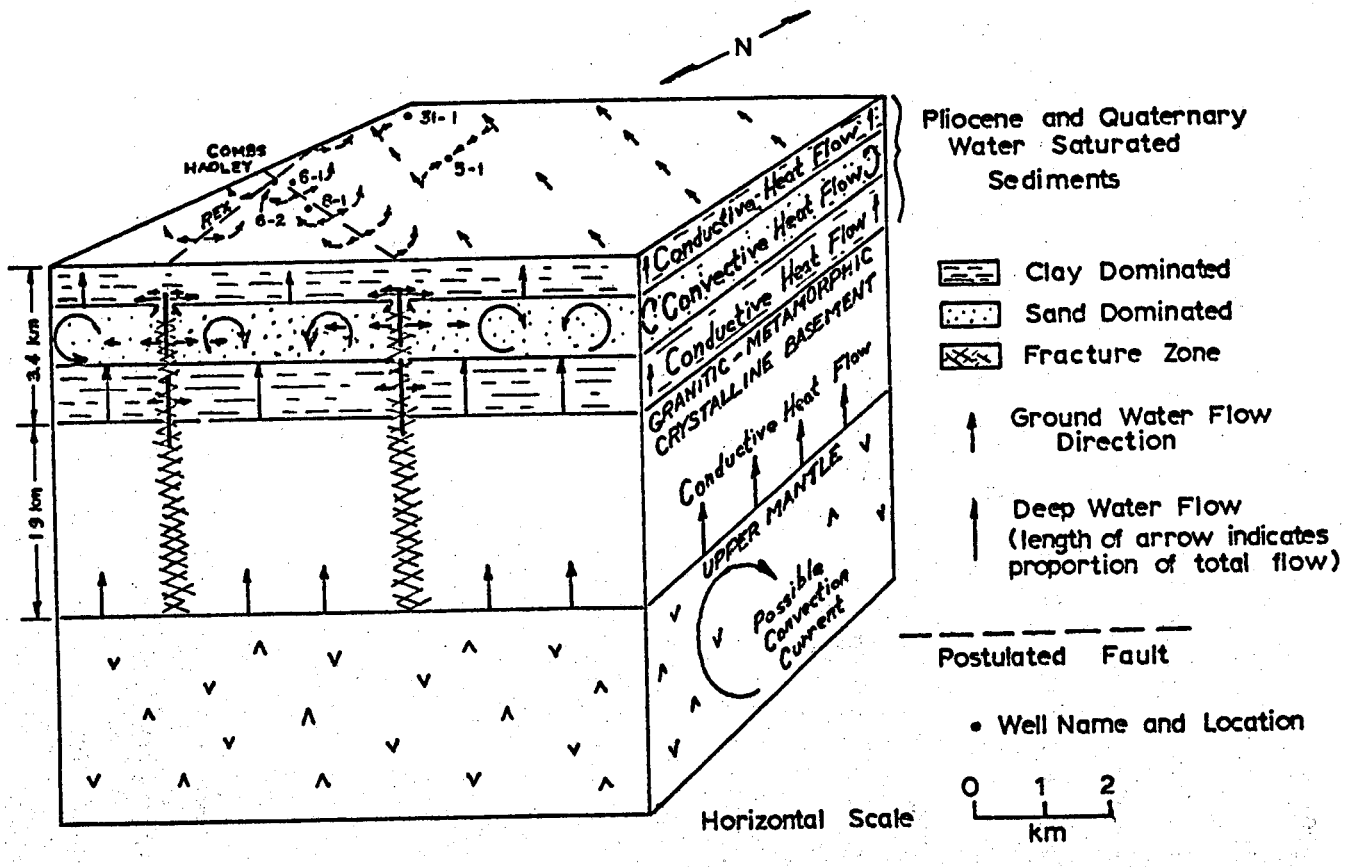

Figure 3.10 Conceptual Model of the East Mesa Geothermal Anomaly. (Adapted from the report of Bailey, 1977)

Sands dominate the sedimentary zone (zone C) from about 800-1900 meters depth. Horizontal permeability in this zone is probably better than in the underlying material because of greater sand contents and continuity and less compaction. Vertical permeability should be good near the fracture zones, and in general should be better than in the underlying beds because of the greater amount of the sand. Except near the fracture zones, relatively fresh water in this sand dominated zone may be prevented from extensive mixing with the more saline water in the sediments below by the restricted vertical permeability of the sediments in the lower zone.

The next 600 meters or so of the sediments (zone B) is dominated by clay. Fractures may form temporarily in these sediments with sudden differential motion, but under light loading fractures in these beds would tend to close by slow flowage unless there are repeated fast movements. Vertical permeability is probably very low in these young sediments, but the numerous shallow wells in them indicate that their horizontal permeability is good.

The upper 200 meters of the valley fill (zone A) appears to have more sand and better porosity than the underlying zone. Vertical permeability is probably much higher than in the underlying zone, but zone A and zone B probably behave in similar ways when subjected to stress.

In summary what vertical permeability exists in the lower four zones is due almost entirely to fractures, whereas except in

the vicinity of a fracture zone, horizontal flow in these zones is largely dependent upon intergranular permeability. The major source of fluid for southern Imperial Valley brines is the underflow from the Colorado River. This water percolates gradually into sediments and/or fractured basement rock over an area considerably larger than the anomaly itself. Heated at depth by an as yet undefined source, the liquid can rise in the high permeability fractured fault zone, convecting energy toward the surface. When a horizontal aquifer is intersected (relatively large horizontal permeability), reservoir charging will occur.

3.4. Mathematical Model

The two dimensional mathematical model of East Mesa geothermal system is shown in Figure 3.11. The fault is hypothesized to be a vertically oriented region of heavily fractured material of finite width (2ye'). The vertical extent of the fault and the second horizontal dimension of the fault are large compared to the width. The fault extends downward through the clay rich region (cap) of thickness ℓ', through the interbedded sediments of the reservoir for a distance L' and finally into the basement rock. It is postulated that the fault is charged at depth by the liquid which has been heated in an extensive basement fractured system. The rate of charge cannot be speculated a priori without a global analysis of the convection process. Liquid rises in the reservoir section of the fault. The presence of clays in the cap suppresses vertical transport there. Water pushed out of the fault by the

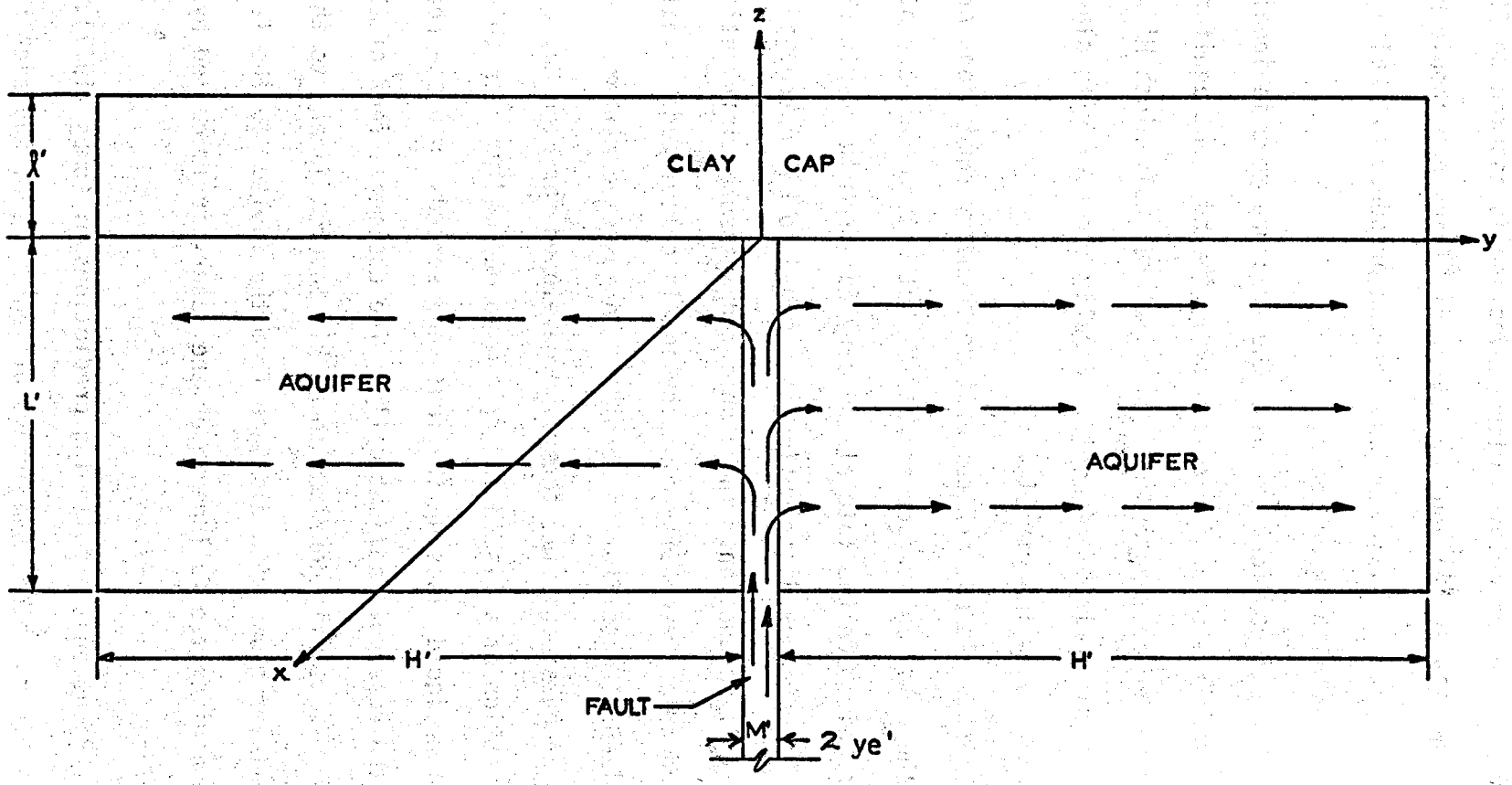

Figure 3.11 Mathematical Model of the East Mesa Geothermal System.

over pressure associated with convection is assumed to flow horizontally in the aquifer. Vertical transport should be less important in the large because of the presence of shaley layers associated with interbedding.

For mathematical purposes the fracture zone is idealized as a vertical slab of porous medium. The adjacent aquifer is represented as a porous medium of lateral half width H' with horizontal permeability only. Finally the overlying clay cap is assumed to be impermeable.

Spatially uniform temperature boundary conditions are imposed on the cold cap surface and at the hot bottom boundary of the reservoir. On the lateral boundary far from the fault (H'>>L'>>ye') the temperature distribution is assumed to be controlled by vertical conduction. The associated pressure distribution can be found once the density distribution is calculated. Finally horizontal mass flux is permitted to conserve matter.

A quasi-analytic theory is developed for high Rayleigh number convection of a liquid in a rigid porous medium. In this approximation liquid rises up the fault and spreads into the near region of the reservoir adiabatically. The cooling effect of the cap in the reservoir is confined to a thin layer adjacent to the interface. The layer grows with distance from the fault. In the far field of the aquifer the full depth of the reservoir is cooled by the surface.

Based on the following predictions of Combs (1977), it is possible to obtain the orders of magnitude of Rayleigh number and

fault width for the East Mesa geothermal system.

Depth to the basement interface = 4.15 km

Clay cap thickness = .8 km

which give

Reservoir thickness = 3.35 km

ℓ = ratio of cap thickness to the reservoir depth = $\frac{\ell'}{L_T}$ = .238

Based on Na-K-Ca geothermometry, formation temperature in the East Mesa area are 200°C ±30°C (Bailey, 1977). Assuming a mean formation temperature of 200°C, we have

$\Delta T' = 175^{\circ}C$ and $\tau = .587$

For an assumed permeability of 10^{-9} cm^2, one obtains R = 338.

Local Rayleigh number may be 10-20 times higher if the local values of the physical properties are used. It is noted that Rayleigh number is also sensitive to changes in permeability.

Assuming an average temperature of about 200°C in the convection-active section of the fault, one finds that 1.011×10^7 cal/sec-km^2 is convected upward. This is about 3 orders of magnitude larger than the purely conductive flux. Fluid experiences a 10% drop in the convection zone temperature while moving away from Mesa Well 6-2 to 5-1 (Figure 3.7). Thus, considering a 10% energy loss to the surroundings, one can then calculate the heat transferred to the surface. This quantity, when measured

from the contours of Figure 3.2, is 4.88×10^6 cal/sec crossing an area of 110 km^2. Upon equating these two quantities, one can then obtain the horizontal fault zone area of 4.827 km^2. Since the thermal activity of the Mesa extends along the primary fault for about 21 km, a fault (fracture zone) width $2\,ye' \approx 230$ m is suggested. One should recognize that this is an order of magnitude estimate. Given the variable nature of input a range $50\text{ m} \leq ye' \leq 150\text{ m}$ might be appropriate. If K were far smaller than 10^9 cm^2 the fault zone area estimate would be far larger, and thus not representative of the relatively localized anomalous properties at the Mesa field.

Fault Zone Equations: The following assumptions are incorporated into the theory:

(i) Fault medium is isotropic, i.e.,

$$K_i' = K'(x',y',z') \tag{3.1}$$

(ii) Fault medium in x'-y' plane is homogeneous

$$K_i' = K_i'(z') \tag{3.2}$$

(iii)

$$\frac{K_i'(z')}{\nu'} = \text{constant} \tag{3.3}$$

This is a qualitative representation of the decrease of ν' with depth (associated with increasing temperature) and the corresponding decrease in permeability $K'(z')$ due to compaction. In actual situations precise compensation is not achieved.

(iv) α_e', C_p', λ_m' are constant.

The basic describing equations can be written in the non-dimensional form

$$V_y + W_z = 0 \tag{3.4}$$

$$V = - P_y \tag{3.5}$$

$$W = - P_z + \frac{T - 1}{\tau} \tag{3.6}$$

$$R(VT_y + WT_z) = T_{yy} + T_{zz} \tag{3.7}$$

Given that $ye << 1$, the appropriate fault variables are

$$\bar{y} = \frac{y}{ye} \quad \text{and} \quad \bar{V} = \frac{V}{ye} \tag{3.8}$$

Equations (3.4) to (3.7) become

$$\bar{V}_{\bar{y}} + W_z = 0 \tag{3.9}$$

$$ye^2 \bar{V} = - P_{\bar{y}} \tag{3.10}$$

$$W = - P_z + \frac{T - 1}{\tau} \tag{3.11}$$

$$\gamma^2(\bar{V}T_{\bar{y}} + WT_z) = T_{\bar{y}\bar{y}} + ye^2 T_{zz} \tag{3.12}$$

where

$$\gamma = R^{1/2} ye = O(1) \tag{3.13}$$

Aquifer Equations: Referring to Figure 3.10, it can be seen that the area normal to the flow in the aquifer is much larger than in the fault. Thus the flow velocities in the aquifer are

expected to be much lower than those in the fault for a prescribed mass flow rate. In dimensional terms, the flow area in the aquifer is (1/ye) times that of the fault; the corresponding flow velocity in the aquifer should be ye times the flow velocity in the fault. Also the continuity of the temperature and pressure is to be maintained at the interface of the fault and the aquifer. The following characteristic variables are used in the aquifer:

$$\text{Characteristic convection velocity} = q_r^{f'} = ye\ q_o^{f'} \tag{3.14}$$

$$q_o^{f'} = g' k'_o\ {}^{o}\alpha_e^{f'} \Delta T / \nu_o^{f'}$$

$$\text{Characteristic viscous stress tensor} = \sigma_r^{f'} = \frac{\mu_o^{f'} q_r^{f'}}{L'} \tag{3.15}$$

$$\text{Characteristic convection pressure} = p_o^{f'} = \frac{q_o^{f'} \mu_o^{f'} L'}{k'_o} \tag{3.16}$$

Appropriate scale variables in the aquifer are L' in z-direction and H' in $\hat{y}$-direction.

The basic conservation equations in the aquifer can be non-dimensionalized with the help of the following non-dimensional variables:

$$\hat{y} = \frac{y'}{H'},\ z = \frac{z'}{L'},\ v = \frac{v^{f'}}{q_r^{f'}},\ w = \frac{w^{f'}}{ye\ q_r^{f'}},\ \sigma_{ij} = \frac{\sigma_{ij}^{f'}}{\sigma_r^{f'}} \tag{3.17}$$

The temperatures in the aquifer are denoted by θ rather than T. During the non-dimensionalization of the momentum equation ($\hat{y}$-direction), it is seen that the pressure terms is of $O(\frac{L'}{H'ye})$. Since the pressure term should balance the Darcy term, which is O(1), the following

relation is obtained:

$$\frac{L'}{H'ye} = O(1)$$

or

$$\frac{H'}{L'} = \frac{d}{ye} \tag{3.18}$$

where d is an $\theta(1)$ number, which determines the far-field end of the aquifer where liquid is fully cooled. Although horizontal motion of water exists, the horizontal temperature gradient is vanishingly small. Hence the major heat transfer at the far end is due to vertical conduction.

Again, considering the orders of magnitudes if different terms in the momentum and energy equations for a typical geothermal reservoir, it can be concluded that the inertia terms and the stress tensor terms represent insignificant effect in the momentum equation. Also, the contribution of the stress tensor term in the energy equation is very small. The following field equations are obtained for a system of constant porosity and small pressure work.

$$v_{\hat{y}} + dw_z = 0 \tag{3.19}$$

$$v = -\frac{k^{\hat{y}}(\hat{x},\hat{y},z)}{\nu d} p_{\hat{y}} \tag{3.20}$$

$$ye^2 w = \frac{k^z(\hat{x},\hat{y},z)}{\nu}\left[-p_z + \alpha_e \frac{\theta - 1}{\tau}\right] \tag{3.21}$$

$$\gamma^2 d^2 cp \left[\frac{v}{d}\theta_{\hat{y}} + w\theta_z\right] = ye^2(\lambda_m\theta_y),y + d^2(\lambda_m\theta_z),z \qquad (3.22)$$

In addition to (3.2) and (3.3) the following assumptions are made in the derivation of the aquifer equations.

(i) vertical permeability $K^{z'}$ is zero.

(ii) C_p' and λ_m' are constant.

It follows that equations (3.19)-(3.22) reduce to:

$$v(z) = -\frac{1}{d} P_{\hat{y}} \qquad (3.23)$$

$$\gamma^2 d\, v(z)\theta_{\hat{y}} = ye^2\theta_{\hat{y}\hat{y}} + d^2\theta_{zz} \qquad (3.24)$$

where γ is given by (3.13). From (3.23) it is clear that the pressure gradient is a pure function of z. It is possible to calculate the pressure gradient in the aquifer if the pressure at the fault boundary and at the far-field boundary of the aquifer is known. Pressure in the fault can be obtained by solving the fault field equations. The hot hydrostatic pressure is specified at $\hat{y} = 1$. Once pressure gradients in the aquifer are known, equation (3.23) can be solved to obtain the aquifer velocity.

3.5 Solution of the Problem

Without Clay Cap

In this case ℓ' of figure 3.11 becomes zero and the impermeable top of the aquifer is at the ambient temperature T_o'. The system of equations (3.9)-(3.12) for the fault are subjected to the following boundary conditions.

$$W(\bar{y},-1) = M \tag{3.25}$$

$$W(\bar{y},0) = 0 \tag{3.26}$$

$$\bar{V}(\pm 1,z) = \pm v(z) \tag{3.27}$$

$$T(\bar{y},0) = 1 \tag{3.28}$$

$$T(\bar{y},-1) = 1 + \tau \tag{3.29}$$

$$T_{\bar{y}}(0,z) = 0 \tag{3.30}$$

where $M = \frac{M'}{Mo'}$ and $Mo' = 2\rho_o^{f'} q_o^{f'} ye'$. (3.31)

To solve the describing mathematical system, let

$$\begin{aligned} T &= To + O(ye^2) \\ P &= Po + O(ye^2) \\ \bar{V} &= \bar{V}o + O(ye^2) \\ W &= Wo + O(ye^2) \end{aligned} \tag{3.32}$$

The describing system for O(1) terms is

$$\bar{V}_{o\bar{y}} + W_{oz} = 0 \tag{3.33}$$

$$P_{o\bar{y}} = 0 \tag{3.34}$$

$$W_o = - P_{oz} + \frac{T_o - 1}{\tau} \tag{3.35}$$

$$\gamma^2(\bar{V}_o T_{o\bar{y}} + W_o T_{oz}) = T_{o\bar{y}\bar{y}} \tag{3.36}$$

$$W_o\ (\bar{y},-1) = M \tag{3.37}$$

$$\bar{V}_o\ (\pm 1,z) = \pm v\ (z) \tag{3.38}$$

$$T_o\ (\bar{y},-1) = 1 + \tau \tag{3.39}$$

$$T_{o\bar{y}}\ (0,z) = 0 \tag{3.40}$$

In a high Rayleigh number flow, where convection heat transfer is much greater than conduction effect, a fluid entering the fault will not cool until it is adjacent to a surface where it must lose heat by conduction. It follows that

$$T = 1 + \tau\ ,\quad z < 0 \tag{3.41}$$

The solution can be written formally as

$$T_o = 1 + \tau \tag{3.42}$$

$$\bar{V}_o = v\ (z)\ \bar{y} \tag{3.43}$$

$$W_o = M - \int_{-1}^{z} v(\alpha)d\alpha \tag{3.44}$$

$$P_o = P_o(-1) + 1 + z - M(1+z) + \int_{-1}^{z} d\sigma \int_{-1}^{\sigma} v(\alpha)d\alpha \tag{3.45}$$

where v(z) remains to be found.

The major heat transfer at the far end of the aquifer is by vertical conduction. As there is no vertical motion, the pressure distribution with depth is simply related to the integral of the vertical density distribution. The aquifer velocity v(z) results from the overall pressure differential between the fault and the far field boundary. For vertical conduction heat transfer and zero horizontal temperature gradient, the far field temperature boundary condition is as follows:

$$\theta'(H',z') = T_o' - \Delta\theta' \frac{z'}{L'} \tag{3.46}$$

or in nondimensional form

$$\theta(1,z) = 1 - \tau z \tag{3.47}$$

The far field pressure is written as

$$p_{HH}^{f'} = - \int_o^{z'} \rho^{f'}(z') g' dz' + p_{atm}'$$

or

$$p_{HH}^{f'} = L' g' \rho_o^{f'} \left[- z - \alpha_e^{f'} T_o' \tau \frac{z^2}{2} \right] + p_{atm}' \tag{3.48}$$

where $\rho^{f'}(z') = \rho_o^{f'}[1 - \alpha_e^{f'}(\theta' - T_o')]$ (3.49)

Cold Hydrostatic pressure becomes

$$p_H^{f'} = - \rho_o^{f'} g' z' + p_{atm}' \tag{3.50}$$

Then because the reference pressure is

$$p_o^{f'} = \rho_o^{f'} g' L' {}^o\alpha_e^{f'} \Delta\theta' \tag{3.51}$$

It follows that

$$p(1,z) = -\frac{z^2}{2} \tag{3.52}$$

From (3.23), aquifer pressure gradient is a pure function of z. It follows that the aquifer pressure gradient can be written as,

$$\frac{\partial p^{f'}}{\partial y'} = \frac{p^{f'}(H',z') - p^{f'}(ye',z')}{H'} \tag{3.53}$$

In nondimensional terms:

$$\frac{\partial p}{\partial \hat{y}} = p(1,z) - p(\frac{ye^2}{d}, z) \tag{3.54}$$

If (3.45) and (3.52) are used in (3.54) one finds

$$\frac{\partial p}{\partial \hat{y}} = -\frac{z^2}{2} - P_o(-1) - 1 - z + M(1+z) - \int_{-1}^{z} d\sigma \int_{-1}^{\sigma} v(\alpha)d\alpha \tag{3.55}$$

Now from (3.23), aquifer velocity becomes

$$v(z) = \frac{z^2}{2d} + \frac{P_o(-1)}{d} + \frac{1}{d} + \frac{z}{d} - \frac{M}{d}(1+z) + \frac{1}{d}\int_{-1}^{z} d\sigma \int_{-1}^{\sigma} v(\alpha)d\alpha \tag{3.56}$$

From (3.56)

$$v(-1) = \frac{1}{2d} + \frac{P_o(-1)}{d} \tag{3.57}$$

Differentiation of (3.56) gives

$$\frac{dv(z)}{dz} = \frac{z}{d} + \frac{1}{d} - \frac{M}{d} + \frac{1}{d}\int_{-1}^{z} v(\alpha)d\alpha \tag{3.58}$$

From (3.58)

$$\frac{dv(-1)}{dz} = -\frac{M}{d} \tag{3.59}$$

Differentiation of (3.58) leads to the following second order ordinary differential equation.

$$\frac{d^2v(z)}{dz} = \frac{1}{d} + \frac{v(z)}{d} \tag{3.60}$$

Although this analysis implies that the solution to (3.60) is valid everywhere in the aquifer except in the thin thermal boundary layer near the top where temperature is not identically $1 + \tau$, it will be shown that the solution is valid to the lowest order in the boundary layer as well.

Therefore, the condition for the conservation of mass in the aquifer up to the O(1) can be written as

$$M = \int_{-1}^{0} v(z)dz \tag{3.61}$$

Solution of (3.60) with the conditions (3.57), (3.59) and (3.61) is given as

$$v(z) = a_1 \cosh \frac{z}{\sqrt{d}} + b_1 \sinh \frac{z}{\sqrt{d}} - 1 \tag{3.62}$$

where

$$a_1 = \frac{M + \cosh \frac{1}{\sqrt{d}}}{\sqrt{d} \sinh \frac{1}{\sqrt{d}}}, \quad b_1 = \frac{1}{\sqrt{d}} \tag{3.63}$$

$$P_o(-1) = \sqrt{d} \left(\frac{1 + M \cosh \frac{1}{\sqrt{d}}}{\sinh \frac{1}{\sqrt{d}}} \right) - d - \frac{1}{2} \tag{3.64}$$

Thus the over pressure in the aquifer is

$$p(\hat{y},z) = d\, v(z)(1-\hat{y}) - \frac{z^2}{2} + O(y_e^2) \tag{3.65}$$

It follows that the fault zone solutions obtained from (3.62), (3.42)-(3.45) and (3.32) are

$$T = 1 + \tau \tag{3.66}$$

$$\bar{V} = \bar{y}v(z) + 0(ye^2) \tag{3.67}$$

$$W = -a_1\sqrt{d}\sinh\frac{z}{\sqrt{d}} - \cosh\frac{z}{\sqrt{d}} + z + 1 + 0(ye^2) \tag{3.68}$$

$$P = d\,v(z) - \frac{z^2}{2} + 0(ye^2) \tag{3.69}$$

Thermal Boundary Layer Near the Top of the Fault

The nondimensional temperature at the top of the fault is 1. There should be a boundary layer to accommodate the temperature drop from $1+\tau$ to 1. Appropriate non-dimensional variables are:

$$\bar{z} = \frac{z}{ye} \quad \text{and} \quad \bar{W} = \frac{W}{ye} \tag{3.70}$$

Substitution of (3.70) into (3.67)-(3.69), (3.62) and (3.65) leads to the following matching conditions for the boundary layer solutions.

$$\bar{V} = \bar{y}(a_1-1) + ye\,\frac{\bar{y}\bar{z}}{d} + 0(ye^2) \tag{3.71}$$

$$\bar{W} = -\bar{z}(a_1-1) - ye\,\frac{\bar{z}^2}{2d} + 0(ye^2) \tag{3.72}$$

$$P = d(a_1-1) + ye\bar{z} + 0(ye^2) \tag{3.73}$$

$$v(\bar{z}) = (a_1-1) + ye\,\frac{\bar{z}}{d} + 0(ye^2) \tag{3.74}$$

$$p(\hat{y},\bar{z}) = d(1-\hat{y})(a_1-1) + ye(1-\hat{y})\bar{z} + 0(ye^2) \tag{3.75}$$

Substitution of (3.70) into (3.9)-(3.12) leads to the following boundary layer equations:

$$\bar{V}_{\bar{y}} + \bar{W}_{\bar{z}} = 0 \tag{3.76}$$

$$ye^2\bar{V} = -P_{\bar{y}} \tag{3.77}$$

$$ye^2\bar{W} = -P_{\bar{z}} + ye\frac{T-1}{\tau} \tag{3.78}$$

$$\gamma^2(\bar{V}T_{\bar{y}} + \bar{W}T_{\bar{z}}) = T_{\bar{y}\bar{y}} + T_{\bar{z}\bar{z}} \tag{3.79}$$

Let the solutions of (3.76)-(3.79) and (3.23) be expressed in the following asymptotic form for small ye.

$$\begin{bmatrix} \bar{V} \\ \bar{W} \\ P \\ T \\ v \\ p \end{bmatrix} = \sum_{n=0} ye^n \begin{bmatrix} V_n \\ W_n \\ P_n \\ T_n \\ v_n \\ p_n \end{bmatrix} \tag{3.80}$$

The lowest order terms describing the fault system have the form:

$$V_{o\bar{y}} + W_{o\bar{z}} = 0 \tag{3.81}$$

$$P_{o\bar{y}} = 0 \tag{3.82}$$

$$P_{o\bar{z}} = 0 \tag{3.83}$$

$$\gamma^2(V_o T_{o\bar{y}} + W_o T_{o\bar{z}}) = T_{o\bar{y}\bar{y}} + T_{o\bar{z}\bar{z}} \tag{3.84}$$

It follows immediately that P_o is a constant. From (3.73), we find that

$$P_o = d(a_1 - 1) \tag{3.85}$$

The O(ye) correction is described by

$$V_{1\bar{y}} + W_{1\bar{z}} = 0 \tag{3.86}$$

$$P_{1\bar{y}} = 0 \tag{3.87}$$

$$- P_{1\bar{z}} + \frac{T_o - 1}{\tau} = 0 \tag{3.88}$$

$$\gamma^2(V_o T_{1\bar{y}} + V_1 T_{o\bar{y}} + W_o T_{1\bar{z}} + W_1 T_{o\bar{z}}) = T_{1\bar{y}\bar{y}} + T_{1\bar{z}\bar{z}} \tag{3.89}$$

While that for $O(ye^2)$ is described by

$$V_{2\bar{y}} + W_{2\bar{z}} = 0 \tag{3.90}$$

$$V_o = - P_{2\bar{y}} \tag{3.91}$$

$$W_o = - P_{2\bar{z}} + \frac{T_1}{\tau} \tag{3.92}$$

$$\gamma^2(V_o T_{2\bar{y}} + V_2 T_{o\bar{y}} + W_o T_{2\bar{z}} + W_2 T_{o\bar{z}} + V_1 T_{1\bar{y}} + W_1 T_{1\bar{z}}) = T_{2\bar{y}\bar{y}} + T_{2\bar{z}\bar{z}} \tag{3.93}$$

Equations (3.87) and (3.88) imply that

$$P_1 = P_1(z) \ , \quad T_o = T_o(z) \tag{3.94}$$

Therefore (3.84) reduces to:

$$\gamma^2 W_o \frac{dT_o}{d\bar{z}} = \frac{d^2 T_o}{d\bar{z}^2} \tag{3.95}$$

which implies that

$$W_o = W_o(\bar{z}) \tag{3.96}$$

The aquifer pressure gradient (to the lowest order) in the thermal boundary layer as obtained from (3.52) and (3.85) is given as follows:

$$\frac{\partial p_o}{\partial \hat{y}} = - d(a_1 - 1) \tag{3.97}$$

From (3.23) and (3.97), one obtains

$$v_o(\bar{z}) = a_1 - 1 \tag{3.98}$$

$$p_o(\hat{y},\bar{z}) = d(a_1-1)(1-\hat{y}) \tag{3.99}$$

The above expressions of the aquifer velocity and the pressure match with the lowest order term of (3.74) and (3.75). Therefore the composite solution for the aquifer velocity which is valid in the whole depth of the aquifer, is given by (3.62) to this order.

The boundary conditions on (3.81) and (3.95) are:

$$V_o(\pm 1,\bar{z}) = \pm v_o(\bar{z}) = \pm(a_1-1) \tag{3.100}$$

$$W_o(\bar{y}, z \to -\infty) = - \bar{z}(a_1-1) \tag{3.101}$$

$$T_0(\bar{y},0) = 1 \tag{3.102}$$

$$T_0(\bar{y},\bar{z} \to -\infty) = 1 + \tau \tag{3.103}$$

Then we find that

$$V_0(\bar{y},\bar{z}) = (a_1-1)\bar{y} \tag{3.104}$$

$$W_0(\bar{y},\bar{z}) = -(a_1-1)\bar{z} \tag{3.105}$$

$$T_0(\bar{z}) = 1 - \tau \operatorname{erf}(A\bar{z}) \tag{3.106}$$

where $A = \sqrt{\frac{\gamma^2}{2}(a_1-1)}$

Since $\gamma\bar{z} = R^{1/2}z$, then a plot T_0 vs. z is independent of ye.

Substitution of (3.104) and (3.105) into (3.91) and (3.92) results into the following equations,

$$(a_1-1)\bar{y} = - P_{2\bar{y}} \tag{3.107}$$

$$-(a_1-1)\bar{z} = - P_{2\bar{z}} + \frac{T_1}{\tau} \tag{3.108}$$

which imply that

$$T_1 = T_1(\bar{z}) \tag{3.109}$$

If (3.94) and (3.109) are used in (3.89), then we obtain

$$\gamma^2\left(W_0 \frac{dT_1}{d\bar{z}} + W_1 \frac{dT_0}{d\bar{z}}\right) = \frac{d^2T_1}{d\bar{z}^2} \tag{3.110}$$

It can be seen readily from (3.110) that

$$W_1 = W_1(\bar{z}) \tag{3.111}$$

Use of (3.94) and (3.106) into (3.88) results in:

$$\frac{dP_1}{d\bar{z}} = - \text{erf}(A\bar{z}) \tag{3.112}$$

which can be solved for the following matching boundary condition (3.73)

$$P_1(\bar{z} \to -\infty) = \bar{z} \tag{3.113}$$

Solution of the above system is as follows:

$$P_1(\bar{z}) = - \bar{z}\, \text{erf}(A\bar{z}) - \frac{1}{\sqrt{\pi}A} e^{-A^2\bar{z}^2} \tag{3.114}$$

The first order correction to the boundary layer pressure gradient in the aquifer as obtained from (3.114) and (3.52) is as follows:

$$\frac{\partial p_1}{\partial \hat{y}} = \bar{z}\, \text{erf}(A\bar{z}) + \frac{1}{A\sqrt{\pi}} e^{-A^2\bar{z}^2} \tag{3.115}$$

From (3.23) and (3.115), following expressions for the aquifer velocity and the over pressure are obtained.

$$v_1(\bar{z}) = - \frac{\bar{z}}{d} \text{erf}(A\bar{z}) - \frac{1}{d\sqrt{\pi}A} e^{-A^2\bar{z}^2} \tag{3.116}$$

$$p_1(\hat{y},\bar{z}) = -(1-\hat{y})\left[\bar{z}\, \text{erf}(A\bar{z}) + \frac{1}{A\sqrt{\pi}} e^{-A^2\bar{z}^2}\right] \tag{3.117}$$

It can be noted again that the expressions (3.116) and (3.117) match with (3.74) and (3.75) respectively to this order.

Now (3.86) and (3.110) can be solved for the following boundary conditions.

$$V_1(\pm 1,\bar{z}) = \pm v_1(\bar{z}) \tag{3.118}$$

$$W_1(\bar{z} \to -\infty) = -\frac{\bar{z}^2}{2d} \tag{3.119}$$

$$T_1(\bar{z} = 0) = 0 \tag{3.120}$$

$$T_1(\bar{z} \to -\infty) = 0 \tag{3.121}$$

The solutions are

$$V_1(\bar{y},\bar{z}) = \bar{y}v_1(\bar{z}) \tag{3.122}$$

$$W_1(\bar{z}) = \frac{1}{4A^2d}\{1 + \mathrm{erf}(A\bar{z})\} + \frac{\bar{z}^2}{2d}\mathrm{erf}(A\bar{z}) + \frac{\bar{z}}{2dA\sqrt{\pi}}e^{-A^2\bar{z}^2} \tag{3.123}$$

$$T_1(\bar{z}) = \frac{\gamma^2\tau}{6\sqrt{\pi}dA^3}\left[1 + \mathrm{erf}(A\bar{z}) - e^{-A^2\bar{z}^2}(1+A^2\bar{z}^2)\right] \tag{3.124}$$

The above results can be used in (3.80) to give

$$\bar{V} = (a_1-1)\bar{y} + ye\bar{y}v_1(\bar{z}) + O(ye^2) \tag{3.125}$$

$$\bar{W} = -(a_1-1)\bar{z} + yeW_1(\bar{z}) + O(ye^2) \tag{3.126}$$

$$P = d(a_1-1) + yeP_1(\bar{z}) + O(ye^2) \tag{3.127}$$

$$T = 1 - \tau\,\mathrm{erf}(A\bar{z}) + yeT_1(\bar{z}) + O(ye^2) \tag{3.128}$$

$$v(\bar{z}) = a_1-1 + yev_1(\bar{z}) + O(ye^2) \tag{3.129}$$

$$p(\hat{y},\bar{z}) = d(a_1-1)(1-\hat{y}) + yep_1(\hat{y},\bar{z}) + O(ye^2) \tag{3.130}$$

Equation (3.18) shows that the far field boundary is determined by d which is a function of the parameters M, R, τ and ye (3.24). Representative values of these parameters selected for comparison are as follows:

$$R = 500$$

$$\tau = 1$$

$$ye = .025$$

For a given set of parameters, d is determined by integrating the parabolic equation (3.24) in the far field region until the numerically determined vertical temperature gradient θ_z is within .8% of the specified value at the far field boundary. Table I shows the values of d for different sets of the parameters. It can be observed that $H'/L' = O(1)$ for $M \leq 1$. As shown by (3.18), this analysis is only valid when $H'/L' = O(1/ye)$. Hence the cases with $M \leq 1$ are not considered in this report.

Figure 3.12 shows the plots of the vertical velocity and the over pressure in the fault vs. depth for different mass flow rates as given by (3.68) and (3.69) respectively. It should be noted that the values of d in this figure are already corrected for the given parameters. Vertical velocity (W) increases with the increase of M, as expected, and becomes zero at the top of the fault. All the water is pushed to the aquifer by the time it reaches the top surface of the fault.

TABLE I

VALUES OF d FOR DIFFERENT SETS
OF PARAMETERS IN THE NO-CAP CASE

d	M	R	τ	ye
<.12	<1	500	1	.025
.12	1	500	1	.025
.3	2	500	1	.025
.47	3	500	1	.025
.64	4	500	1	.025
.47	2	750	1	.025
.64	2	1000	1	.025
.35	2	500	2	.025
1.34	2	500	1	.05

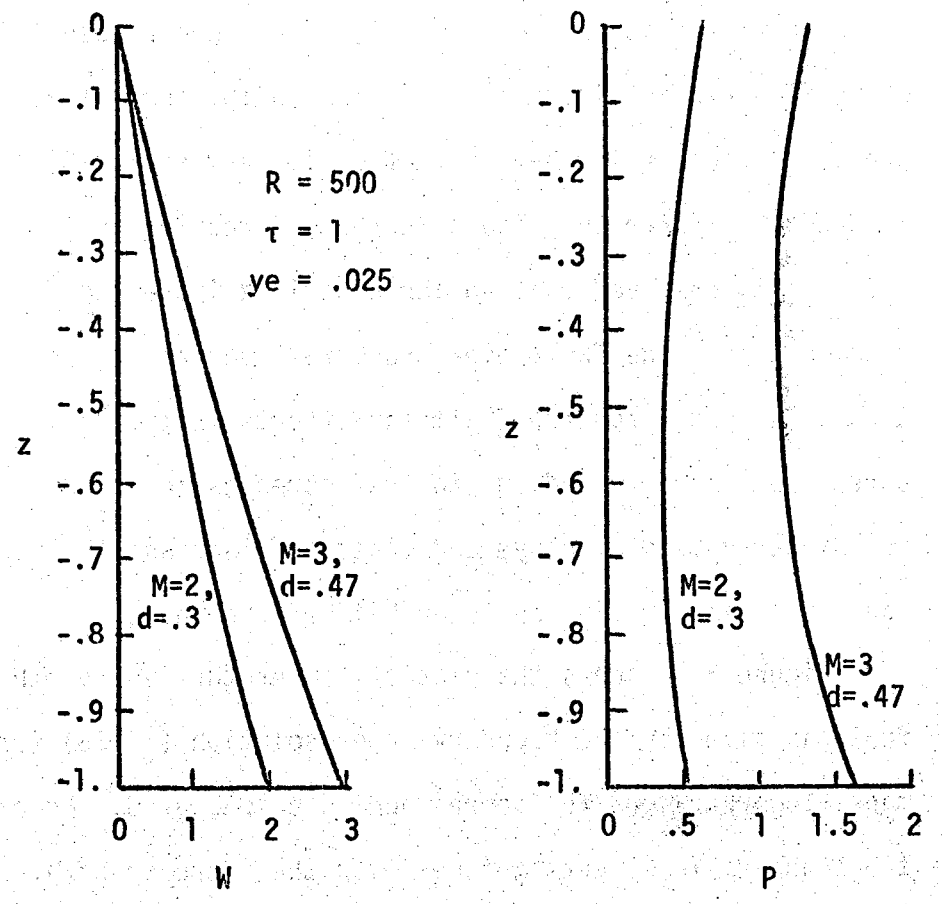

Figure 3.12 Vertical Velocity and Over Pressure Distribution along the Depth of the Fault for Different Mass Flow Rates.

Overall magnitudes of the overpressure increase with increasing mass flow rate. For high mass flow rates ($M > 2$) overpressures are highest at the inlet of the fault, decreasing upwards and then again increasing towards the top of the fault. The pressure increase towards the top of the fault is caused by the stagnation point at $z = 0$. It can be seen that the pressure gradient changes from negative at the bottom of the fault ($z = -1$) to the positive at the top ($z = 0$); in between pressure is minimum where its gradient is zero. Equation (3.10) shows that the fault pressure gradient in the $\bar{y}$ direction is very small, $O(ye^2)$, which is needed to force the liquid in the $\bar{y}$ direction in the fault. Also, it is observed that an increase in R increases d which, in turn, enhances the fault over pressures required to push the fluid through a longer aquifer. Similar effects in the fault over pressures are also observed due to the increases in ye and τ. Also, the higher values of R, ye and τ seem to increase the vertical fault velocity (W) in the lower half of the fault.

Figure 3.13 shows the plot of temperature vs. depth of the fault as given by the boundary layer solution (3.128) for different mass flow rates and the corresponding values of d. As expected the boundary layer gets thinner with the increase of M. Also note that the depth scale is smaller in this figure and the maximum depth plotted is only 18% of the total depth of the fault. It is observed that an increase in ye increases d and reduces the fault temperatures slightly. Since the lowest order term of (3.128) is independent of ye, this decrease is, therefore, caused by an

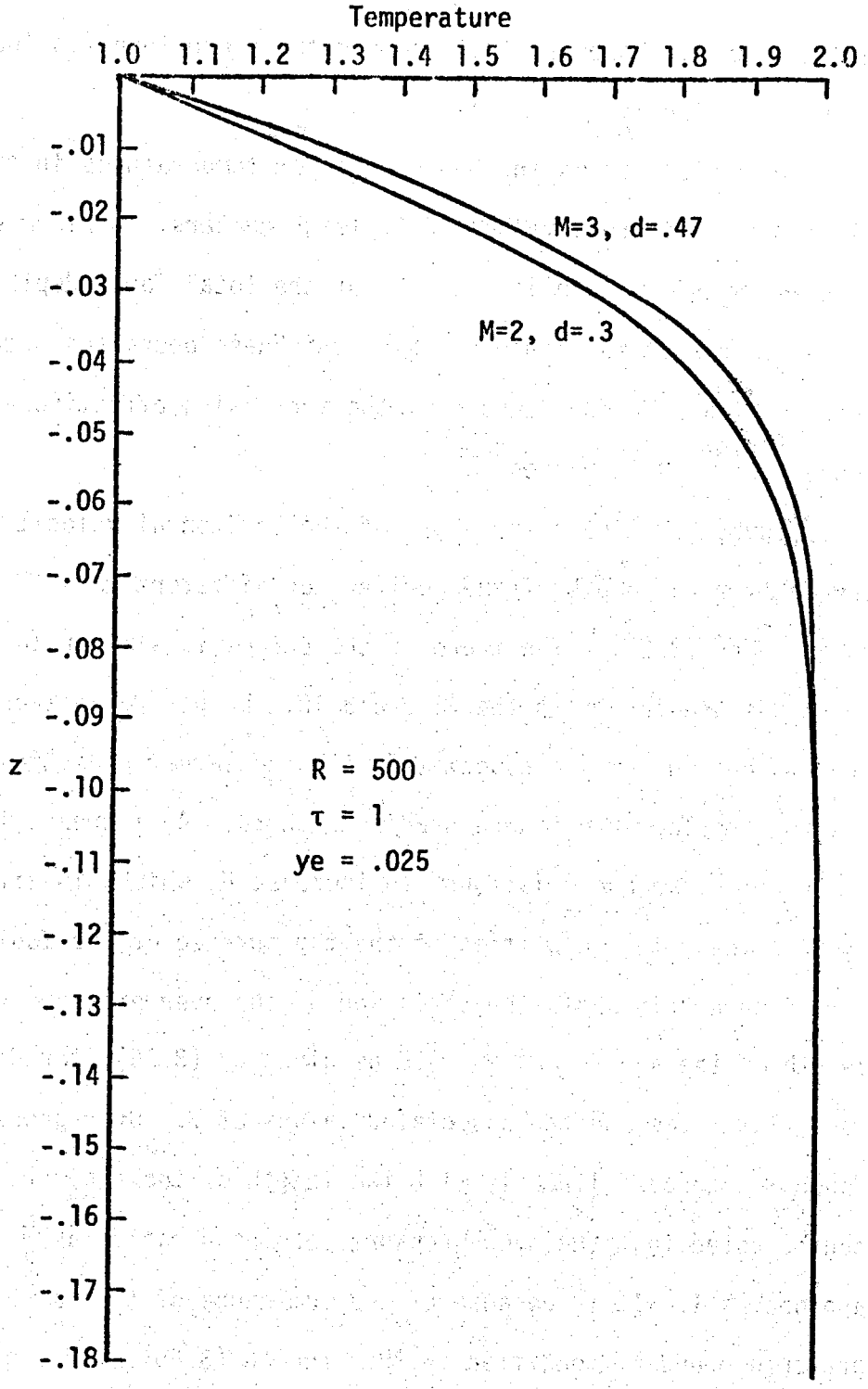

Figure 3.13 Effect of Mass Flow Rate on the Temperature of the Fault as per Depth

increase of d. However, fault temperatures are found to increase with increasing τ.

Figure 3.14 shows the boundary layer temperatures in the fault (3.128) for different values of Rayleigh numbers. Maximum depth plotted in this figure is also 18% of the total fault depth. It can be seen that the boundary layer thickness decreases with increasing R. This is caused by the increasing effectiveness of convection as R increases.

Figure 3.15 shows the plots of the horizontal velocity in the aquifer vs. depth of the aquifer for different mass flow rates as given by (3.62). The trend of the curves is similar to the over pressure curves in the Figure 3.12. Larger velocities at the top of the aquifer are associated with the larger pressures which lead to the larger pressure gradients there. An increase in the values of R, ye and τ is found to increase d, which, in effect, reduces the water velocities at the top surface of the aquifer.

Figure 3.16 shows the variation of the over pressure vs. the length of the aquifer at z = -.5 as given by (3.65), for different mass flow rates and the associated values of d. Over pressure is found to decrease linearly with the length of the aquifer. It can be noted that the over pressure becomes negative as $\hat{y}$ approaches 1. It is because of the dominance of the far end pressure boundary condition in that region (3,65). It can also be seen that the overall values of the over pressures increase with increasing mass flow rate, as expected. For a given M, over pressures increase with the increase of d (or of R, ye and τ) as

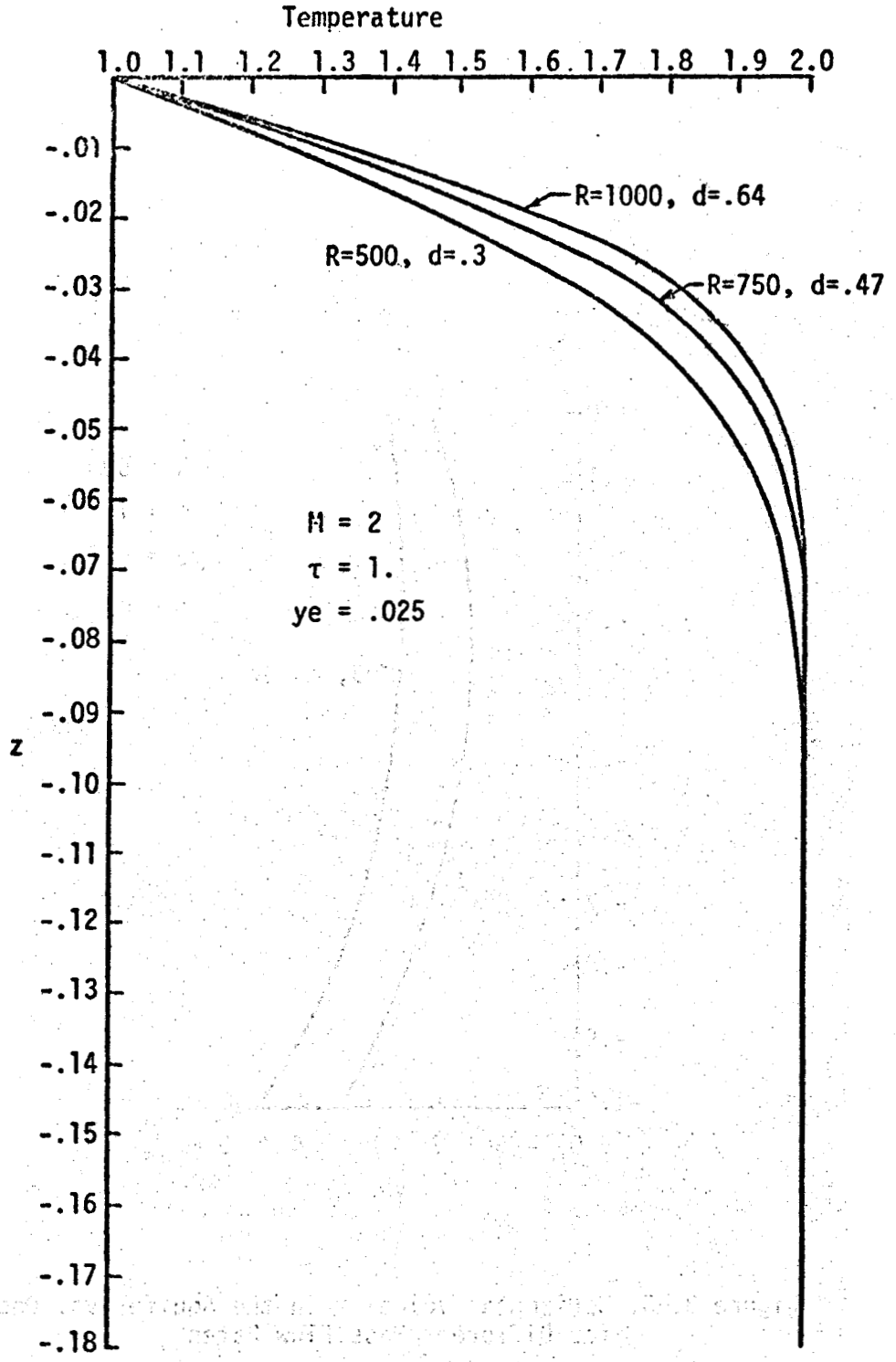

Figure 3.14 Effect of Rayleigh Number on Temperature of Fault as per Depth

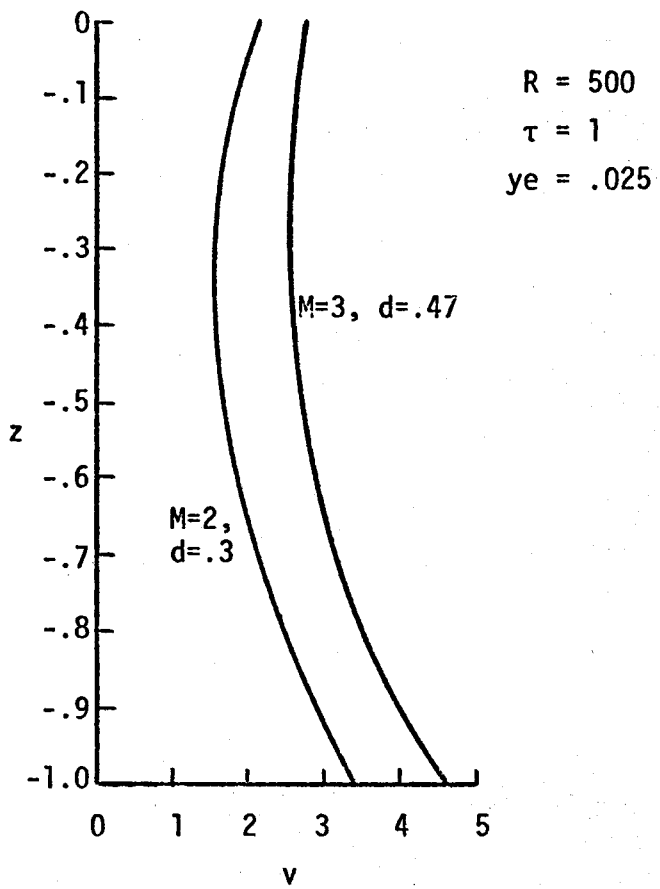

Figure 3.15 Horizontal Velocity in the Aquifer vs. Depth for Different Mass Flow Rates

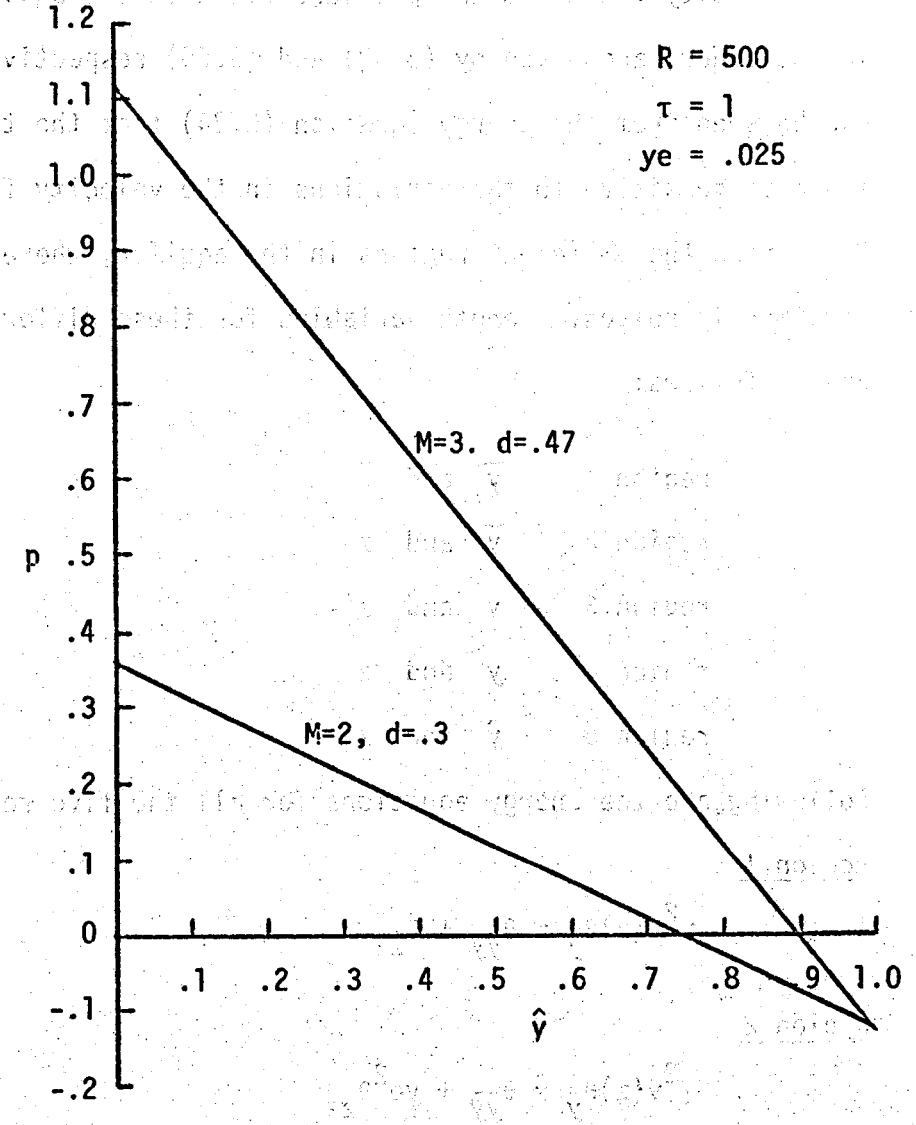

Figure 3.16 Over Pressure in the Aquifer vs. $\hat{y}$ for Different Values of M at $\bar{z}$ = -.5

higher pressures are needed to push the given amount of the fluid through a longer aquifer.

Temperature Distributions in the Aquifer

Velocity field and the pressure field in the aquifer, to the lowest order, are given by (3.62) and (3.65) respectively. It can be seen from the energy equation (3.24) that the temperature field is sensitive to the variations in the velocity field. Figure 3.17 shows the different regions in the aquifer, where energy equation is solved. Length variables for these different regions are as follows:

region 1 $\bar{y}$ and $\bar{z}$

region 2 $\bar{y}$ and z

region 3 y and z^*

region 4 y and z

region 5 $\hat{y}$ and z

Following are the energy equations for all the five regions.

Region 1

$$\gamma^2 v(\bar{z})\theta_{\bar{y}} = \theta_{\bar{y}\bar{y}} + \theta_{\bar{z}\bar{z}} \tag{3.131}$$

Region 2

$$\gamma^2 v(z)\theta_{\bar{y}} = \theta_{\bar{y}\bar{y}} + ye^2\theta_{zz} \tag{3.132}$$

Region 3

$$\gamma^2 v(z^*)\theta_y = ye\theta_{yy} + \theta_{z^*}\theta_{z^*} \tag{3.133}$$

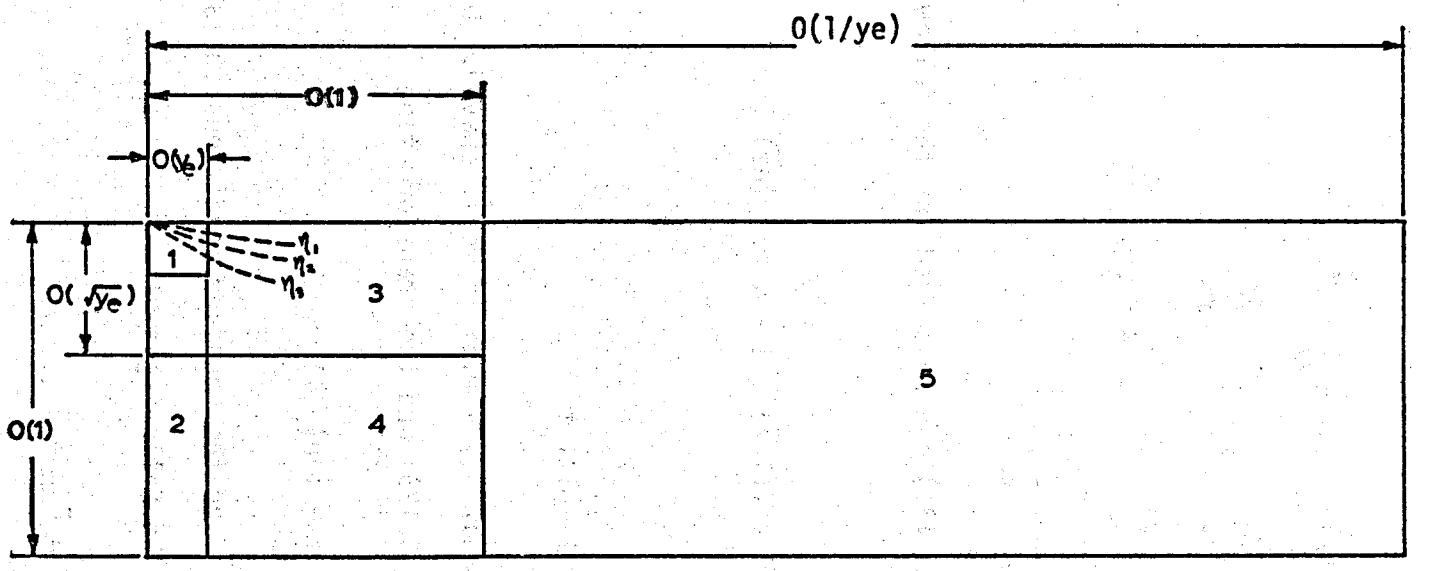

Figure 3.17 Five Different Regions in the Aquifer.

Region 4

$$\gamma^2 v(z)\theta_y = ye(\theta_{yy} + \theta_{zz}) \tag{3.134}$$

Region 5

$$\gamma^2 d\, v(z)\theta_{\hat{y}} = ye^2\theta_{\hat{y}\hat{y}} + d^2\theta_{zz} \tag{3.135}$$

where $y = \frac{y'}{L'} = \frac{\hat{y}d}{ye}$, $z = \frac{z'}{L'} = \frac{\hat{z}d}{ye}$

$$\bar{y} = \frac{y'}{ye'} = \frac{y}{ye} = \frac{\hat{y}d}{ye^2} , \quad \bar{z} = \frac{z'}{ye'} = \frac{z}{ye} \tag{3.136}$$

$$z^* = \frac{z'}{\sqrt{L'ye'}} = \frac{z}{ye^{1/2}}$$

Equation (3.131) can be solved for the following boundary conditions.

$$\theta(1,\bar{z}) = T(1,\bar{z}) = 1 - \tau \text{ erf } (A\bar{z}) \tag{3.137}$$

$$\theta(\bar{y},o) = 1 \tag{3.138}$$

$$\theta(y,-\infty) = 1 + \tau \tag{3.139}$$

It is required that $\theta(\bar{y} \to \infty,\bar{z})$ is well behaved. With the lowest order terms of (3.129) and the transformation

$$\theta = 1 + \tau + \bar{\theta}(\bar{y},\bar{z}) \tag{3.140}$$

Equation (3.131) and the boundary conditions (3.137)-(3.139) are transformed to the following system.

$$2A^2\bar{\theta}_{\bar{y}} = \bar{\theta}_{\bar{y}\bar{y}} + \bar{\theta}_{\bar{z}\bar{z}} \tag{3.141}$$

$$\bar{\theta}(1,\bar{z}) = -\tau\ [1 + \text{erf}(A\bar{z})] \qquad -\infty \le \bar{z} \le 0 \tag{3.142}$$

$$\bar{\theta}(\bar{y},0) = -\tau \qquad 1 \leq \bar{y} \leq \infty \tag{3.143}$$

$$\bar{\theta}(\bar{y},-\infty) = 0 \qquad 1 \leq \bar{y} \leq \infty \tag{3.144}$$

To solve the above system, the following Fourier Sine Integral Transform is used.

$$\theta_s(\bar{y},\omega) = \int_{-\infty}^{0} \bar{\theta}(\bar{y},\bar{z}) \sin \omega\bar{z}\, d\bar{z} \tag{3.145}$$

Its inverse is given by

$$\bar{\theta}(\bar{y},\bar{z}) = \frac{2}{\pi} \int_{-\infty}^{0} \theta_s(\bar{y},\omega) \sin \omega\bar{z}\, d\omega \tag{3.146}$$

Taking the integral transform of (3.141) with the boundary conditions (3.143) and (3.144), the following ordinary differential equation is obtained.

$$\frac{d^2\theta_s}{d\bar{y}^2} - 2A^2 \frac{d\theta_s}{d\bar{y}} - \omega^2\theta_s = -\omega\tau \qquad 1 \leq \bar{y} \leq \infty \tag{3.147}$$

Boundary conditions are:

$$\theta_s(1,\omega) = \frac{\tau}{\omega}\left(1 - \bar{e}^{\omega^2/4A^2}\right) \tag{3.148}$$

$$\theta_s(\infty,\omega) = \text{Bounded.} \tag{3.149}$$

The transform solution can be expressed as

$$\theta_s(\bar{y},\omega) = \frac{\tau}{\omega}\left[1 - e^{\left\{-\frac{\omega^2}{4A^2} - A^2 + \sqrt{A^4+\omega^2} + \left(A^2-\sqrt{A^4+\omega^2}\right)\bar{y}\right\}}\right] \tag{3.150}$$

An inversion of (3.150) yields

$$\bar{\theta}(\bar{y},\bar{z}) = -\tau - \frac{2\tau}{\pi}\int_{-\infty}^{0} e^{\{-\frac{\omega^2}{4A^2} - A^2 + \sqrt{A^4+\omega^2} + (A^2 - \sqrt{A^4+\omega^2})\bar{y}\}}\frac{\sin \omega z}{\omega}\, d\omega \tag{3.151}$$

Thus from (3.140), one finds

$$\theta(\bar{y},\bar{z}) = 1 - \frac{2\tau}{\pi}\int_{-\infty}^{0} e^{\{-\frac{\omega^2}{4A^2} - A^2 + \sqrt{A^4+\omega^2} + (A^2 - \sqrt{A^4+\omega^2})\bar{y}\}}\frac{\sin \omega\bar{z}}{\omega}\, d\omega \tag{3.152}$$

To find the result for $\bar{y} \to \infty$, substitute

$$\bar{y} = \frac{1}{\varepsilon} >> 1 \tag{3.153}$$

into (3.152) to obtain

$$\theta(\bar{y},\bar{z})$$

$$= 1 - \frac{2\tau}{\pi}\int_{0}^{\infty} e^{\{-\frac{\omega^2}{4A^2} - A^2 + A^2(1+\frac{\omega^2}{A^4})^{1/2} - \frac{A^2}{\varepsilon}(\sqrt{1+\frac{\omega^2}{A^4}} - 1)\}}\frac{\sin \omega\bar{z}}{\omega}\, d\omega \tag{3.154}$$

For $\varepsilon \to 0$, the integrand in (3.154) is exponentially small, except when $\omega << 1$. The integrand can be evaluated for

$$\omega << 1 \quad \text{and} \quad \omega\bar{z} << 1 \tag{3.155}$$

The asymptotic estimate can be written as

$$\theta(\bar{y},\bar{z}) = 1 - \frac{2\tau}{\pi}\int_{0}^{\omega} e^{\{\frac{\omega^2}{4A^2} - \frac{\omega^2}{2\varepsilon A^2}\}}\bar{z}\, d\omega \tag{3.156}$$

which can be integrated to give

$$\theta(\bar{y},\bar{z}) = 1 - \sqrt{\frac{2}{\pi}}\,\tau A\,\frac{\bar{z}}{\bar{y}^{1/2}} \tag{3.157}$$

where $$\omega = O(\varepsilon^{1/2}) \tag{3.158}$$

Equation (3.157) indicates that a similarity variable $(\bar{z}/\bar{y}^{1/2})$ will be significant in region 3. The order of the magnitude of $\bar{z}$ can be obtained from (3.155) and (3.158), with the following result.

$$\bar{z} \ll O(\frac{1}{\varepsilon^{1/2}}) \tag{3.159}$$

The limitation to be imposed on the solution (3.157), as obtained from (3.153) and (3.159), is as follows:

$$\frac{\bar{z}}{\bar{y}^{1/2}} \ll O(1)\ , \qquad \bar{y} \to \infty \tag{3.160}$$

Solution of (3.132) in the region 2 is

$$\theta(\bar{y},z) = 1 + \tau \tag{3.161}$$

because the cooled thermal region does not extend below the thin surface boundary layer.

Use of (3.136) in (3.62) gives the following expression for the aquifer velocity.

$$v(z^*) = a_1 - 1 + O(ye^{1/2}) \tag{3.162}$$

Equation (3.133), containing O(1) terms for the region 3, can be written as

$$2A^2\theta_y = \theta_{z^*}\theta_{z^*} \tag{3.163}$$

with the following boundary conditions

$$\theta(y,0) = 1 \tag{3.164}$$

$$\theta(y,-\infty) = 1 + \tau \tag{3.165}$$

A similarity solution can be obtained which is compatible with the solution in region 1 (in which the boundary layer is born) Elementary methods yield,

$$\theta(y,z^*) = 1 - \tau \operatorname{erf}\left(\frac{A}{\sqrt{2}}\eta\right), \quad \eta = \frac{z^*}{y^{1/2}} \tag{3.166}$$

Expressing (3.166) in the variables of region 1 $(\bar{y},\bar{z})$ the following equation results.

$$\theta(\bar{y},\bar{z}) = 1 - \tau \operatorname{erf}\left(\frac{A}{\sqrt{2}} \frac{\bar{z}}{\bar{y}^{1/2}}\right) \tag{3.167}$$

Referring to Spiegel (1968)

$$\operatorname{erf}(x) \simeq \frac{2}{\sqrt{\pi}} x \ , \quad x << 1 \tag{3.168}$$

For $\bar{z}/\bar{y}^{1/2} << 1$, (3.167) becomes

$$\theta(\bar{y},\bar{z}) \simeq 1 - \sqrt{\frac{2}{\pi}} \tau A \frac{\bar{z}}{\bar{y}^{1/2}} \tag{3.169}$$

It can be seen that (3.169) matches with the outer limit (3.157) of region 1. It is clear from (3.166) that the temperature boundary layer thickens along the lines $\eta = O(1)$ and $y \to \infty$ as shown in Figure 3.17 by lines for η_1, η_2, η_3, etc.

The basic temperature solution for region 4 is

$$\theta(y,z) = 1 + \tau \tag{3.170}$$

here again the same argument, as given for region 2, can be used.

Solution (3.166) and the quadrature solution (3.152) are plotted in Figure 3.18 at different depths of the aquifer and at different values of y away from the fault centerline. It can be noted that the quadrature solution approaches the similarity solution and finally merges in it for large values of y.

It is possible to obtain the analytic solution of (3.135) in region 5 when $\hat{y} << 1$ and $z << 1$ but $z/\hat{y}^{1/2} = O(1)$, which can be matched with (3.166).

The Taylor's series expansions,

$$v(z \to o) = v(o) + zv'(o) + \frac{z^2}{2} v''(o) + \ldots \tag{3.171}$$

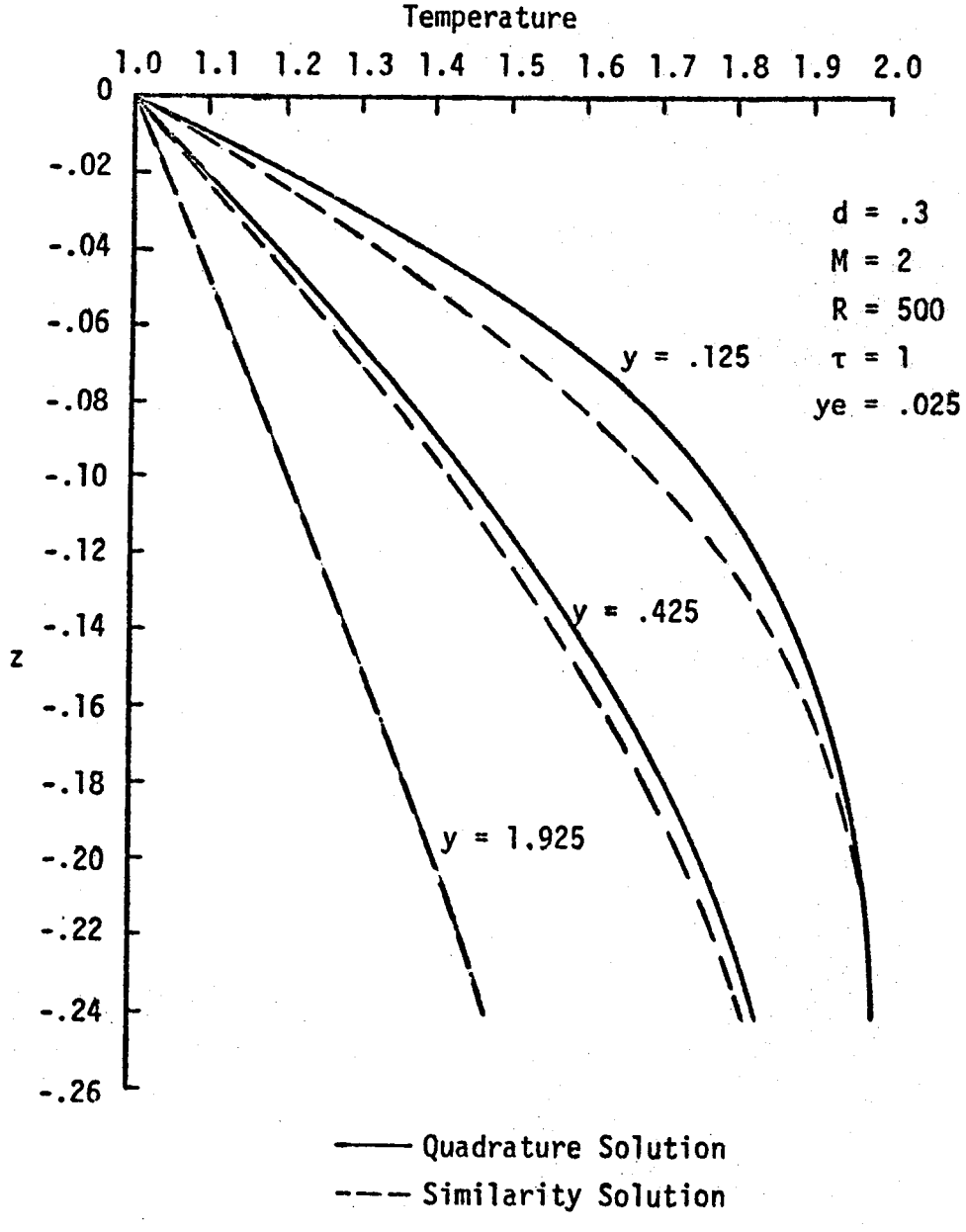

Figure 3.18 Near Fault Temperatures in the Aquifer

or

$$v(z\to o) = (a_1-1) + \frac{z}{d} + \frac{a_1}{2d} z^2 + \ldots \tag{3.172}$$

are used to describe the velocity field. The temperature field is expressed as

$$\theta(\hat{y},z) = \theta_o(\eta) + \hat{y}^{1/2}\theta_1(\eta) + \hat{y}\theta_2(\eta) + O(\hat{y}^{3/2}) \tag{3.173}$$

where $$\eta = \frac{z}{\hat{y}^{1/2}} \tag{3.174}$$

Substituting (3.172), (3.173) and (3.174) into (3.135) one can construct the following systems.

Order (1)

$$\frac{d^2\theta_o}{d\eta^2} + \frac{A^2}{d}\eta\frac{d\theta_o}{d\eta} = 0 \tag{3.175}$$

$$\theta_o(\hat{y},z = 0) = 1 \tag{3.176}$$

$$\theta_o(\hat{y}\to 0,z) = 1 + \tau \tag{3.177}$$

Order $(\hat{y}^{1/2})$

$$\frac{d^2\theta_1}{d\eta^2} + \frac{\eta A^2}{d}\frac{d\theta_1}{d\eta} - \frac{A^2}{d}\theta_1 = \frac{\gamma^2\tau A}{\sqrt{2\pi d}\,d^2}\eta^2 e^{-\frac{A^2\eta^2}{2d}} \tag{3.178}$$

$$\theta_1(\hat{y},z = 0) = 0 \tag{3.179}$$

$$\theta_1(\hat{y}\to 0,z) = 0 \tag{3.180}$$

Solutions of (3.175)-(3.177) and (3.178)-(3.180) when substituted in (3.173) result in the following expression for the temperature in region 5 when both $\hat{y}$ and z are small.

$$\theta(\hat{y},z) = 1 - \tau\ \mathrm{erf}\left(\frac{A}{\sqrt{2d}}\frac{z}{\hat{y}^{1/2}}\right) + \frac{\hat{y}^{1/2}\tau\gamma^2}{4\sqrt{2d}\,A^2}\left[\frac{z}{\sqrt{2d\hat{y}}}\left\{1 + \mathrm{erf}\left(\frac{Az}{\sqrt{2d\hat{y}}}\right)\right\}\right.$$

$$\left. - \frac{Az^2}{\sqrt{\pi d\hat{y}}}\, e^{-\frac{A^2z^2}{2d\hat{y}}}\right] + O(\hat{y}) \qquad (3.181)$$

It can be noted that the O(1) terms of this expression match with (3.166) of region 3.

Temperatures in region 5 are obtained by integrating (3.135) numerically as explained in Appendix A. Solution (3.181) is taken as the initial condition at $\hat{y} = .05$ for the numerical integration. Figure 3.19 shows the variation of the temperature as per depth of the aquifer for different values of $\hat{y}$. $\hat{y} = 1$ represents the far end of the aquifer, which is d/ye times its depth. This figure shows the reduction in the temperatures of the liquid as it moves away from the fault, losing heat to the surroundings. It can be noted that the far field boundary condition is satisfied for this value of d. Figure 3.20 shows the isotherms in the aquifer for the temperatures of Figure 3.19. It is apparent from this figure that the horizontal temperature gradient decreases as the liquid moves away from the fault and becomes negligibly small near the far end.

Figure 3.21 shows the effect of mass flow rate on the surface temperature gradients both for the fault and the aquifer. Heat transfer at the surface is seen to increase with increasing mass flow rate, as expected. Matching of the three regions is also shown for M = 2. It can also be noted that the length of the

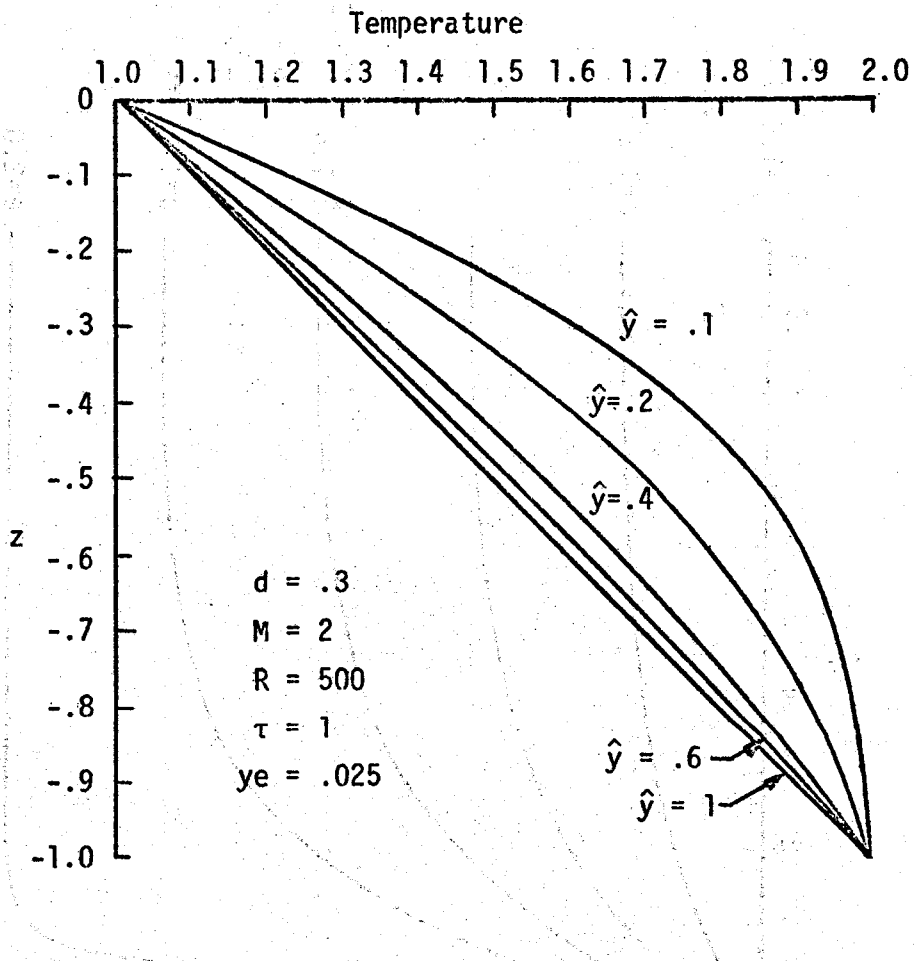

Figure 3.19 Temperatures in the Aquifer at Different Locations Away from the Fault

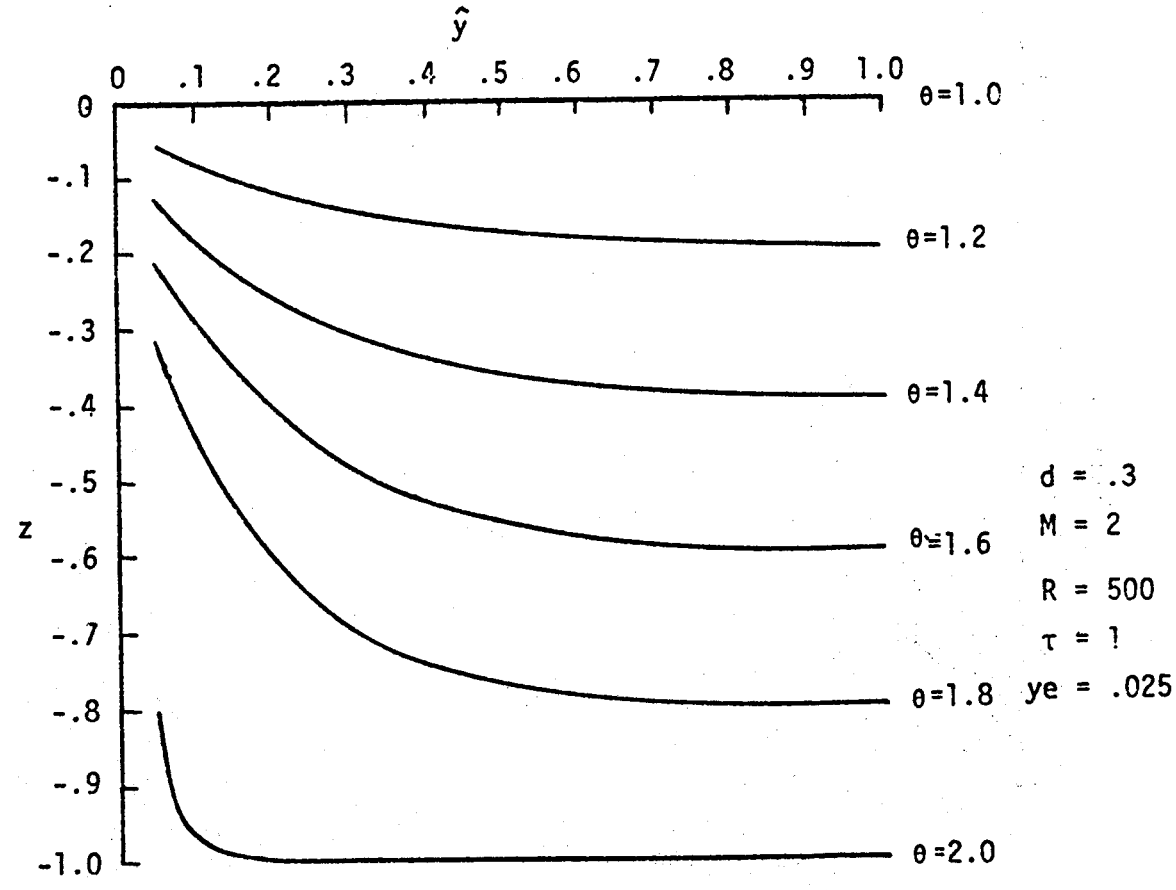

Figure 3.20 Isotherms in the Aquifer

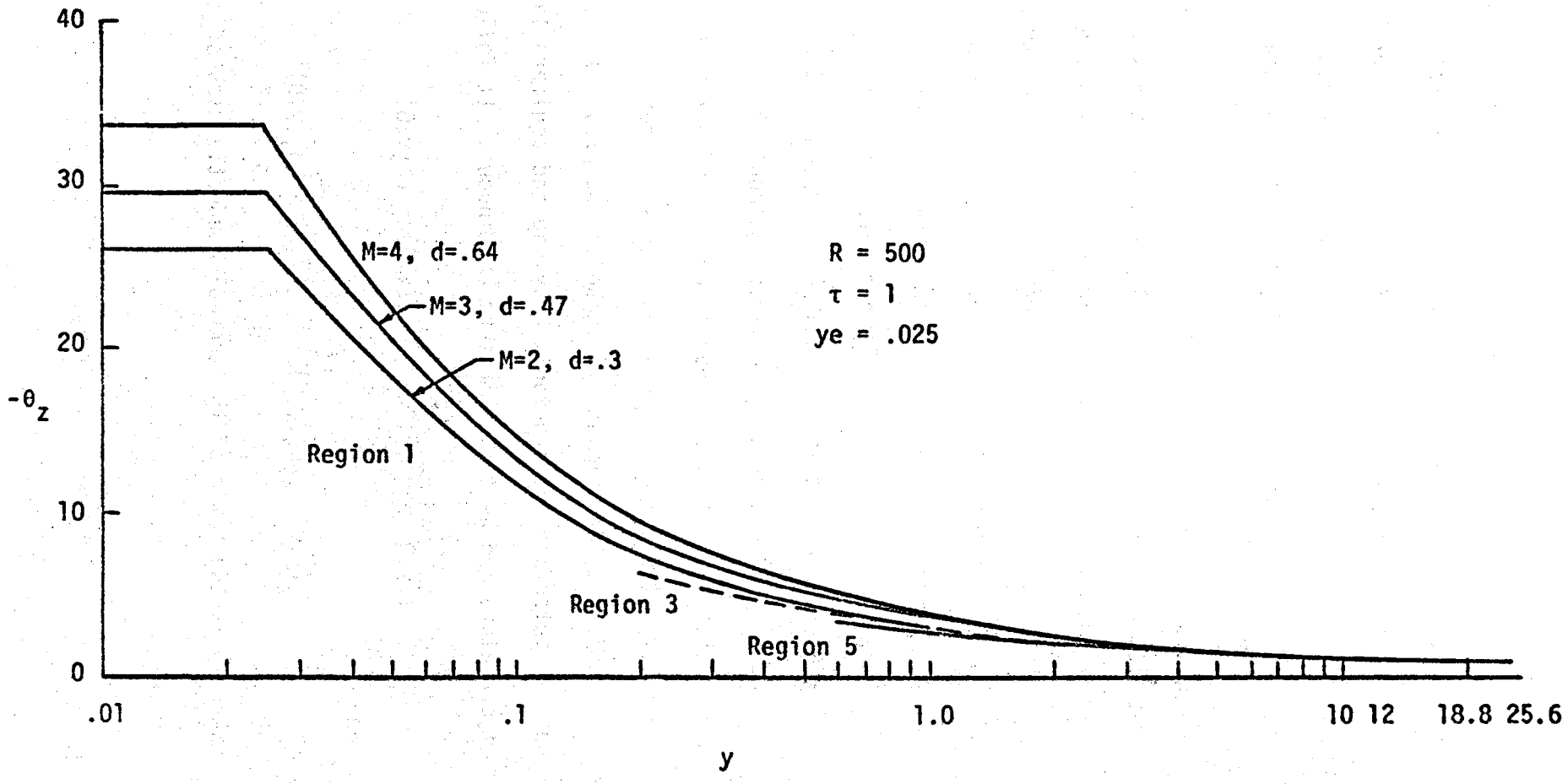

Figure 3.21 Effect of Mass Flow Rate on the Surface Temperature Gradients along the Length of the Aquifer

aquifer in each case is different. It is because of different values of d associated with different mass flow rates.

Figures 3.22, 3.23 and 3.24 show the effects of R, τ and ye on the surface heat flux. As expected, an increase in R, τ and ye enhances the temperature gradients at the surface.

The Clay Cap Case

In this case an impermeable layer of thickness ℓ' is supposed to cap the aquifer as shown in Figure 3.11. Relative to the capless case there will be a reduction in the heat transfer to the surface that depends on ℓ' and the thermal conductivity. Two different thermal conductivity zones are considered in this analysis, because the impermeable clay-rich sediments have a lower thermal conductivity than the sand rich aquifer (Bear, 1972). Change of the temperature gradients at about .8 km in East Mesa Wells (Figure 3.7) also supports the idea of a thermal conductivity contrast. The boundary conditions, to which fault and aquifer are subjected, are similar to those in the previous case. However, at the interface between fault-clay cap and aquifer-clay cap, temperature and heat flux must be continuous. It follows that

$$T(\bar{y},0) = \theta^c(\bar{y},0), \qquad \theta(\hat{y},0) = \theta^c(\hat{y},0) \tag{3.182}$$

and

$$T_z(\bar{y},0) = \lambda\theta_z^c(\bar{y},0), \quad \theta_z(\hat{y},0) = \lambda\theta_z^c(\hat{y},0) \tag{3.183}$$

where λ is the ratio of the thermal conductivities of the cap and the aquifer.

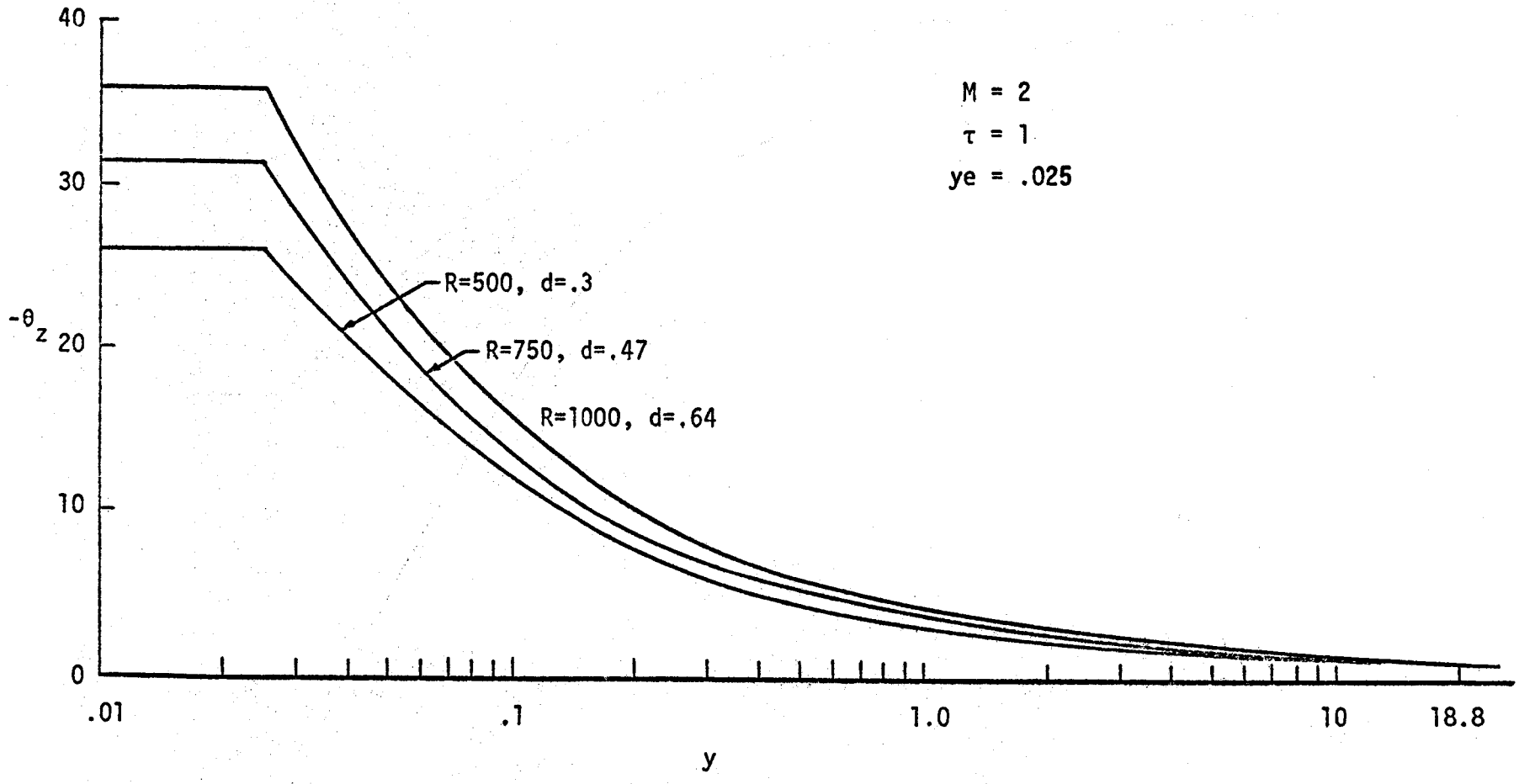

Figure 3.22 Effect of Rayleigh Number on the Surface Temperature Gradients along the Length of the Aquifer

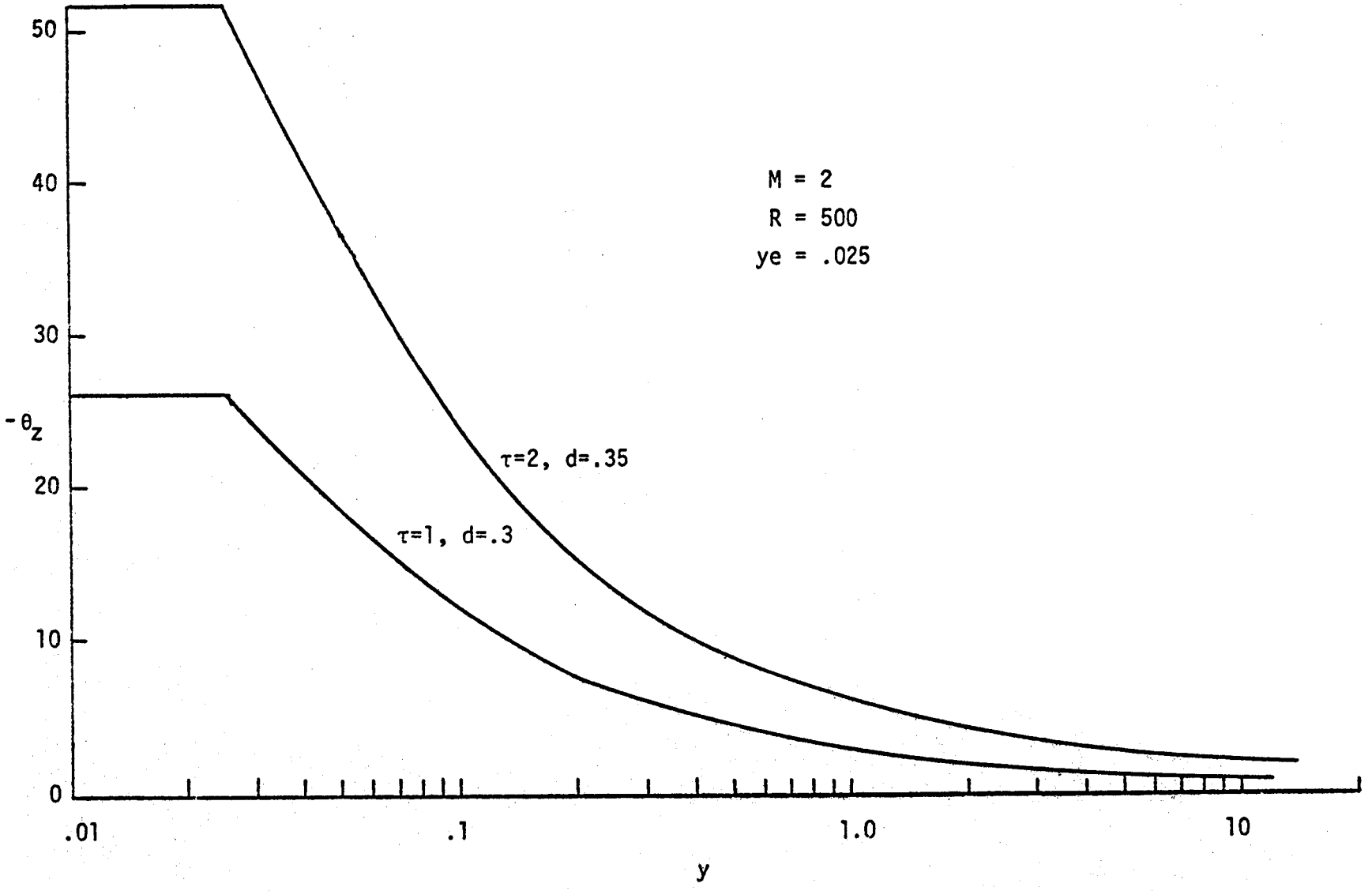

Figure 3.23 Effect of τ on the Surface Temperature Gradients along the Length of the Aquifer

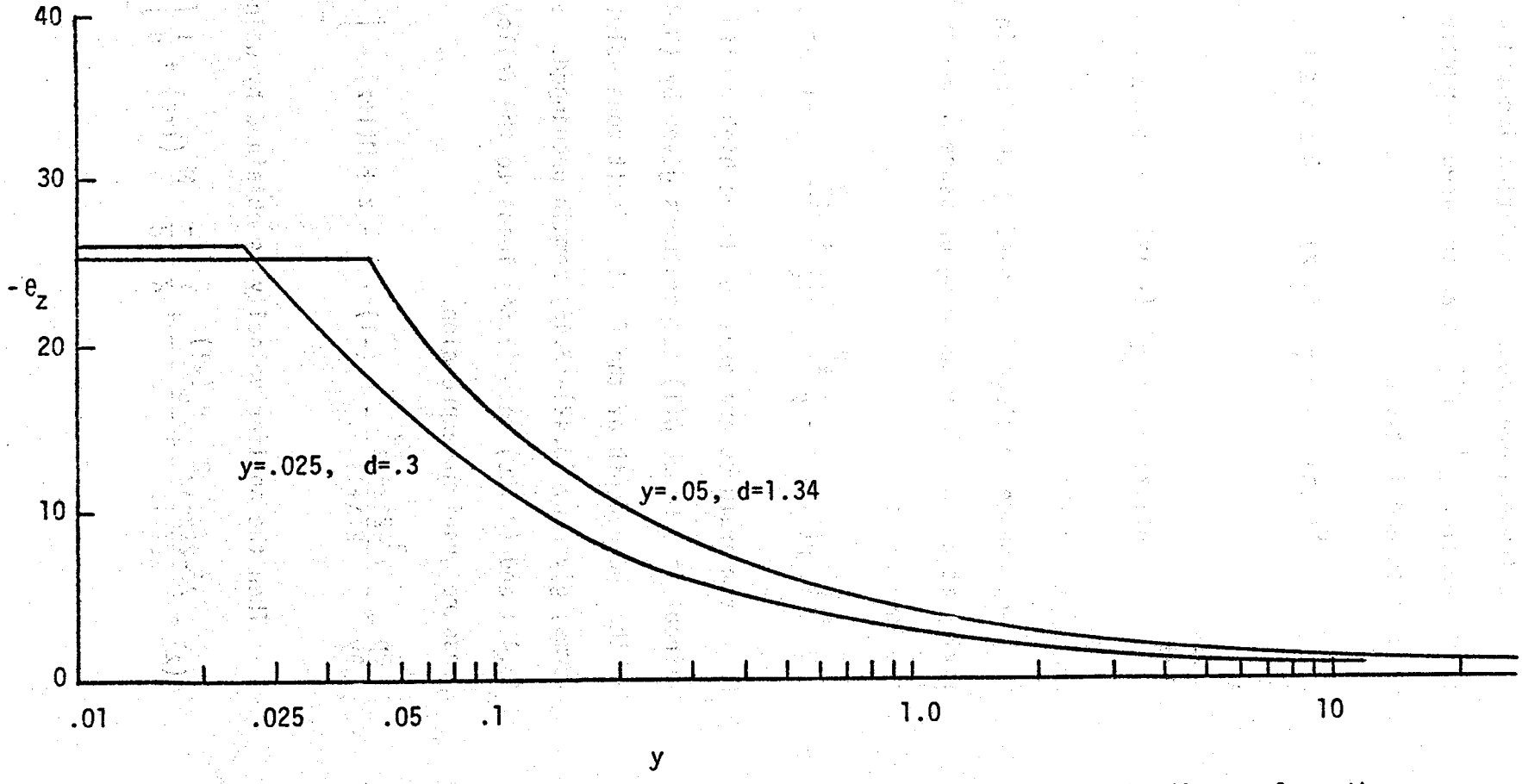

Figure 3.24 Effect of Semi-Fault width on the Surface Temperature Gradients along the Length of the Aquifer

The temperature boundary condition imposed at the far end of the aquifer ($y' = H'$) is again based on purely vertical conduction and is given as

$$\theta^c(1,z) = 1 + \frac{\tau}{\lambda+\ell}(\ell-z) \qquad 0 \le z \le \ell \tag{3.184}$$

and

$$\theta(1,z) = 1 + \frac{\tau}{\lambda+\ell}(\ell-\lambda z) \qquad -1 \le z \le 0 \tag{3.185}$$

where $\ell = \ell'/L'$.

The change in slope is caused by the jump in thermal conductivity at $z = 0$. Corresponding pressure boundary condition in the aquifer is

$$p(1,z) = -\frac{1}{2}\frac{\ell^2 - 2\ell z + \lambda z^2}{\lambda+\ell} \qquad -1 \le z \le 0 \tag{3.186}$$

Fault temperatures are expected to be higher with clay cap than without it. Hence O(1) temperatures given by (3.42) are valid in the whole depth of the fault. Fault zone solutions of O(1) terms, given by (3.42)-(3.45) remain unchanged. Substitution of (3.45) and (3.186) into (3.54) leads to the following horizontal pressure gradient expression.

$$\frac{\partial p}{\partial \hat{y}} = -\frac{\ell^2-2\ell z+\lambda z^2}{2(\lambda+\ell)} - P_o(-1) - 1 - z + M(1+z) - \int_{-1}^{z} d\sigma \int_{-1}^{\sigma} v(\alpha)d\alpha \tag{3.187}$$

Then the aquifer velocity is obtained by using (3.23).

$$v(z) = \frac{\ell^2-2\ell z+\lambda z^2}{2d(\lambda+\ell)} + \frac{P_o(-1)}{d} + \frac{1}{d} + \frac{z}{d} - \frac{M}{d}(1+z) + \frac{1}{d}\int_{-1}^{z} d\sigma \int_{-1}^{\sigma} v(\alpha)d\alpha \tag{3.188}$$

Differentiating (3.188) twice with respect to z yields the following ordinary differential equation,

$$\frac{d^2v(z)}{dz^2} = \frac{v(z)}{d} + \frac{\lambda}{d(\lambda+\ell)} \tag{3.189}$$

which must satisfy the conditions

$$v(-1) = \frac{P_o(-1)}{d} + \frac{\ell^2 + 2\ell + \lambda}{2d(\lambda+\ell)} \tag{3.190}$$

and

$$\frac{dv(-1)}{dz} = -\frac{M}{d} \tag{3.191}$$

The solution can be written as

$$v(z) = a_2 \cosh \frac{z}{\sqrt{d}} + b_2 \sinh \frac{z}{\sqrt{d}} - \frac{\lambda}{\lambda+\ell} \tag{3.192}$$

where

$$a_2 = \frac{M + \frac{\lambda}{\lambda+\ell} \cosh \frac{1}{\sqrt{d}}}{\sqrt{d} \sinh \frac{1}{\sqrt{d}}} \quad , \quad b_2 = \frac{\lambda}{\sqrt{d}\,(\lambda+\ell)} \tag{3.193}$$

and

$$P_o(-1) = -\frac{\ell^2+2\ell+\lambda+2\lambda d}{2(\ell+\lambda)} + \frac{\lambda}{\lambda+\ell} \frac{\sqrt{d}}{\sinh \frac{1}{\sqrt{d}}} + M\sqrt{d} \coth \frac{1}{\sqrt{d}} \tag{3.194}$$

It follows that the fault zone solutions obtained from (3.192), (3.42)-(3.45) and (3.32) are

$$T = 1 + \tau \tag{3.195}$$

$$\overline{V} = \bar{y}v(z) + O(ye^2) \tag{3.196}$$

$$W = - a_2\sqrt{d}\,\sinh\frac{-z}{\sqrt{d}} + b_2\sqrt{d}\left(1 - \cosh\frac{-z}{\sqrt{d}}\right) + \frac{\lambda z}{\lambda+\ell} + O(ye^2) \tag{3.197}$$

$$P = d\,v(z) - \frac{\ell^2 - 2\ell z + \lambda z^2}{2(\lambda+\ell)} + O(ye^2) \tag{3.198}$$

The over pressure in the aquifer derived from (3.23), (3.186) and (3.192) is

$$p(\hat{y},z) = d\,v(z)(1-\hat{y}) - \frac{\ell^2 - 2\ell z + \lambda z^2}{2(\lambda+\ell)} + O(ye^2) \tag{3.199}$$

The factor d, which determines the far-field boundary of the aquifer, depends on the parameters ℓ, λ, M, R, τ and ye as shown by (3.24) and (3.192). Besides R, τ and ye, other comparing parameters in the East Mesa area are (Combs, 1977),

clay cap thickness = ℓ' = .8 km

$$\ell = \frac{\ell'}{L'} = \frac{.8}{3.35} \simeq .24$$

Thermal conductivity of the clay cap = 4.6×10^{-3} cal/cm-sec-^{o}K
Thermal conductivity of the aquifer = 6.4×10^{-3} cal/cm-sec-^{o}K

$$\lambda = \frac{4.6 \times 10^{-3}}{6.4 \times 10^{-3}} \simeq .7$$

Table II shows the values of d for different sets of the parameters, obtained by integrating the parabolic equation (3.24). It can be observed that for $M \leq 0.5$, $H'/L' = O(1)$ implying that the asymptotic analysis, based on $H'/L' = O(\frac{1}{ye}) \gg O(1)$, fails. The following observations can be made from this table.

TABLE II

VALUES OF d FOR DIFFERENT SETS
OF PARAMETERS IN THE CLAY-CAP CASE

d	ℓ	λ	M	R	τ	ye
.24	.24	.7	1	500	1	.025
.28	.50	.7	1	500	1	.025
.22	.24	1.0	1	500	1	.025
.14	.24	.7	.5	500	1	.025
.49	.24	.7	2	500	1	.025
.74	.24	.7	3	500	1	.025
.18	.24	.7	1	338	1	.025
.50	.24	.7	1	1000	1	.025
.24	.24	.7	1	500	.6	.025
1.04	.24	.7	1	500	1	.05
.32	.24	.7	1	338	.6	.034

An increase in λ is associated with a decrease in d. Faster convergence to the far field boundary condition occurs because of increased cap heat transfer. An increase in M, R, τ and ye, all of which lead to enhancement of convection, increase d because, in general, they tend to increase the temperature at a given point in the cooled part of the aquifer. The cap heat transfer reduction, caused by an increase in thickness implies that a longer aquifer is required to stabilize the temperatures.

It is clear from (3.192), (3.197), (3.198) and (3.199) that v(z), W, P, and p depend explicitly on ℓ, λ and M. However, an increase in R, τ and ye increases d (Table IV) which implicitly affect aquifer velocity, vertical fault velocity, fault over pressure and aquifer over pressure. Velocity of the liquid near the top surface and the bottom surface of the aquifer are found to decrease with increasing d. This is required to accommodate the existing pressure gradients there. However, the velocity increase in the middle portion of the aquifer is due to the conservation of the specified mass flow rate. The effect of cap thickness on the horizontal aquifer velocity is shown in Figure 3.25. It can be seen that the horizontal aquifer velocities are higher in the lower half of the aquifer for higher cap thicknesses. This is due to increased pressure gradients found in that portion of the

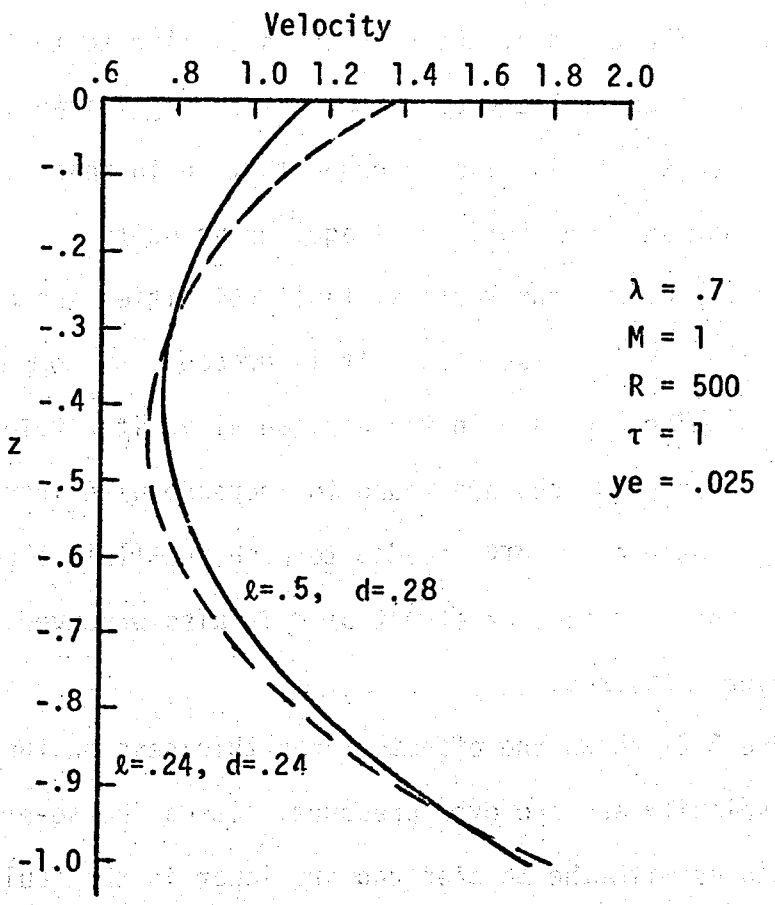

Figure 3.25 Effect of Cap Thickness on the Horizontal Velocity in the Aquifer

aquifer because of the reduced hot hydrostatic pressure associated with the lighter (warmer) liquid at the far-field boundary. Velocities reduce correspondingly in the upper half of the aquifer to conserve mass.

Figure 3.26 shows the effect of the thermal conductivity ratio on the aquifer velocity. Lower λ reduces heat transfer throughout the cap and hence maintains higher temperatures in the aquifer. The trend of the results is similar to that in Figure 3.25 but the velocities do not differ significantly for this change of λ. It is also observed that an increase in mass flow rate increases the horizontal aquifer velocity.

It is found that the vertical fault velocities increase slightly with the increase of d. It is probably to compensate for the corresponding decrease in the horizontal aquifer velocity. Also fault over pressures are found to increase with increasing d. Larger pressures are needed to push the fluid through a longer distance. A similar effect of d is also observed on the aquifer over pressures.

Figure 3.27 shows the effect of cap thickness on the fault vertical velocity and the over pressure. It can be seen that the over pressures with the thicker cap are lower in the fault. This difference is primarily caused by the reduced far-field pressure boundary condition which in turn establishes a different pressure at the fault so that the same amount of liquid is pushed through the aquifer. It is also observed that the vertical fault velocities are slightly lower for a thicker cap. This can be

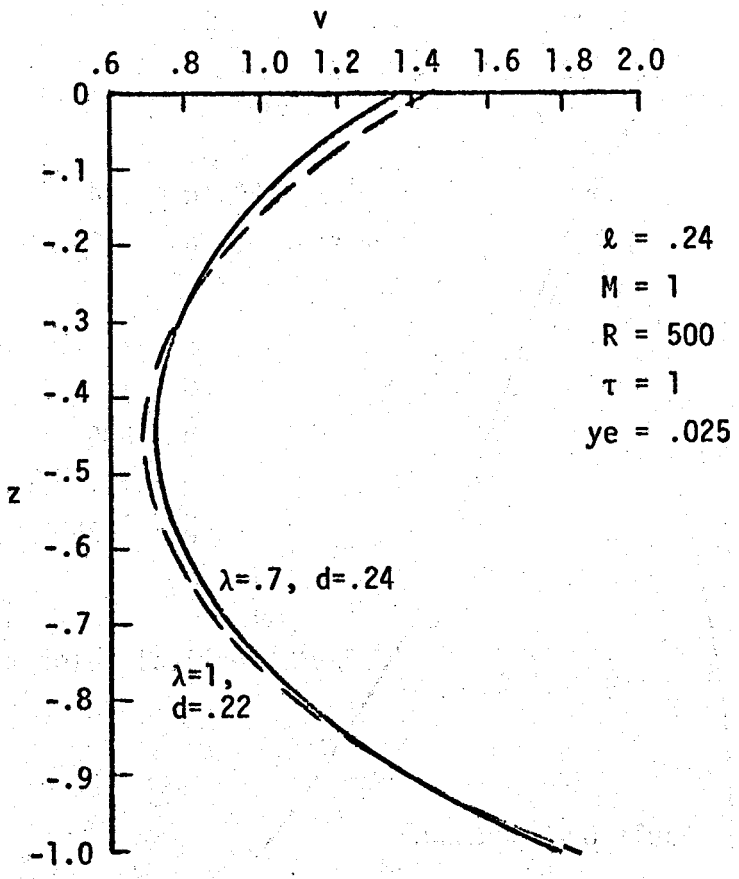

Figure 3.26 Thermal Conductivity Ratio Effect on the Horizontal Velocity in the Aquifer

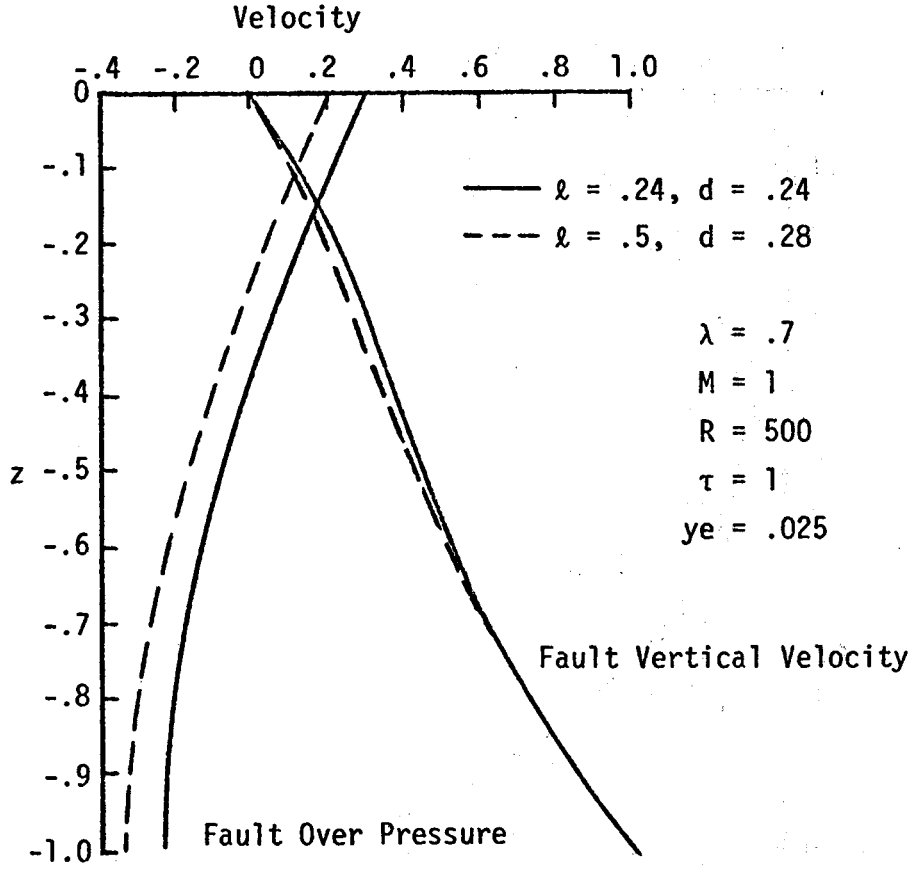

Figure 3.27 Effect of Cap Thickness on the Fault Vertical Velocity and Over Pressure

explained with the help of Figure 3.25 where horizontal aquifer velocities in the lower half of the aquifer are higher for a thicker cap. These higher velocities transport a relatively larger amount of fluid in the aquifer and thereby correspondingly reduce the vertical velocities in the fault

It is also observed that the increase in λ causes a very slight increase in both the vertical velocity and the over pressures in the fault. It is clear from Figure 3.26 that the horizontal aquifer velocities decrease with increasing λ in the lower half of the aquifer and hence correspondingly increase the vertical fault velocities. Also higher λ transfers more heat through the cap so that the aquifer fluid is relatively cool. The cool liquid of higher density will give rise to higher hot hydrostatic pressure at the far end of the aquifer. To make up for the needed pressure gradient, fault over pressures are expected to increase with increasing λ.

Figures 3.28 and 3.29 show the effect of mass flow rate on the vertical velocity and the over pressures in the fault respectively. As expected, both the vertical velocity and the over pressures increase with increasing mass flow rate.

Figure 3.30 shows the effect of cap thickness on the over pressures in the aquifer. It can be seen that the over pressures with a thicker cap are lower in the aquifer. As the far end hot hydrostatic pressure becomes lower for thicker cap (lighter liquid), aquifer over pressures adjust to lower values to allow nearly the same pressure gradient for any given M.

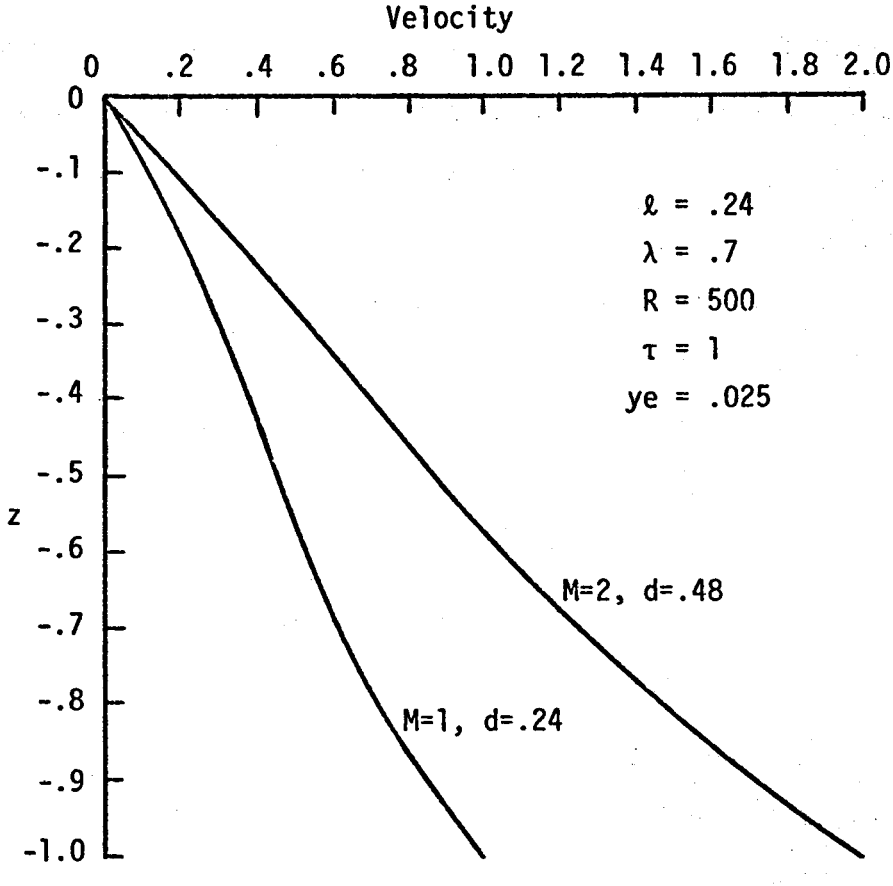

Figure 3.28 Effect of Mass Flow Rate on the Vertical Velocity in the Fault

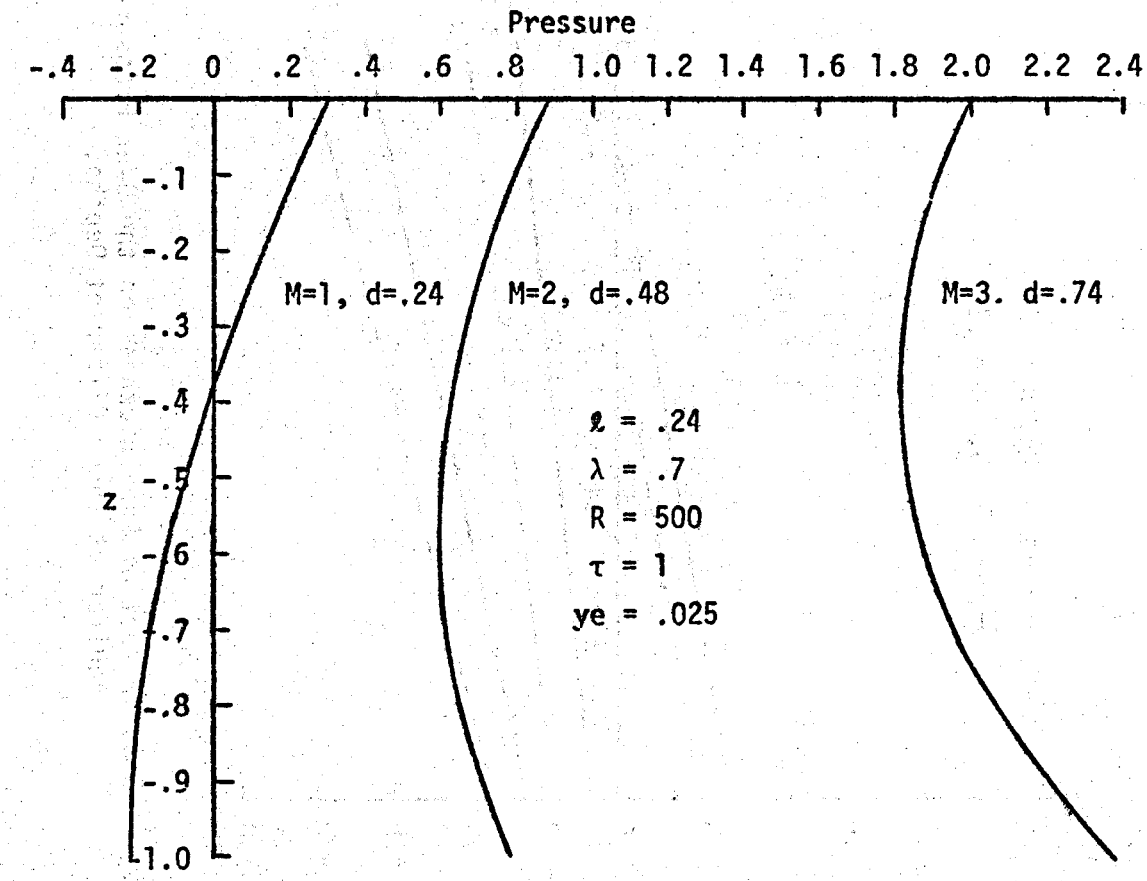

Figure 3.29 Effect of Mass Flow Rate on the Pressure in the Fault as per Depth

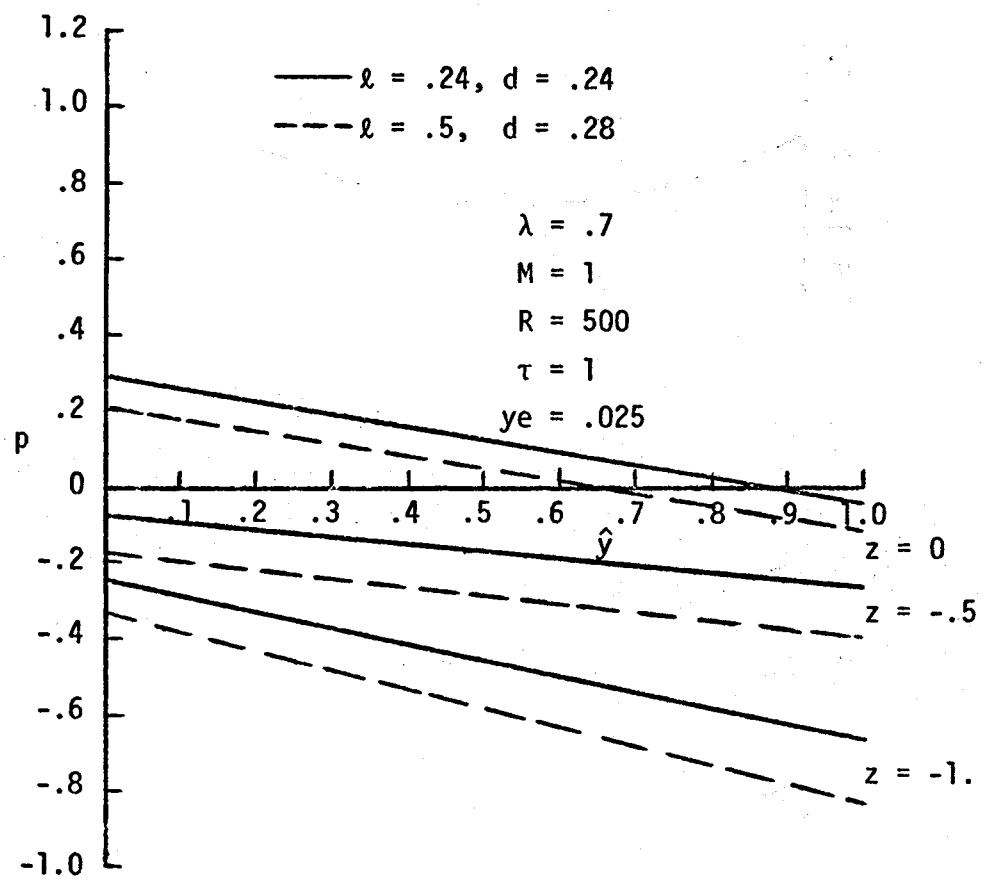

Figure 3.30 Effect of Cap Thickness on the Over Pressure in the Aquifer at Three Different Depths.

An increase in λ seems to increase the over pressures in the aquifer very slightly. Higher λ gives rise to higher over pressures because larger heat transfer results in a cooler, heavier fluid. An additional contributing factor is the effect of the far-field pressure boundary condition as explained in the previous paragraph.

Figure 3.31 shows the effect of mass flow rate on the over pressures in the aquifer. Higher mass flow rates give rise to larger pressure gradients, as expected.

Once the O(1) temperature solutions in the fault zone are obtained the next step is to look into the temperature distributions in the clay cap and the aquifer. Figure 3.32 shows the regions in which the temperature distributions will be examined. Energy equations (3.131) to (3.135) remain unchanged for the regions 1 to 5 in the aquifer. In regions 6 and 7 in the clay cap the energy equations are:

Region 6

$$\theta^c_{yy} + \theta^c_{zz} = 0 \tag{3.200}$$

Region 7

$$ye^2\theta^c_{\hat{y}\hat{y}} + d^2\theta^c_{zz} = 0 \tag{3.201}$$

Besides (3.182) and (3.183), other boundary conditions for (3.200) are:

$$\theta^c_y(0,z) = 0 \tag{3.202}$$

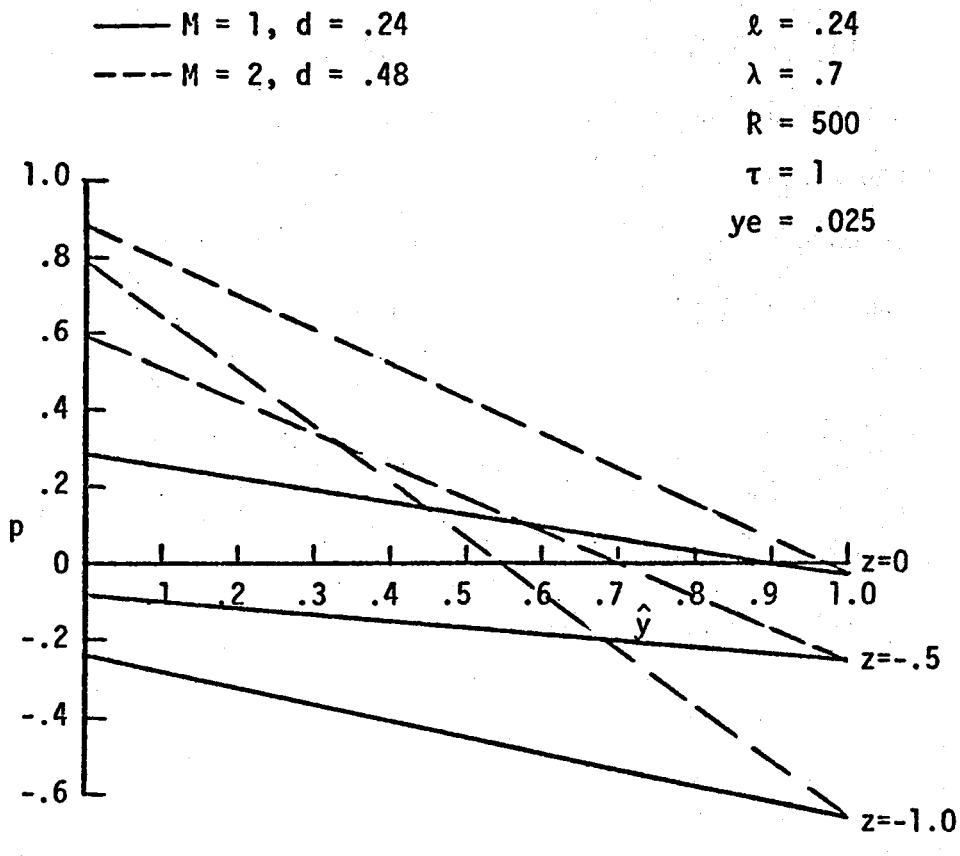

Figure 3.31 Effect of Mass Flow Rate on the Over Pressure vs. Length of the Aquifer at Different Depths

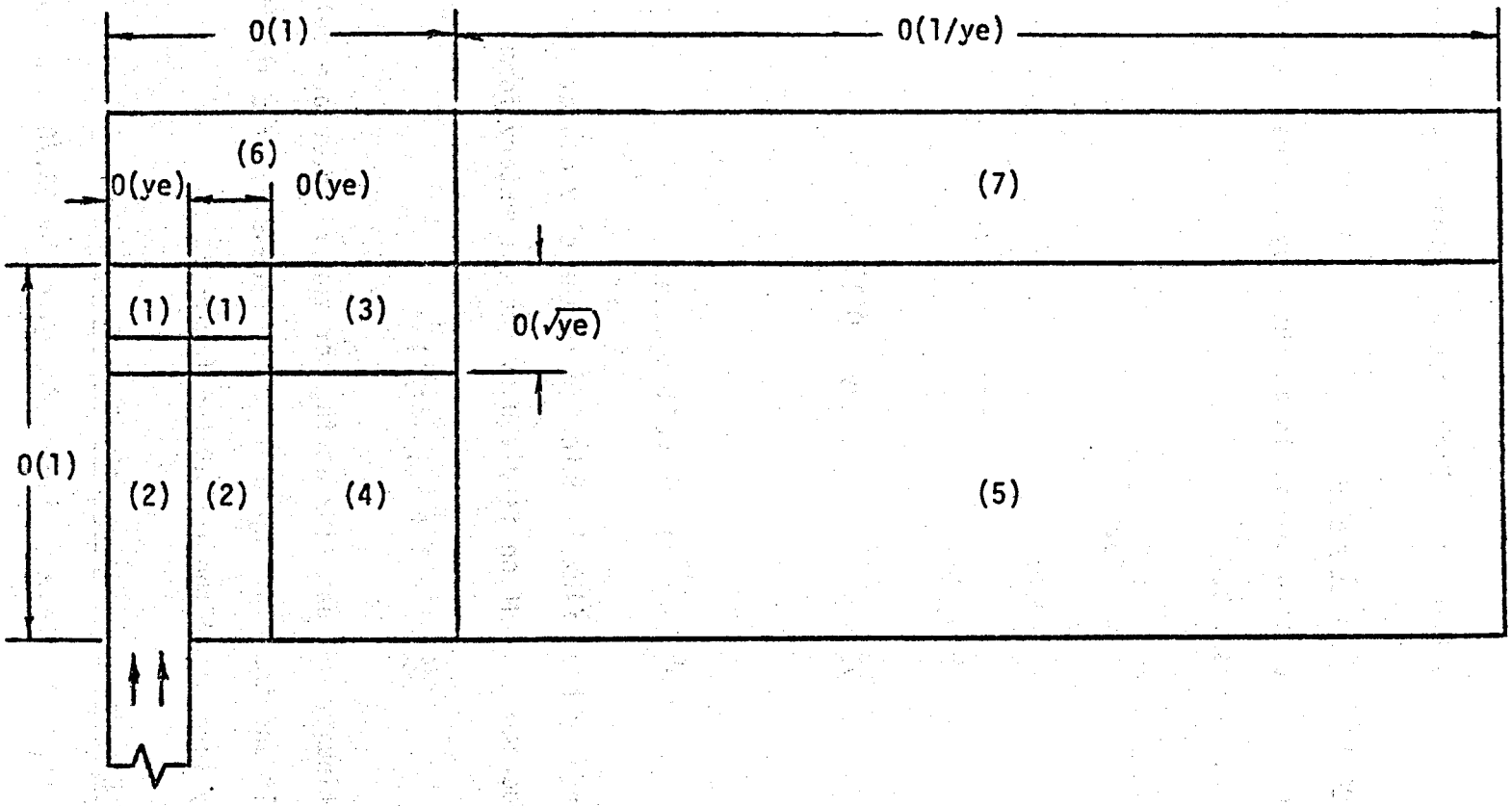

Figure 3.32 Different Regions in the Fault, Aquifer and the Clay Cap

$$\theta^c(y,\ell) = 1 \tag{3.203}$$

$$\theta^c(y\to\infty,z) = \text{Increases algebraically at most} \tag{3.204}$$

Solutions in Regions 1 and 6

The basic temperature field in the clay cap near the fault (region 6) is described by

$$\theta^c_{oyy} + \theta^c_{ozz} = 0 \tag{3.205}$$

$$\theta^c_{oy}(0,z) = 0 \tag{3.206}$$

$$\theta^c_o(y,\ell) = 1 \tag{3.207}$$

$$\theta^c_o(y,0) = 1 + \tau, \quad y = 0(1) \tag{3.208}$$

where

$\theta^c_o(y\to\infty,z)$ is well behaved.

Since no heat flux is entering in the clay cap at y = 0 face, the temperature solution is given by the elementary form,

$$\theta^c_o(z) = 1 + \tau(1 - z/\ell) \tag{3.209}$$

The continuity of heat flux at the horizontal interface between the fault and the clay cap implies the necessity of a thermal boundary layer near the top of the fault.

Thermal Boundary Layer near the Interface

Appropriate scale variables are given by (3.70) and corresponding boundary layer equations are given by (3.76)-(3.79).

Using the asymptotic expansions (3.80) and collecting the terms for O(1), O(ye) and O(ye^2), the results in (3.94), (3.96), (3.109) and (3.111) can again be derived. The lowest order solutions are given by

$$T_o = 1 + \tau \tag{3.210}$$

$$V_o = (a_2 - \frac{\lambda}{\lambda+\ell})\bar{y} \tag{3.211}$$

$$W_o = -(a_2 - \frac{\lambda}{\lambda+\ell})\bar{z} \tag{3.212}$$

$$P_o = d(a_2 - \frac{\lambda}{\lambda+\ell}) - \frac{\ell^2}{2(\lambda+\ell)} \tag{3.213}$$

The related pressure and velocity fields in the aquifer are:

$$p_o = (1 - \hat{y})\, d(a_2 - \frac{\lambda}{\lambda+\ell}) - \frac{\ell^2}{2(\lambda+\ell)} \tag{3.214}$$

$$v_o = (a_2 - \frac{\lambda}{\lambda+\ell}) \tag{3.215}$$

Equations, describing the O(ye) terms are:

$$V_{1\bar{y}} + W_{1\bar{z}} = 0 \tag{3.216}$$

$$P_{1\bar{y}} = 0 \tag{3.217}$$

$$- P_{1\bar{z}} + 1 = 0 \tag{3.218}$$

$$- \gamma^2(a_2 - \frac{\lambda}{\lambda+\ell})\bar{z}\,\frac{dT_1}{d\bar{z}} = \frac{d^2T_1}{d\bar{z}^2} \tag{3.219}$$

Boundary conditions are:

$$V_1\ (\pm 1, \bar{z}) = \pm \frac{b_2\bar{z}}{\sqrt{d}} \tag{3.220}$$

$$W_1\ (\bar{y},\bar{z}\to-\infty) = -\frac{b_2}{2\sqrt{d}}\bar{z}^2 \tag{3.221}$$

$$P_1\ (\bar{y},\bar{z}\to-\infty) = \bar{z} \tag{3.222}$$

$$\frac{dT_1}{d\bar{z}}\ (\bar{y},0) = -\frac{\tau\lambda}{\ell} \tag{3.223}$$

$$T_1\ (\bar{y},\bar{z}\to-\infty) = 0 \tag{3.224}$$

Solutions of this system are:

$$V_1 = \frac{b_2}{\sqrt{d}}\bar{y}\bar{z} \tag{3.225}$$

$$W_1 = -\frac{b_2}{2\sqrt{d}}\bar{z}^2 \tag{3.226}$$

$$P_1 = \bar{z} \tag{3.227}$$

$$T_1 = -\frac{\sqrt{\pi}\,\tau\lambda}{2B\ell}\{1 + \text{erf}\,(B\bar{z})\} \tag{3.228}$$

where $$B = \sqrt{\frac{\gamma^2}{2}(a_2 - \lambda/\lambda+\ell)} \tag{3.229}$$

Associated pressure and velocity fields in the aquifer are

$$p_1 = b_2\sqrt{d}\,\bar{z}\,(1-\hat{y}) + \frac{\ell\bar{z}}{\lambda+\ell} \tag{3.230}$$

$$v_1 = \frac{b_2}{\sqrt{d}}\bar{z} \tag{3.231}$$

The above results can be used in (3.80) to give

$$\bar{V} = (a_2 - \frac{\lambda}{\lambda+\ell})\bar{y} + ye\,\frac{b_2}{\sqrt{d}}\,\bar{z}\bar{y} + O(ye^2) \tag{3.232}$$

$$\bar{W} = -(a_2 - \frac{\lambda}{\lambda+\ell})\bar{z} - ye\,\frac{b_2\bar{z}^2}{2\sqrt{d}} + O(ye^2) \tag{3.233}$$

$$P = d(a_2 - \frac{\lambda}{\lambda+\ell}) - \frac{\ell^2}{2(\lambda+\ell)} + ye\,\bar{z} + O(ye^2) \tag{3.234}$$

$$T = 1 + \tau - ye\,\frac{\sqrt{\pi}\,\tau\lambda}{2B\ell}\left[1 + \mathrm{erf}\,(B\bar{z})\right] + O(ye^2) \tag{3.235}$$

$$v(\bar{z}) = (a_2 - \frac{\lambda}{\lambda+\ell}) + ye\,\frac{b_2}{\sqrt{d}}\,\bar{z} + O(ye^2) \tag{3.236}$$

$$p(\hat{y},\bar{z}) = d(a_2 - \frac{\lambda}{\lambda+\ell})(1-\hat{y}) - \frac{\ell^2}{2(\lambda+\ell)} + ye\left[b_2\sqrt{d}\,\bar{z}(1-\hat{y}) + \frac{\ell\bar{z}}{\lambda+\ell}\right] + O(ye^2) \tag{3.237}$$

Note that equations (3.232)-(3.235) are valid in the fault zone only, i.e., $-1 \le \bar{y} \le 1$. Solutions of (3.132) and (3.134) for the regions 2 and 4 are given by (3.161) and (3.170), respectively. The solution structure for $1 \le \bar{y} \le \infty$ (the aquifer) appears to be more complex and will not be considered further because reasonable progress can be made without them.

It is possible to obtain a similarity solution for region 3, where similarity variable is defined as follows.

$$\eta = z^*/y^{1/2} \tag{3.238}$$

Let

$$\theta(y,z^*) = 1 + \tau + (y\ ye)^{1/2}\theta_1(\eta) + O(ye) \qquad (3.239)$$

Equation (3.192), when expressed in terms of z^*, is as follows:

$$v(z^*) = (a_2 - \frac{\lambda}{\lambda+\ell}) + O(ye^{1/2}) \qquad (3.240)$$

Substitution of (3.239) in the O(1) terms of (3.133) results in the following equation for θ_1.

$$B^2(\theta_1 - \eta \frac{d\theta_1}{d\eta}) = \frac{d^2\theta_1}{d\eta^2} \qquad (3.241)$$

Boundary conditions on θ_1 are

$$\frac{d\theta_1}{d\eta}(\eta = 0) = -\frac{\tau\lambda}{\ell} \qquad (3.242)$$

$$\theta_1(\eta \to -\infty) = 0 \qquad (3.243)$$

Equation (3.242) represents the continuity of the heat flux at the interface between regions 3 and 6. The solution of the system (3.241)-(3.243) is

$$\theta_1(\eta) = -\frac{\tau\lambda\sqrt{2}}{\ell B\sqrt{\pi}}\left[\sqrt{\frac{\pi}{2}}\, B\eta \{1 + \mathrm{erf}(\frac{B}{\sqrt{2}}\eta)\} + e^{-\frac{B^2}{2}\eta^2}\right] \qquad (3.244)$$

Then the temperature in the region 3, obtained from (3.239) and (3.244) is

$$\theta(y,z^*) = 1 + \tau - (\frac{2\,y\ ye}{\pi})^{1/2}\frac{\tau\lambda}{B\ell}\left[\sqrt{\frac{\pi}{2}}\frac{Bz^*}{y^{1/2}}\{1 + \mathrm{erf}(\frac{B}{\sqrt{2}}\frac{z^*}{y^{1/2}})\} + e^{-\frac{B^2 z^{*2}}{2y}}\right] + O(ye) \qquad (3.245)$$

It follows that the interface temperature in regions 1 and 3 are:

$$T(\bar{y},0) = 1 + \tau - \frac{ye\sqrt{\pi}\,\tau\lambda}{2B\ell} + O(ye^2), \quad -1 \le \bar{y} \le 1 \tag{3.246}$$

$$\theta(y,0) = 1 + \tau - (y\,ye)^{1/2}\sqrt{\frac{2}{\pi}}\,\frac{\tau\lambda}{B\ell} + O(ye) \tag{3.247}$$

Temperatures in the region 6 for $|\bar{y}| \le 1$ can be expressed as

$$\theta^c(y,z) = \theta_0^c(z) + ye\,\theta_1^c(y,z) + O(ye^2) \tag{3.248}$$

where $\theta_0^c(z)$ is given by (3.209).

The first order correction is described by the equations obtained from (3.248), (3.200), (3.202), (3.203) and (3.246).

$$\theta_{1yy}^c + \theta_{1zz}^c = 0 \tag{3.249}$$

$$\theta_{1y}^c(0,z) = 0 \tag{3.250}$$

$$\theta_1^c(y,\ell) = 0 \tag{3.251}$$

$$\theta_1^c(y,0) = -\frac{\sqrt{\pi}\,\tau\lambda}{2B\ell} \qquad |\bar{y}| \le 1 \tag{3.252}$$

Also $\theta_1^c(y\to\infty,z)$ should be well behaved. Again using the same argument, as used to derive (3.209), the solution of the above system is

$$\theta_1^c(z) = -\frac{\sqrt{\pi}\,\tau\lambda}{2B\ell}(1 - z/\ell), \quad |\bar{y}| \le 1 \tag{3.253}$$

From (3.209), (3.248) and (3.253), one obtains

$$\theta^c(y,z) = 1 + \tau\left(1 - \frac{z}{\ell}\right) - ye\,\frac{\sqrt{\pi}\,\tau\lambda}{2B\ell}\left(1 - \frac{z}{\ell}\right) + O(ye^2), \quad |\bar{y}| \le 1 \tag{3.254}$$

Solutions (3.235) and (3.254) are plotted in Figures 3.33-3.38 where the effect of the parameters ℓ, λ, M, R, τ and ye on the temperature is shown. It should be noted that the vertical scale used in the cap is different than that used in the fault zone.

Figure 3.33 shows the effect of cap thickness on the temperatures in the fault and the cap. Temperatures in the aquifer increase with increasing cap thickness because of increased resistance to the heat flow in the cap.

Effect of the thermal conductivity ratio (λ) on the temperatures in the fault and the cap is shown in Figure 3.34. Temperatures are found to decrease with increasing λ because of the relative increase in the heat transfer. For $\lambda = 1$ the slope is continuous at $z = 0$ when the scale change in Figure 3.34 is considered. Figure 3.35 shows the effect of mass flow rate on the temperatures in the fault and the cap. Higher mass flow rate gives rise to higher temperatures as expected. Effect of R and τ on the temperatures in the fault and the cap is shown in Figures 3.36 and 3.37, respectively. Temperatures are found to decrease for lower values of R and τ as expected.

Figure 3.38 shows the effect of the fault half width on the temperatures in the fault and the cap. As obvious from (3.235) and (3.254), temperatures decrease with increased ye.

Equation (3.247) implies that the temperature in region 6 can be written as

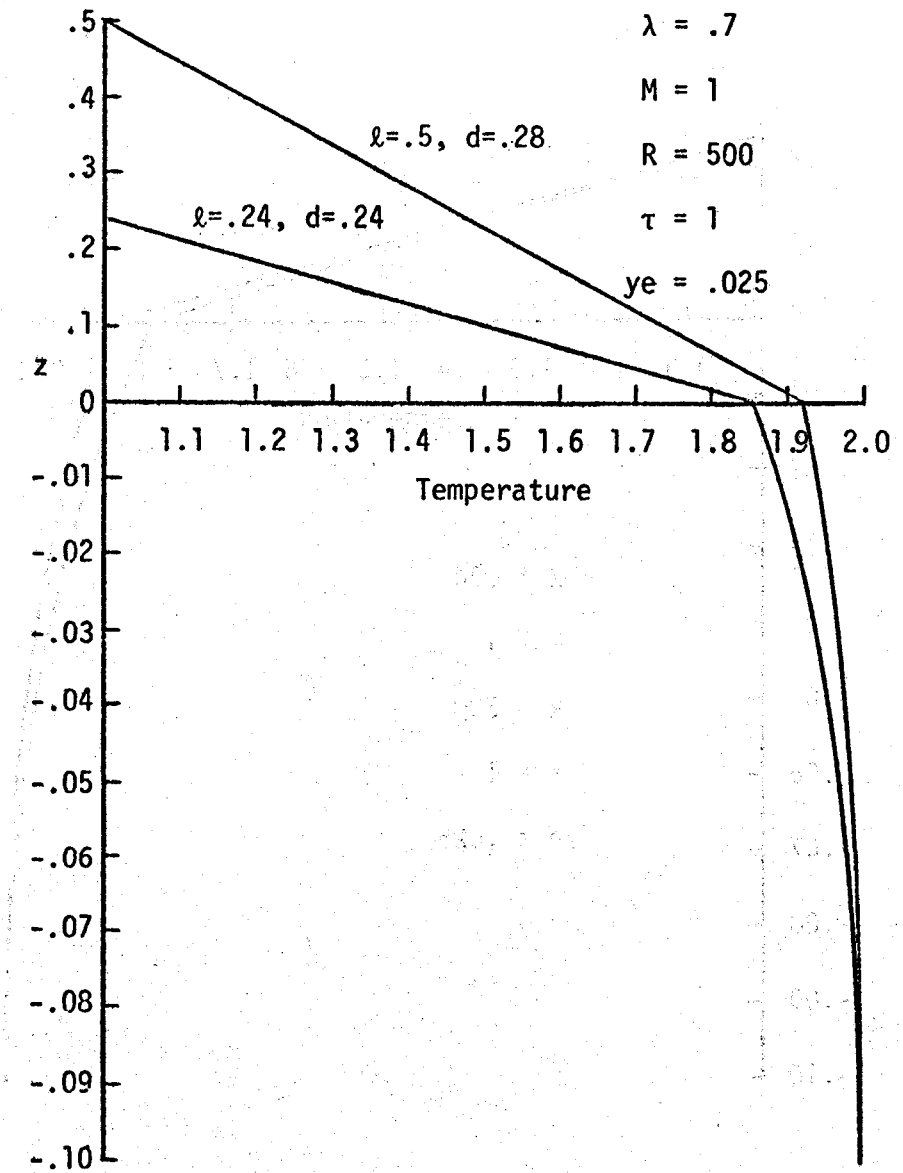

Figure 3.33 Effect of Cap Thickness on the Temperatures in the Fault and the Cap as per Depth

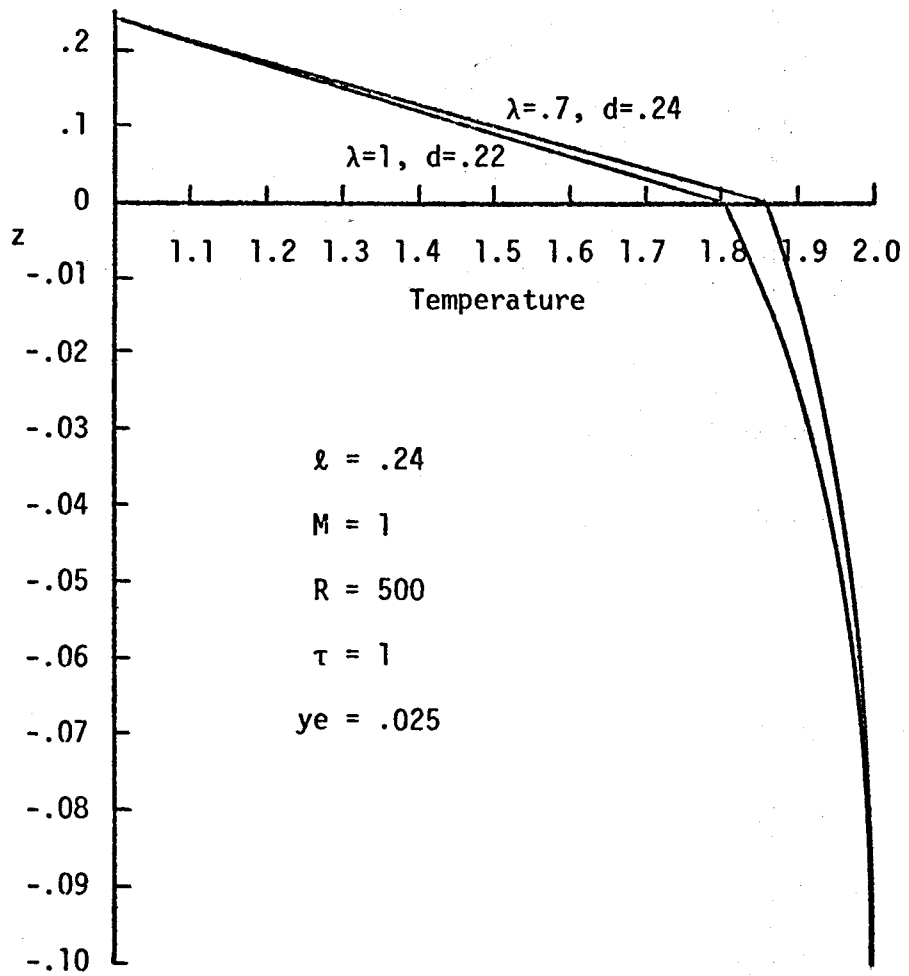

Figure 3.34 Effect of Thermal Conductivity Ratio on the Temperatures in the Fault and the Cap vs. Depth

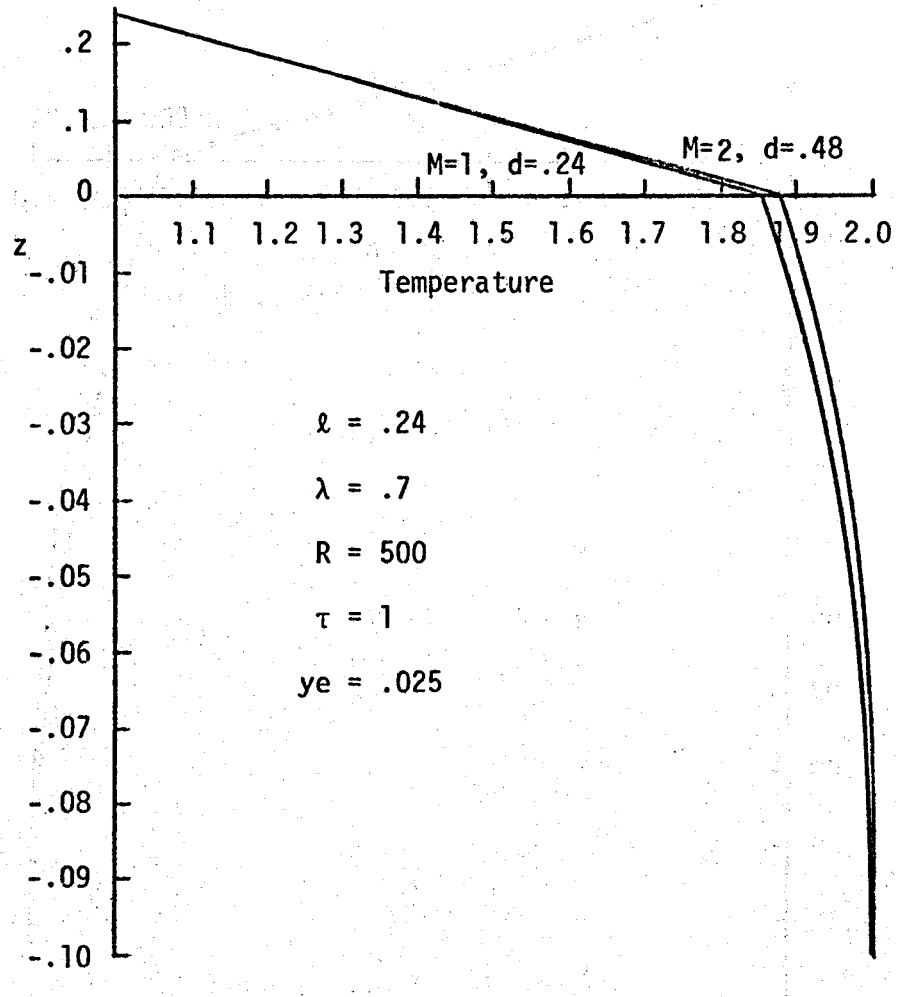

Figure 3.35 Effect of Mass Flow Rate on the Temperatures in the Fault and the Cap as per Depth

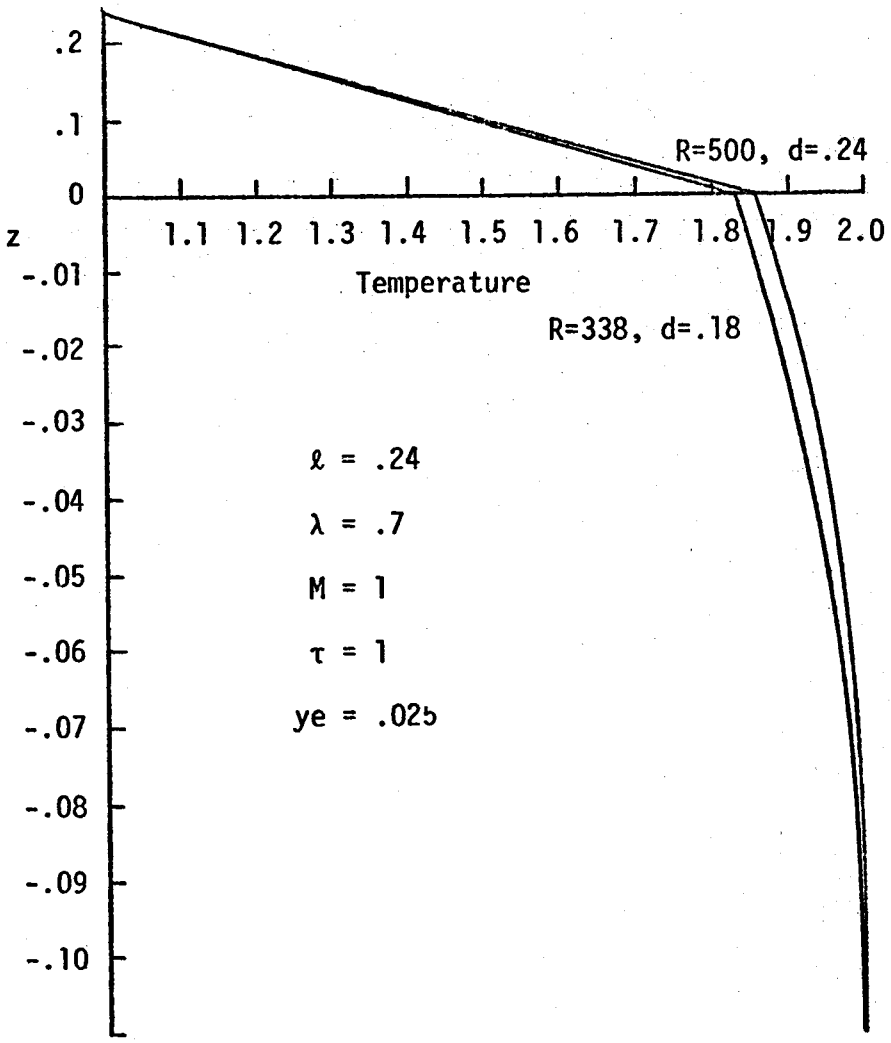

Figure 3.36 Effect of Rayleigh Number on the Temperature in the Fault and the Cap as per Depth

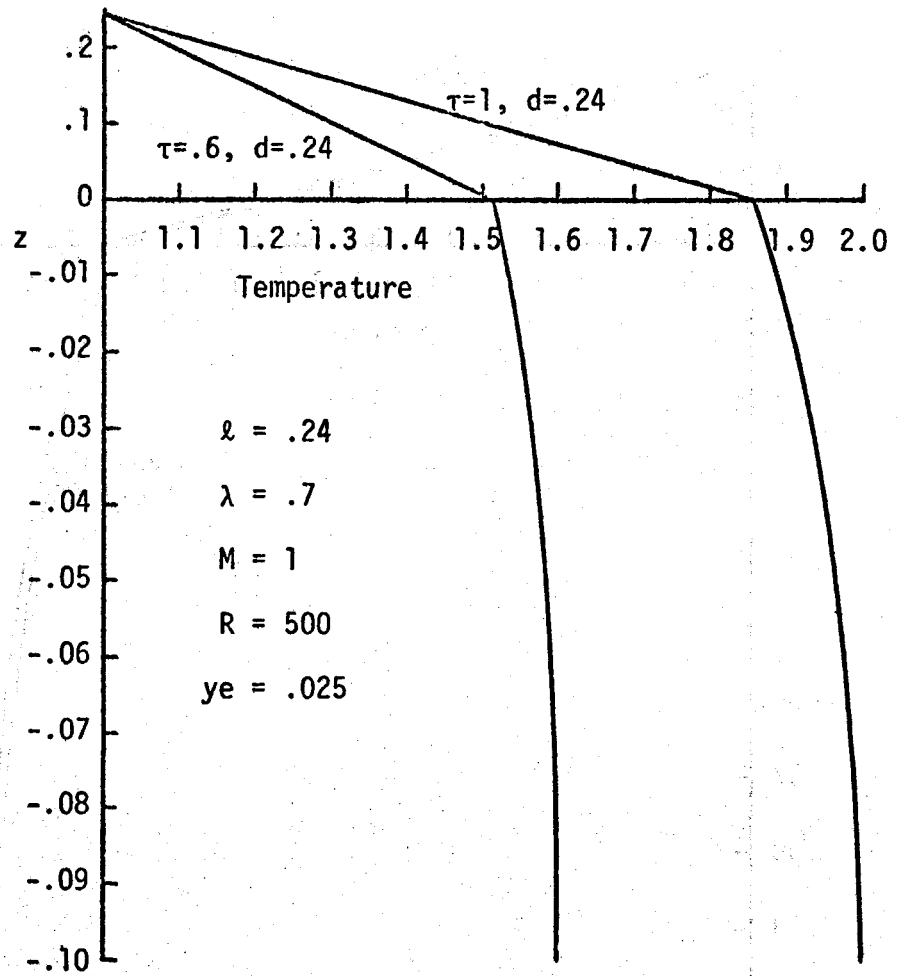

Figure 3.37 Effect of τ on the Temperature in the Fault and the Cap as per Depth

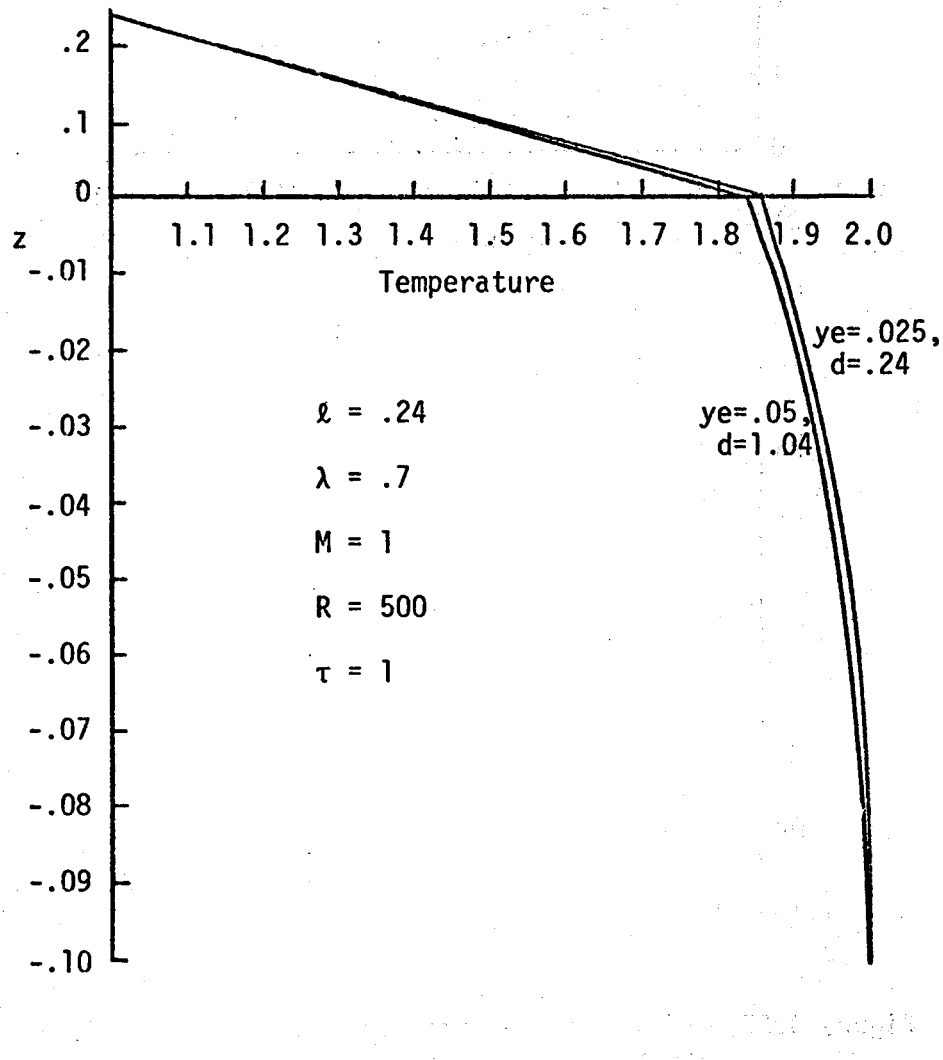

Figure 3.38 Effect of Semi-Fault Width on the Temperatures in the Fault and the Cap as per Depth

$$\theta^c(y,z) = \theta_o^c(z) + ye^{1/2}\sqrt{\frac{2}{\pi}}\frac{\tau\lambda}{B\ell}\theta_2^c(y,z) + O(ye) \tag{3.255}$$

where $\theta_o^c(z)$ is given by (3.209).

It follows from (3.200), (3.202)-(3.204), (3.247) and (3.255) that

$$\theta_{2yy}^c + \theta_{2zz}^c = 0 \tag{3.256}$$

$$\theta_2^c(y,\ell) = 0 \tag{3.257}$$

$$\theta_2^c(y,0) = -\sqrt{y} \tag{3.258}$$

$$\theta_2^c(0,z) = 0 \tag{3.259}$$

$$\theta_2^c(y\to\infty,z) \text{ is non-exponential} \tag{3.260}$$

Boundary condition (3.259) shows that $O(ye^{1/2})$ correction vanishes as $y \to 0$.

A solution for θ_2^c can be found by using the Fourier sine integral transform with respect to y.

The solution is

$$\theta_2^c(y,z) = -\frac{1}{2\ell}\left[\int_0^\infty \frac{\sin\frac{\pi}{\ell}(\ell-z)\,\xi^{1/2}\,d\xi}{\cosh\frac{\pi}{\ell}(|y-\xi|) + \cos\frac{\pi}{\ell}(\ell-z)} - \int_0^\infty \frac{\sin\frac{\pi}{\ell}(\ell-z)\,\xi^{1/2}\,d\xi}{\cosh\frac{\pi}{\ell}(y+\xi) + \cos\frac{\pi}{\ell}(\ell-z)}\right] \tag{3.261}$$

A series solution also obtained for the above system, is as follows:

$$\theta_2^c(y,z)$$

$$= \frac{1}{\ell} \sum_{n=1}^{\infty} \frac{1}{(-1)^n} \sin \frac{n\pi}{\ell}(\ell - z) \int_0^{\infty} \xi^{1/2} \left[e^{-\frac{n\pi}{\ell}(|y-\xi|)} - e^{-\frac{n\pi}{\ell}(y+\xi)} \right] d\xi \tag{3.262}$$

It is also possible to obtain an asymptotic solution for the system (3.256)-(3.260) for large values of y. As is clear from (3.258), the leading term of the solution should be of $O(y^{1/2})$. Let

$$\theta_2^c(y,z) = -y^{1/2}\,\theta_{21}^c(z) + \theta_{22}^c(y,z) + \ldots \tag{3.263}$$

Substitution of (3.263) in (3.256)-(3.260) results in the following system of equations:

$$\frac{1}{4y^{3/2}}\,\theta_{21}^c(z) + \theta_{22}^c yy - y^{1/2}\,\theta_{21}^c zz + \theta_{22}^c zz = 0 \tag{3.264}$$

$$\theta_{21}^c(\ell) = 0 \tag{3.265}$$

$$\theta_{21}^c(0) = 1 \tag{3.266}$$

$$\theta_{22}^c(y,\ell) = 0 \tag{3.267}$$

$$\theta_{22}^c(y,0) = 0 \tag{3.268}$$

$$\theta_{22}^c(y \to \infty, z) = \text{Bounded} \tag{3.269}$$

Boundary condition (3.259) is not to be satisfied since this solution is applicable for large values of y only. Solutions of the above system are:

$$\theta_{21}^{c}(z) = 1 - z/\ell \tag{3.270}$$

$$\theta_{22}^{c}(y,z) = \frac{1}{24y^{3/2}}\left[-3z^2 + \frac{z^3}{\ell} + 2\ell z\right] \tag{3.271}$$

which give

$$\theta_{2}^{c}(y\to\infty,z) = -y^{1/2}(1 - \tfrac{z}{\ell}) + \frac{1}{24\ y^{3/2}}\left[-3z^2 + \frac{z^3}{\ell} + 2\ell z\right] + O(\frac{1}{y^{7/2}}) \tag{3.272}$$

Equation (3.272) can also be obtained by expanding (3.262) for large values of y. If (3.209), (3.255) and (3.272) are combined, one can show that the temperatures in the cap for large values of y are described by

$$\theta^{c}(y\to\infty,z) = 1 + \tau(1 - \tfrac{z}{\ell}) + ye^{1/2}\sqrt{\frac{2}{\pi}}\frac{\tau\lambda}{B\ell}\left[-y^{1/2}(1 - \tfrac{z}{\ell}) + \frac{1}{24y^{3/2}}(-3z^2 + \frac{z^3}{\ell} + 2\ell z) + O(\frac{1}{y^{7/2}})\right] + O(ye) \tag{3.273}$$

Values of θ_2^c, obtained from (3.261) and (3.272), are plotted in Figure 3.39 for different values of y and at different depths of the cap. It is seen that the exact solution (3.261) approaches the asymptotic solution (3.272) and finally merges in it for $y > 1$. Figure 3.40 shows the temperatures in the regions 6, 3 and 4 for different values of y.

Temperatures in the region 7 can be obtained by solving (3.201). The O(1) temperatures are given by the following expression.

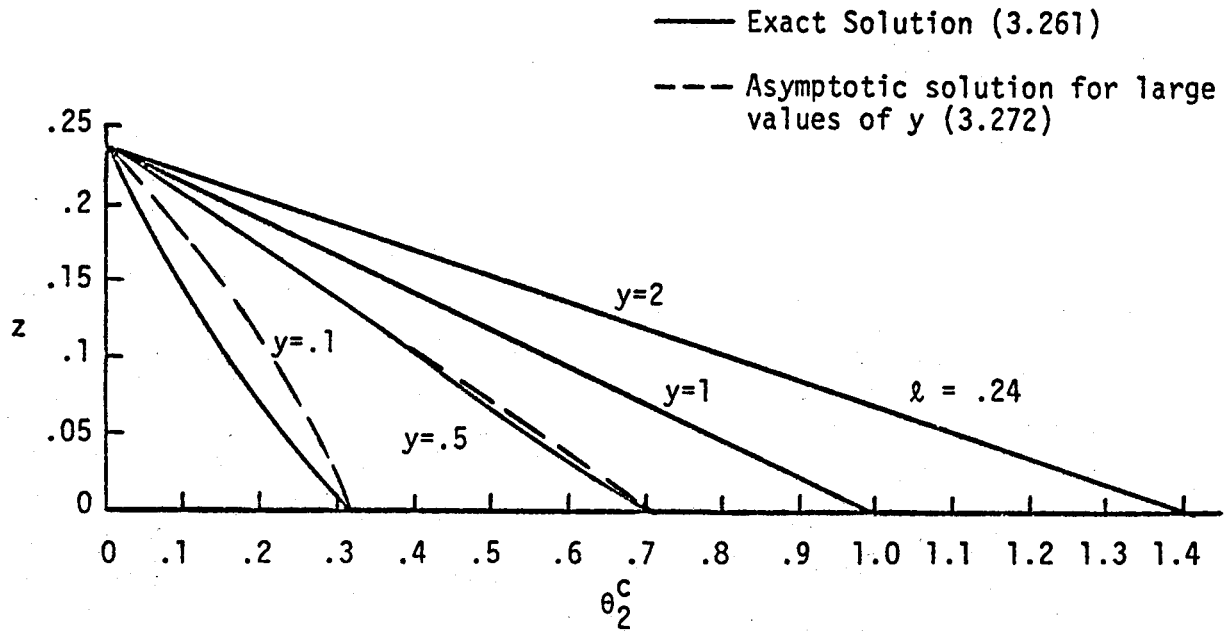

Figure 3.39 Matching of the Exact and the Asymptotic Solutions

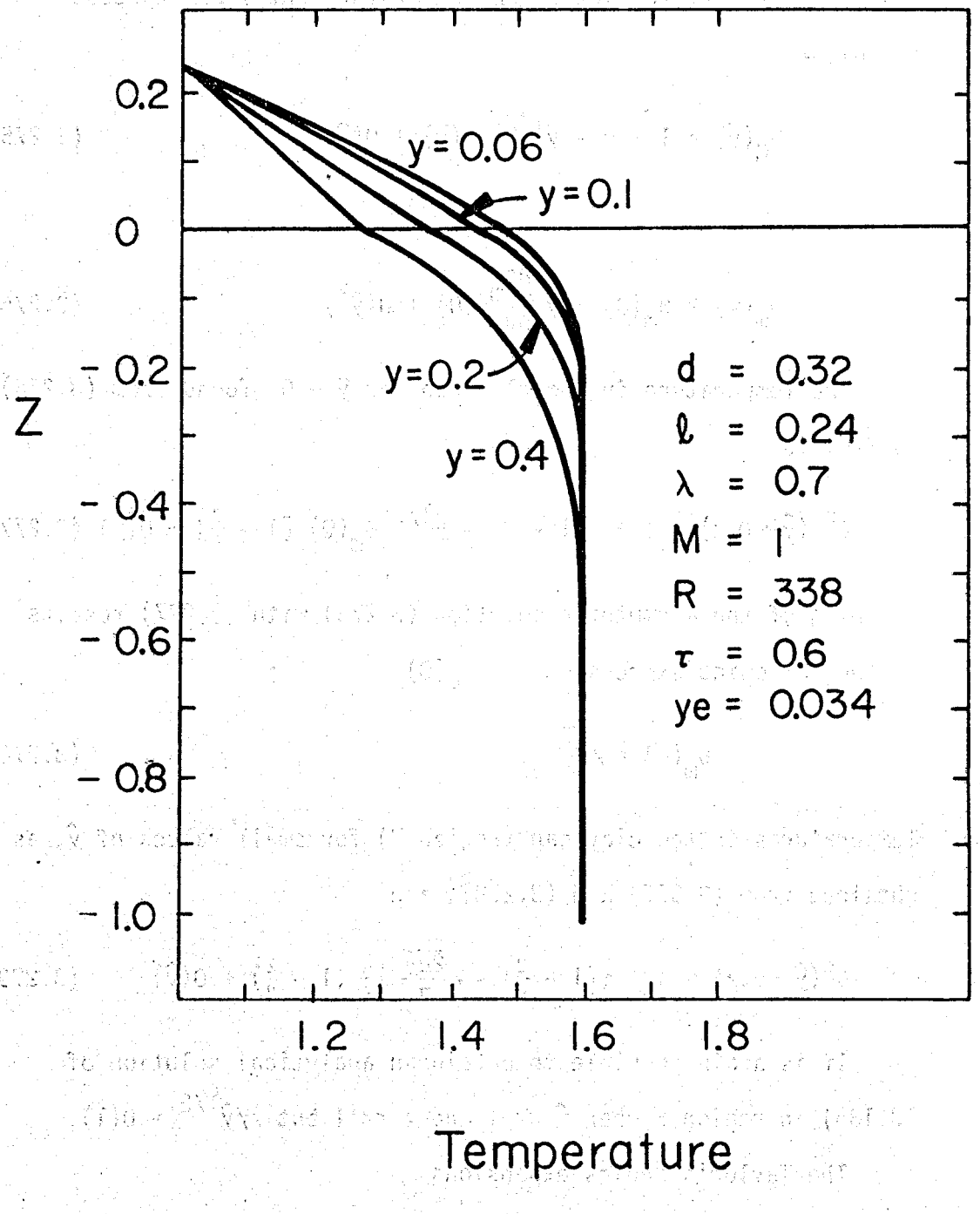

Figure 3.40 Near Fault Temperatures in the Aquifer and the Cap for Different Values of y.

$$\theta^c(\hat{y},z) = \theta_M(\hat{y}) + \frac{z}{\ell}[1 - \theta_M(\hat{y})] \tag{3.274}$$

For <u>small</u> $\hat{y}$, let the interface temperature $\theta_M(\hat{y})$ be expressed as follows:

$$\theta_M(\hat{y}) = 1 + \tau - \hat{y}^{1/2}\,\theta_m(\hat{y}) + O(\hat{y}) \tag{3.275}$$

where

$$\theta_m(\hat{y}) = \theta_m(0) + \hat{y}\,\frac{d\theta_m}{d\hat{y}}(0) + O(\hat{y}^2) \tag{3.276}$$

The temperature in the clay cap for $\hat{y} \to 0$, found from (3.274)-(3.276) is

$$\theta^c(\hat{y}\to 0,z) = 1 + \tau(1 - \tfrac{z}{\ell}) - \hat{y}^{1/2}\,\theta_m(0)\,[1 - \tfrac{z}{\ell}] + O(\hat{y}) \tag{3.277}$$

Matching of the asymptotic solution (3.273) with (3.277) results in the following expression for $\theta_m(0)$.

$$\theta_m(0) = \sqrt{\frac{2d}{\pi}}\,\frac{\tau\lambda}{B\ell} \tag{3.278}$$

Temperatures in the clay cap (region 7) for small values of $\hat{y}$, as obtained from (3.277) and (3.278), are

$$\theta^c(\hat{y}\to o,z) = 1 + \tau(1 - \tfrac{z}{\ell}) - \sqrt{\frac{2d\hat{y}}{\pi}}\,\frac{\tau\lambda}{B\ell}\,(1 - \tfrac{z}{\ell}) + O(\hat{y}) \tag{3.279}$$

If is again possible to obtain an analytical solution of (3.135) in region 5 when $\hat{y} \ll 1$ and $z \ll 1$ but $z/\hat{y}^{1/2} = O(1)$.

The Taylor's series expansions

$$v(z \to 0) = (a_2 - \frac{\lambda}{\lambda+\ell}) + \frac{b_2}{\sqrt{d}}\,z + \frac{a_2}{2d}\,z^2 + \ldots \tag{3.280}$$

are used to describe the velocity field. The temperature field is expressed as

$$\theta(\hat{y},z) = 1 + \tau + \hat{y}^{1/2}\,\theta_1(\eta) + O(\hat{y}) \tag{3.281}$$

where η is given by (3.174).

Then from (3.135), (3.279), (3.280) and (3.281) one finds

$$\frac{d^2\theta_1}{d\eta^2} + \frac{B^2}{d}\,\eta\,\frac{d\theta_1}{d\eta} - \frac{B^2}{d}\,\theta_1 = 0 \tag{3.282}$$

$$\theta_1(\eta = 0) = -\sqrt{\frac{2d}{\pi}}\,\frac{\tau\lambda}{B\ell} \tag{3.283}$$

$$\theta_1(\eta \to -\infty) = 0 \tag{3.284}$$

The solution is

$$\theta_1(\eta) = -\sqrt{\frac{2d}{\pi}}\,\frac{\tau\lambda}{B\ell}\left[\frac{B\sqrt{\pi}}{\sqrt{2d}}\,\eta\,\{1 + \operatorname{erf}\,(\frac{B}{\sqrt{2d}}\,\eta)\} + e^{-\frac{B^2}{2d}\eta^2}\right] \tag{3.285}$$

Substitution of (3.285) into (3.281) results in the following expression for the temperature in the aquifer (region 5) for small values of $\hat{y}$.

$$\theta(\hat{y},z) = 1 + \tau - \sqrt{\frac{2d\hat{y}}{\pi}}\,\frac{\tau\lambda}{B\ell}\left[\frac{Bz}{\hat{y}^{1/2}}\sqrt{\frac{\pi}{2d}}\,\{1 + \operatorname{erf}\,(\frac{B}{\sqrt{2d}}\,\frac{z}{\hat{y}^{1/2}})\} + e^{-\frac{B^2}{2d}\frac{z^2}{\hat{y}}}\right] + O(\hat{y}) \tag{3.286}$$

It may be noted that (3.286) matches with (3.245) of region 3. Once the initial condition (3.286) is known, temperatures in the region 5 can be obtained by the numerical integration of the parabolic equation (3.135) for the following boundary conditions.

$$\theta(\hat{y},0) = \theta_M(\hat{y}) \tag{3.287}$$

$$\theta(\hat{y},-1) = 1 + \tau \tag{3.288}$$

Interface temperature $\theta_M(\hat{y})$ is calculated at each step of $\hat{y}$ for the continuous heat flux and the temperature. For an assumed initial value of the interface temperature, equations (3.135) and (3.274) are solved simultaneously and a successive value of $\theta_M(\hat{y})$ is calculated. The actual interface temperature is obtained when the difference between the two successive values is negligibly small. Code CLAYCAP, given in Appendix B is used to obtain the interface temperature

Figure 3.41 shows the temperatures in the cap and the aquifer for different locations of $\hat{y}$ and z. Again $\hat{y} = 1$ represents the far end of the aquifer. The value of d used for this case is already corrected for the parameters shown in the figure. Again, a trend similar to Figure 3.19 is seen here.

Isotherms, related to the temperatures of Figure 3.41, are plotted in Figure 3.42. Cap surface temperature gradients for this case are plotted in Figure 3.43. Discontinuity in the slope in Figure 3.43 arises because the solutions in the two regions are known to different orders.

Figure 3.44 shows the effect of cap thickness on the surface temperature gradients for all values of y. A thicker cap, providing a higher resistance to heat flow, will reduce the heat transfer to the surface. As expected, surface temperature

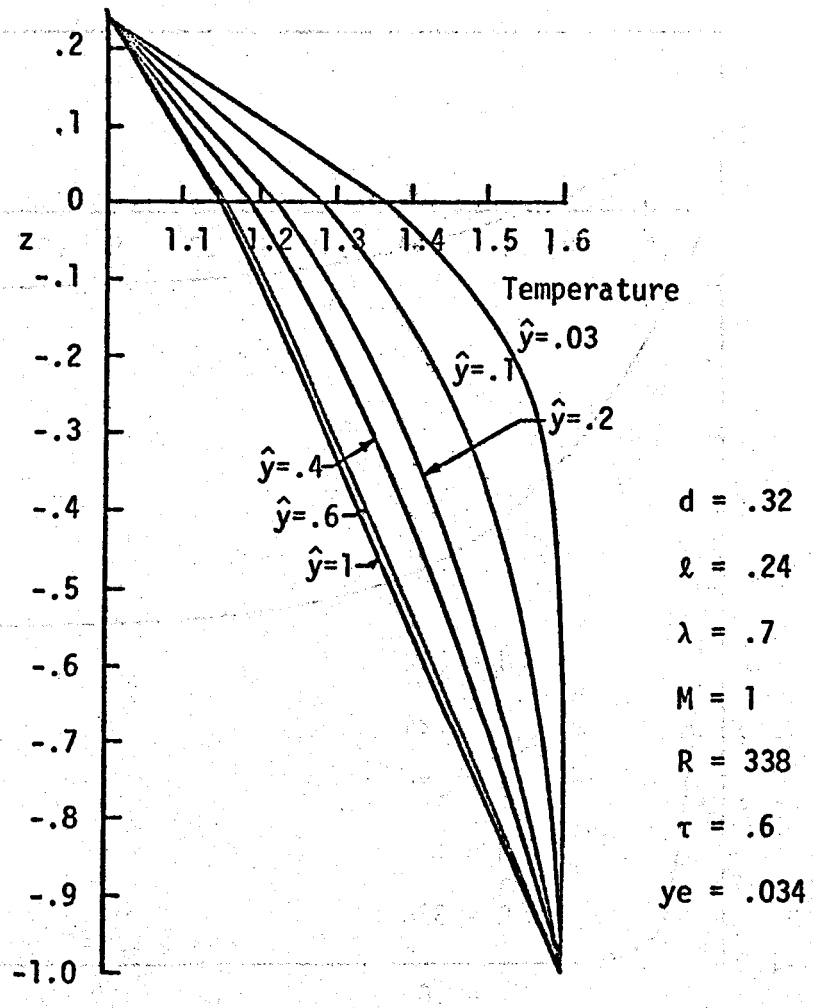

Figure 3.41 Temperature in the Aquifer and the Clay Cap at Different Locations away from the Fault

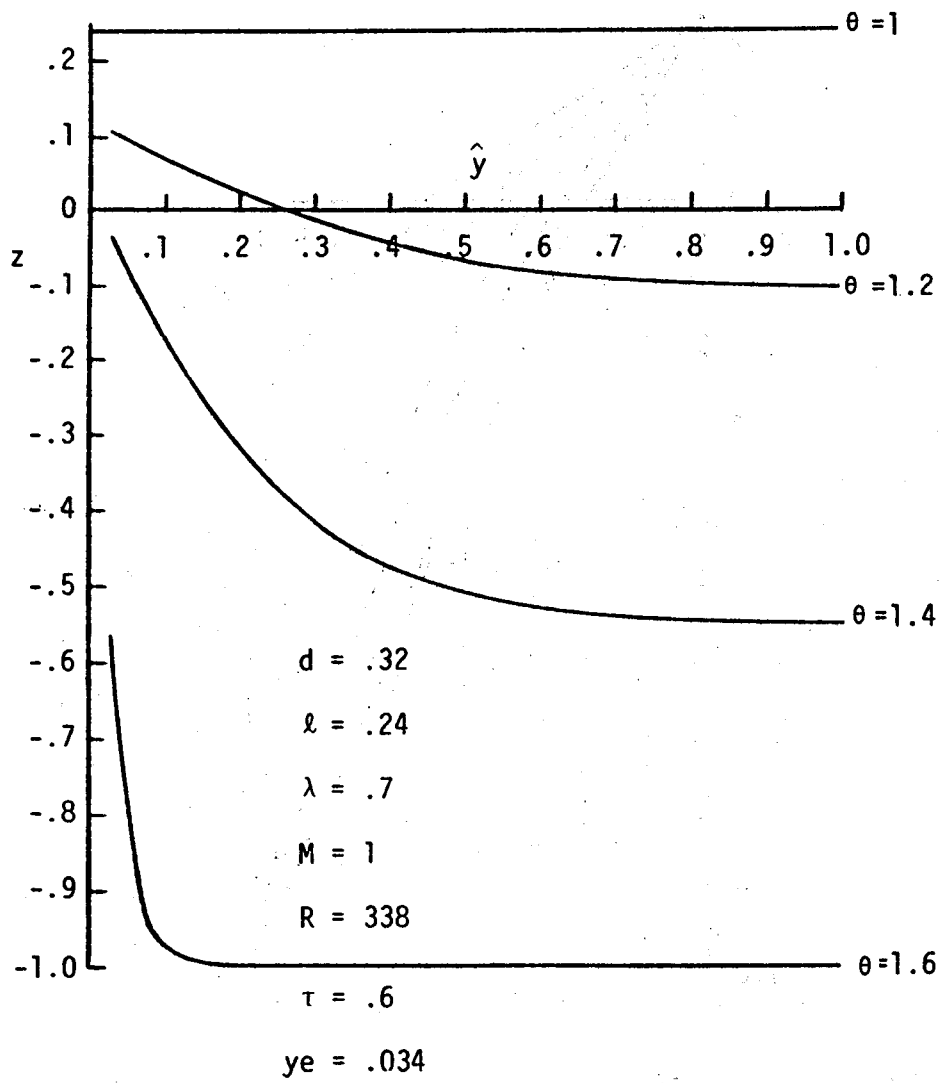

Figure 3.42 Isotherms in the Aquifer and the Clay Cap

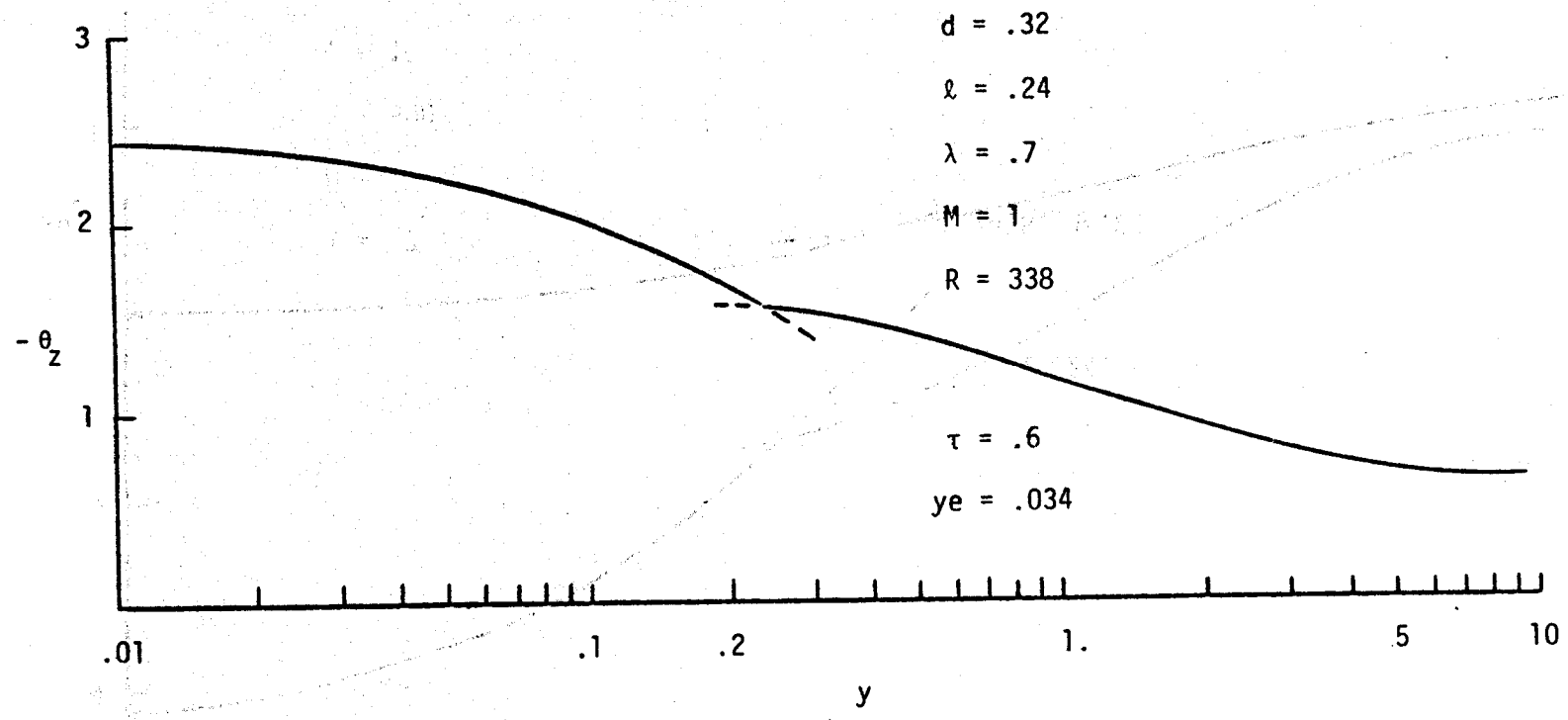

Figure 3.43 Surface Temperature Gradients vs. Length of the Aquifer

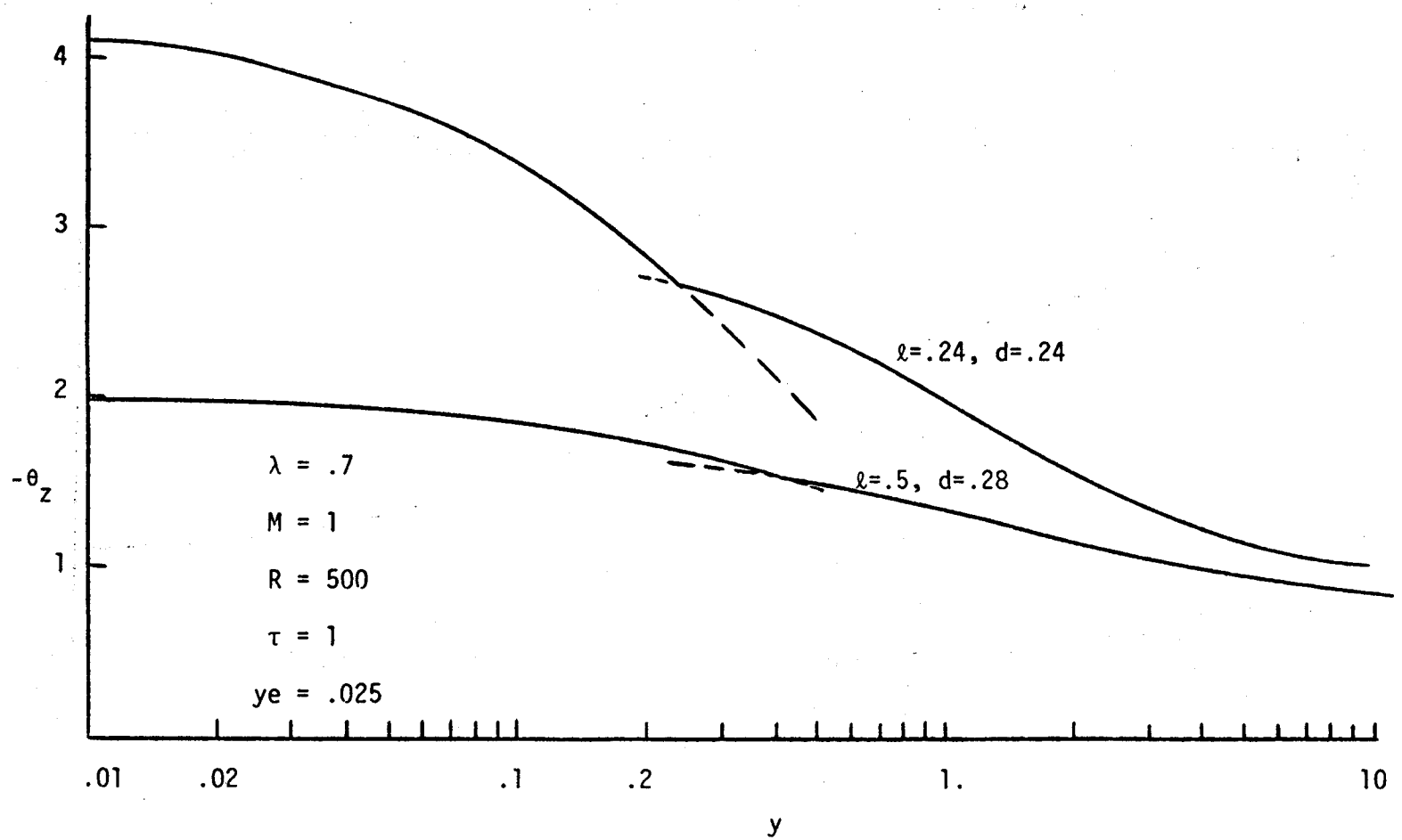

Figure 3.44 Effect of Cap Thickness on the Surface Temperature Gradients Along the Length of the Aquifer

gradients are lower for higher cap thickness.

Effect of thermal conductivity ratio (λ) on the surface temperature gradients is shown in Figure 3.45. It may be seen that the gradients at the surface are lower for higher values of λ. An increase in λ increases the heat transfer to the surface and thus reduces the temperatures in the cap and the aquifer. Lower temperatures, in turn, give rise to lower temperature gradients as confirmed by the Figure 3.45.

Figures 3.46, 3.47, 3.48 and 3.49 show the effects of M, R, τ and ye on the surface heat flux. As expected, an increase in M, R, τ and ye enhances the temperature gradients at the surface.

3.6 Conclusions and Remarks

A mathematical model for fault zone controlled charging of a geothermal reservoir is developed. The model is used to describe:

(A) A reservoir extending to the earth's surface with an impermeable upper boundary, and

(B) A reservoir covered by an impermeable clay rich layer like that at East Mesa.

A quasi-analytic theory is developed for high Rayleigh number convection of a liquid in a rigid porous medium. In this approximation liquid rises up the fault and spreads into the near regions of the reservoir adiabatically. The cooling effect of the cap in the reservoir is confined to a thin layer adjacent to

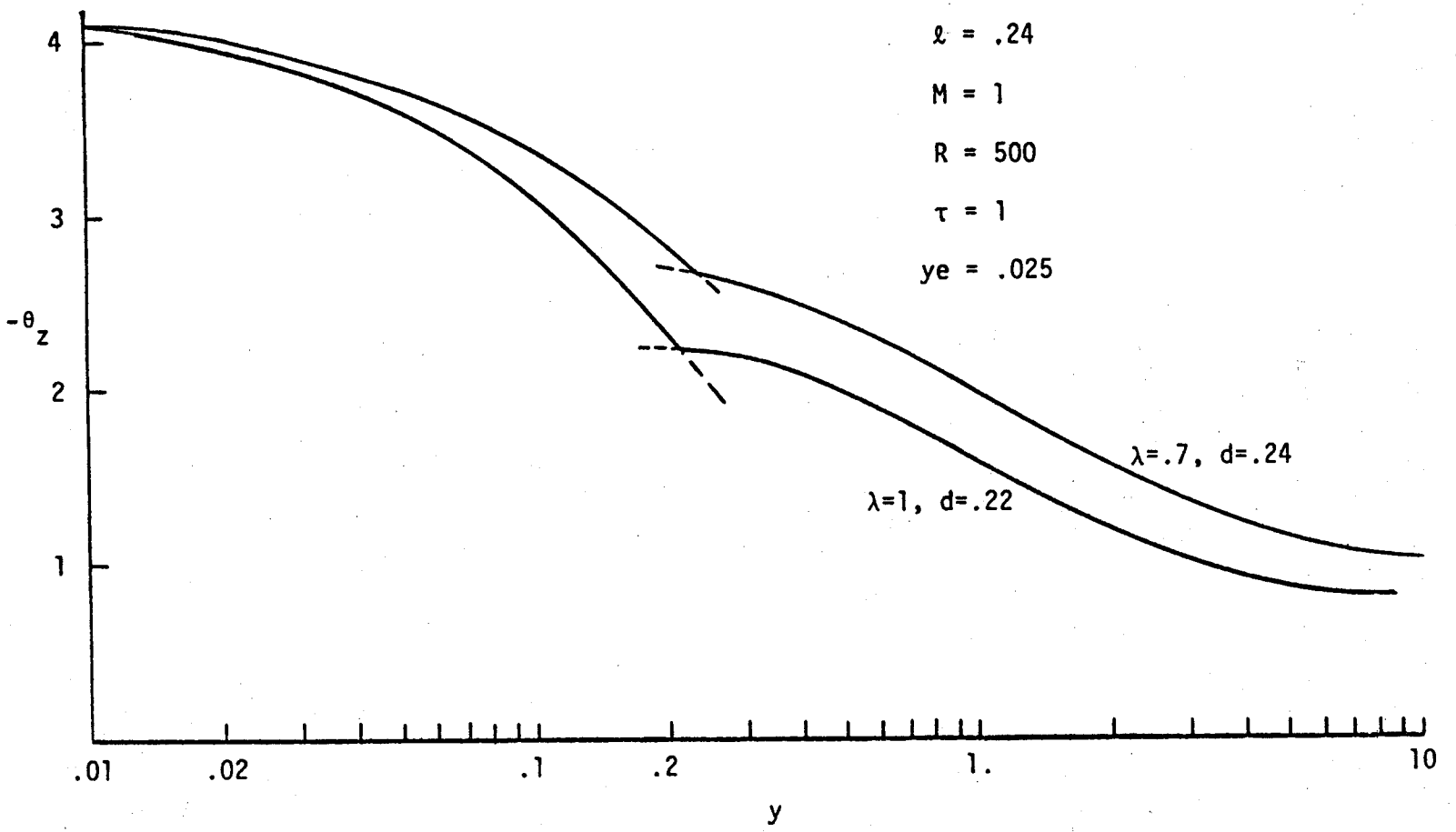

Figure 3.45 Effect of Thermal Conductivity Ratio on the Surface Temperature Gradients along the Length of the Aquifer

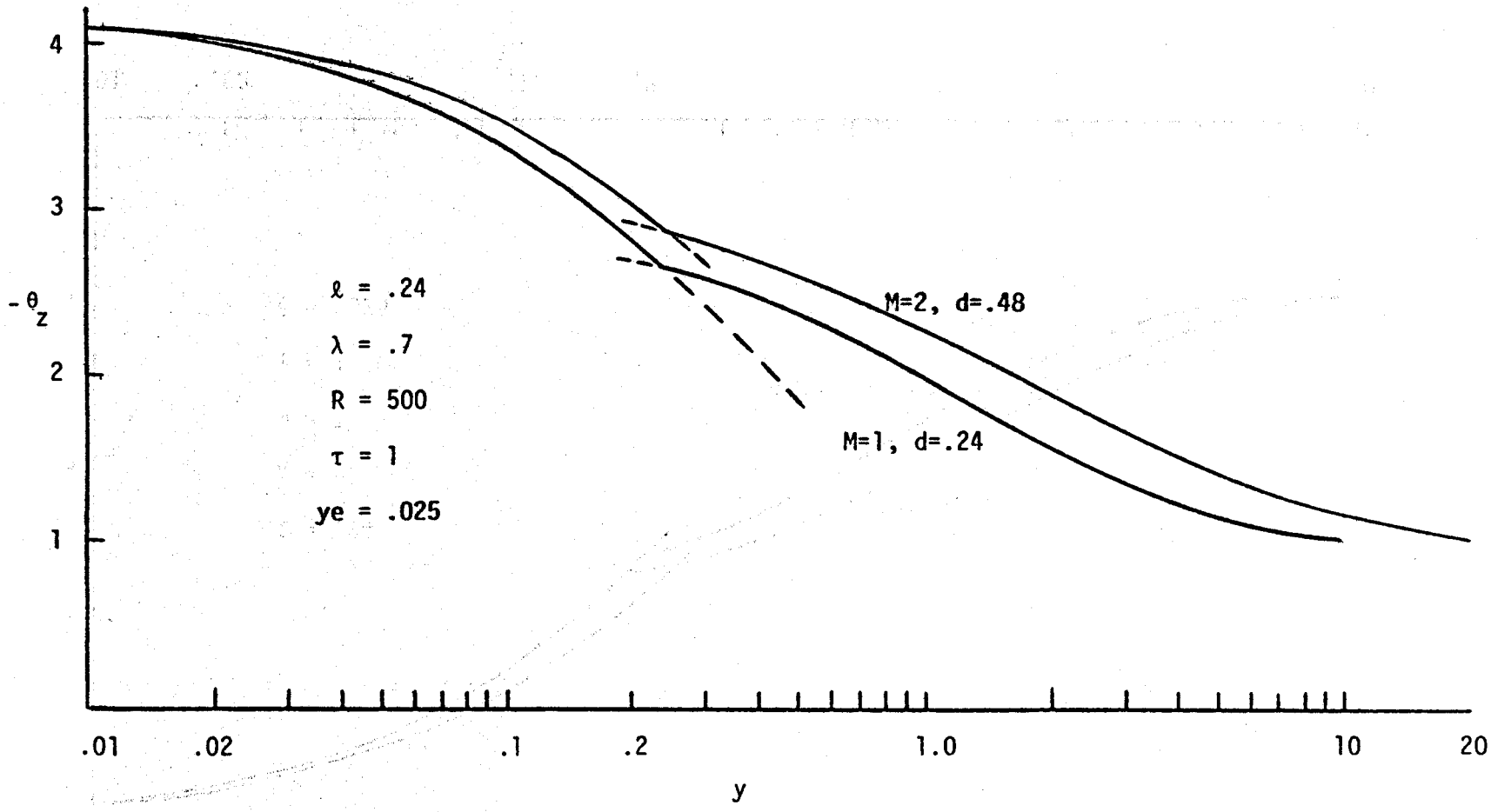

Figure 3.46 Effect of Mass Flow Rate on the Surface Temperature Gradients Along the Length of the Aquifer

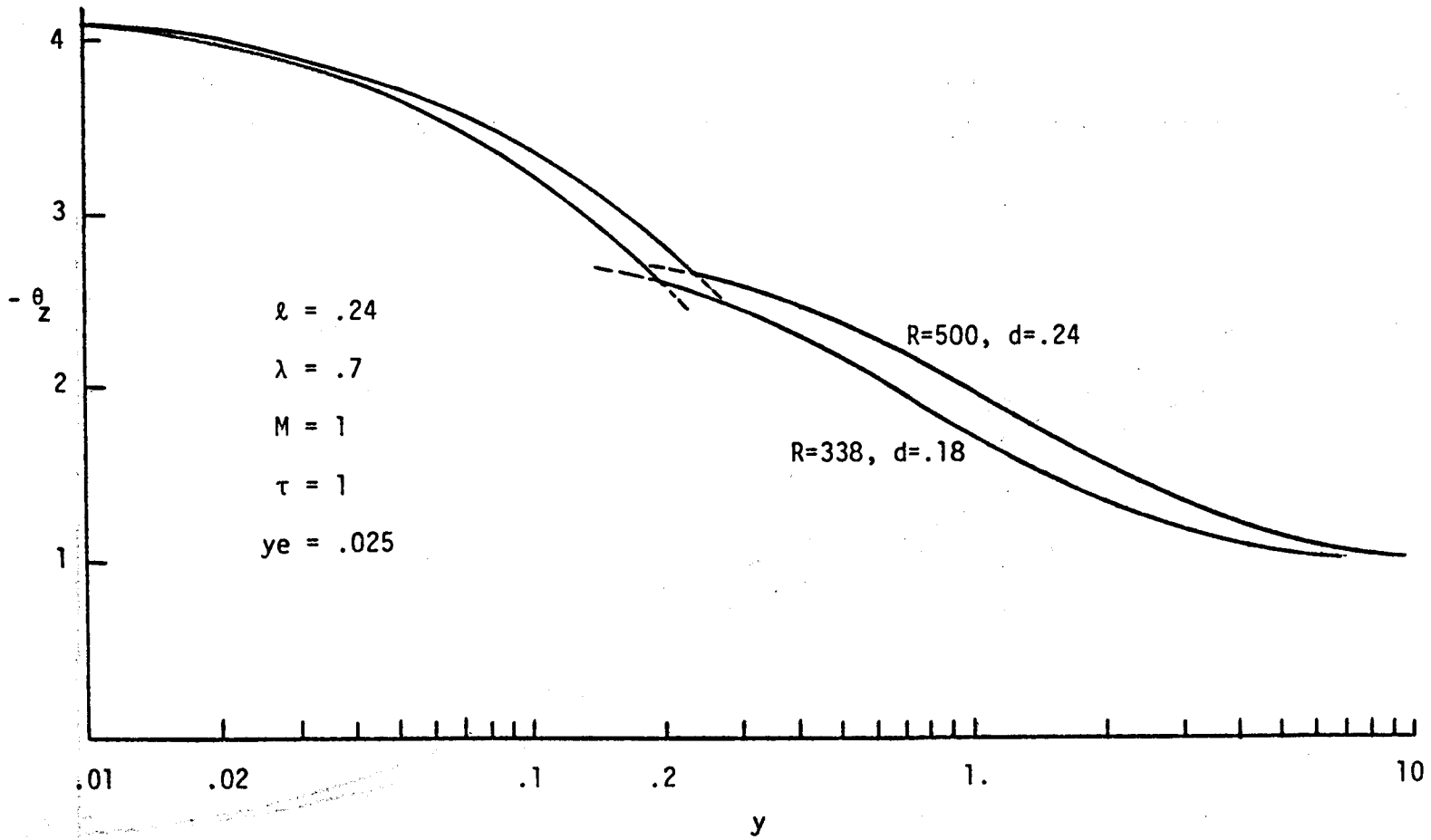

Figure 3.47 Effect of Rayleigh Number on the Surface Temperature Gradients Along the Length of the Aquifer

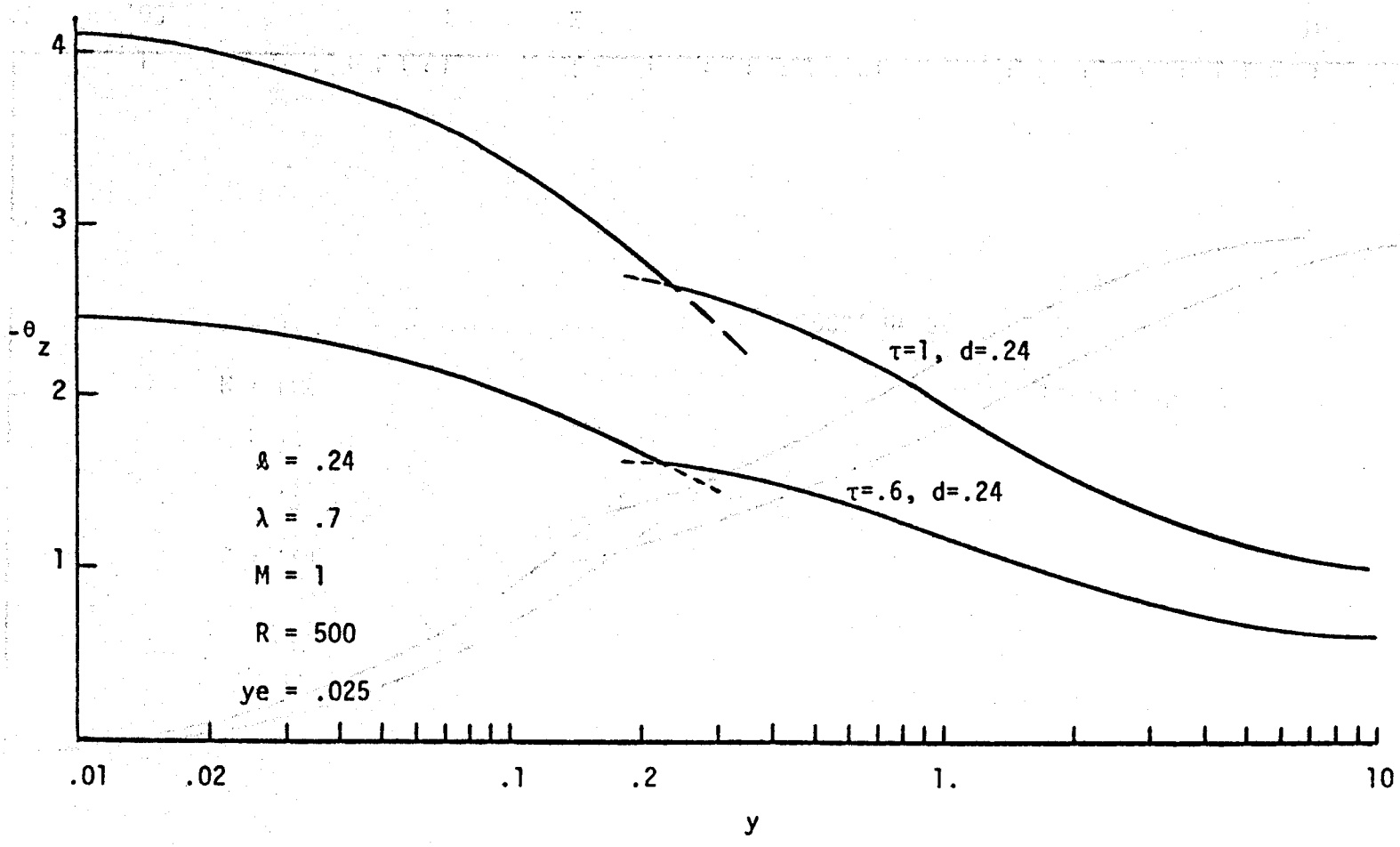

Figure 3.48 Effect of τ on the Surface Temperature Gradients Along the Length of the Aquifer

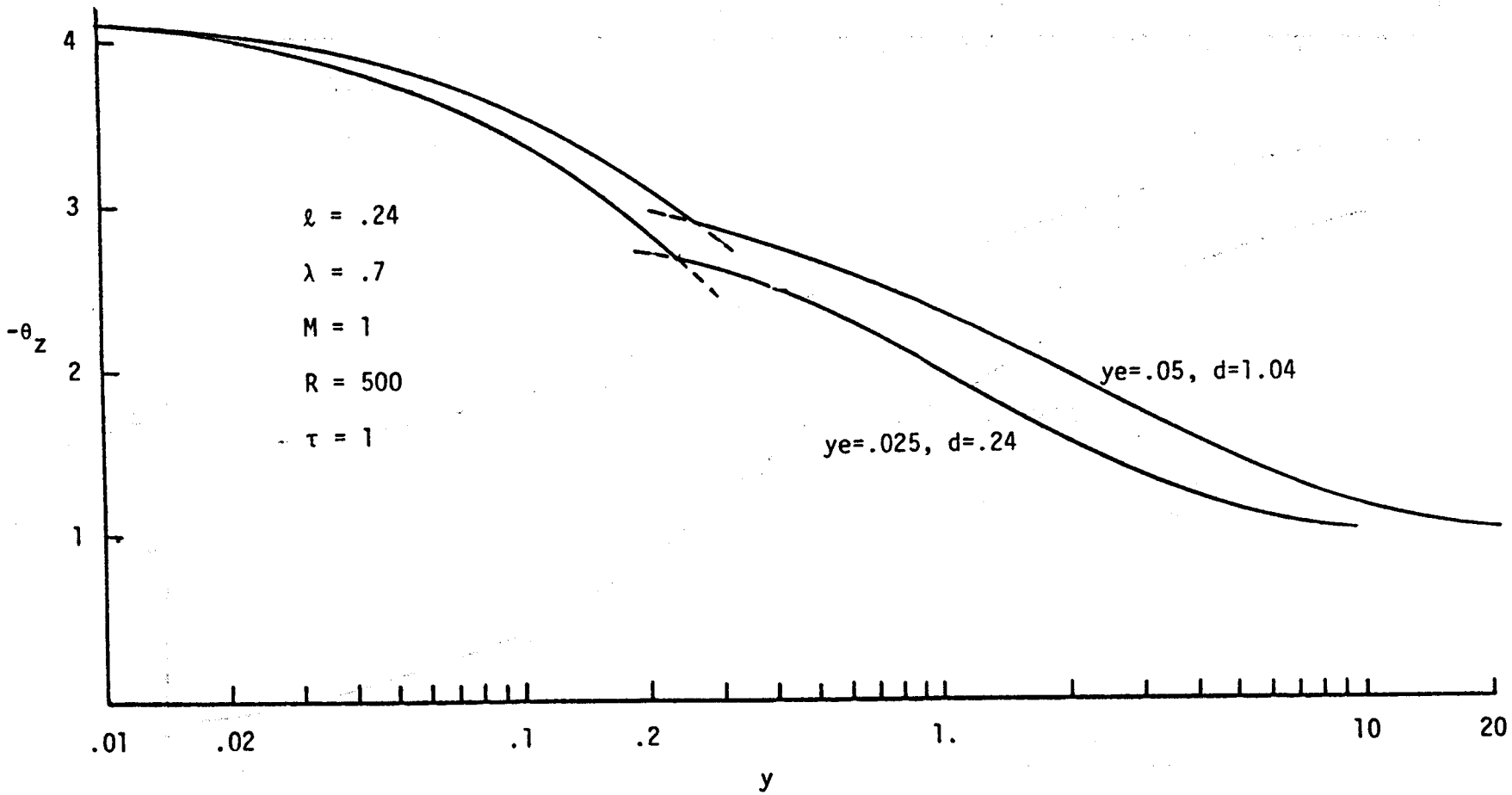

Figure 3.49 Effect of Semi-Fault Width on the Temperature Gradients vs. the Length of the Aquifer

the interface. This layer grows with distance from the fault. In the far field of the aquifer the full depth of the reservoir is cooled by the surface and the horizontal temperature gradient of the liquid becomes very small. The parabolic equation (3.24) is integrated until this condition is achieved and the number d, which defines the far end of the boundary, is thus determined. Effects of the parameters ℓ, λ, M, R, τ and ye are studied on the pressures, velocities, temperatures and their gradients at different locations in the fault, cap and the aquifer. General dependence of these parameters is summarized as follows.

(i) Horizontal aquifer velocities are higher in the lower half for a thicker cap. This is due to increased pressure gradients found in that portion of the aquifer because of the reduced hot hydrostatic pressure associated with the lighter (warmer) liquid at the far field boundary. Velocities are reduced correspondingly in the upper half of the aquifer to conserve mass. The change of λ (.7-1.) does not seem to change aquifer velocity significantly.

(ii) It is found that the over pressure with a thicker cap is lower in the fault. This difference is caused primarily by the reduced far field pressure boundary condition which in turn establishes a different pressure at the fault to push the same amount of liquid through the aquifer. Fault over pressures are found to increase with increasing d. This is true since larger pressures will be needed to push the fluid through a longer aquifer. An increase in λ (.7-1.) also increases the fault over

pressures, though the difference is very small. This occurs because of an increased hot hydrostatic pressure at the far end of the aquifer due to relatively heavier (colder) liquid, which in turn affects fault over pressures. An increase in mass flow rate increases the fault over pressures as expected.

(iii) Temperatures in the fault and clay cap seem to increase with increasing ℓ. This is because of a relative reduction in heat conduction in the cap. Temperatures are found to decrease with increasing λ as expected. An increase in M, R and τ enhances the temperatures in the fault and the cap. However, temperatures are found to decrease with increase in fault width. This is probably due to increased d associated with the larger fault width.

(iv) Effects of d, ℓ, λ and M on aquifer over pressures are similar to those on the fault over pressures.

(v) Temperatures in the aquifer are found to decrease with increasing $\hat{y}$. This is due to the loss of heat to the surface. Surface temperature gradients are lower for a thicker cap because of increased thermal resistance. On the other hand, an increase in λ increases the surface heat flux. Also an increase in M, R, τ and ye enhances the temperature gradients at the surface.

(vi) Flat temperature profiles exist in Mesa Wells 8-1, 44-7 and 48-7 in the depth intervals of 1200-1800 m, 1500-1850 m and 1800-2100 m, respectively. One could interpret these flat portions as zones that are strongly affected by fault zone flow. Temperature variations in the hotter wells are smaller compared

with those in the colder wells. These lower gradients represent the upflow in the vicinity of the wells. Increased temperature gradients below about 2 km (low permeability zone) represent heat transfer basically by conduction. This model does not allow for such a low permeability zone. It is also possible that the high Rayleigh number assumption is too strong.

(vii) The ratio of the heat transfer near the fault to that in the far field region can be obtained from (3.184) and (3.209):

$$\frac{\theta_z^c(0,z)}{\theta_z^c(1,z)} = 1 + \frac{\lambda}{\ell}$$

When $\lambda = .715$ and $\ell = .238$, then the ratio is about 4. A similar ratio can also be obtained from the Figure 3.2. Thus the results predicted from the analysis are very close to those measured at the East Mesa site.

References

Bailey, T.P., A hydrogeological and subsurface study of Imperial Valley geothermal anomalies, Imperial Valley, California. Geological Sciences, University of Colorado, Unpublished report, 1977, p. 101.

Bear, J., Dynamics of fluid in porous media. American Elsevier Publishing Company, Inc. 1972, 764.

Biehler, S., Geophysical study of Salton Trough of southern California, Pasadena, California. PhD thesis, California Institute of Technology, 1964, 139 pp.

Biehler, S., Gravity studies in the Imperial Valley in cooperative geological-geophysical-geochemical investigations of geothermal resources in the Imperial Valley. UCR-IGPP Report, 1971, 29-42.

Black, H.T., A subsurface study of the Mesa geothermal anomaly, Imperial Valley, California. Unpublished report, University of Colorado, 1975, 58.

Burst, J. F., Diagenesis of Gulf Coast clayey sediments and its possible relation to petroleum migration. AAPG Bulletin, 1969, 53(1), 73-93.

Cheng, P., and Chang, I.D., Buoyancy induced flows in a saturated porous medium adjacent to impermeable horizontal surfaces. Int. J. Heat Mass Transfer, 1976, 19, 1267-1272.

Cheng, P., The influence of lateral mass flux on free convection boundary layers in a saturated porous medium. Int. J. Heat Mass Transfer, 1977, 20, 201-206.

Cheng, P., and Lau, K.H., Steady state free convection in an unconfined geothermal reservoir. J. Geophysical Research, 1974, 79(29), 4425-4431.

Combarnous, M.A. and Bories, S.A., Hydrothermal convection in porous media. Advances in Hydrosciences, 1975, 10, 232-307.

Combs, J., and Hadley, D., Microearthquake investigation of the Mesa geothermal anomaly, Imperial Valley, California, EOS. Trans. Am. Geophys. Union, 1975, 54, 1213.

Combs, J., and Swanberg, C., Heat flow on the East Mesa KGRA, Imperial Valley, California. Geophysics, 1977. (In preparation)

Combs, J., and Hadley, D., Microearthquake investigation of the Mesa geothermal anomaly, Imperial Valley, California. Geophysics, 1977, 42(1), 17-33.

Combs, J., Seismic refraction and basement temperature investigation of the East Mesa known geothermal resources area, southern California. Geothermal Resources Council, Transactions, 1977, 1, 45-47.

Coplen, T.B., Isotopic geochemistry of water from the Imperial Valley. In Cooperative geological-geophysical-geochemical investigations of geothermal resources in the Imperial Valley of California, UCR-IGPP Report, 1971, 113-118.

Coplen, T.B., Origin of the salt of the Imperial Valley and surrounding watershed areas. In Cooperative investigations of geothermal resources in the Imperial Valley area and their potential value for desalting of water and other purposes, IGPP-UCR 72-33, 1972, E1-E33.

Coplen, T.B., Cooperative geochemical resource assessment at the mesa-geothermal system. University of California, Riverside. IGPP, 1976.

Coplen, T.B., Kolesar, P., Taylor, R.C., Kendall, C., and Mooser, C., Investigations of the Dunes geothermal anomaly, Imperial Valley, California; Part 4. University of California, Riverside. IGPP, 1975.

Donaldson, I.G. Temperature gradients in the upper layers of the earth's crust due to convective water flows. Journal of Geophysical Research, August 1962, 67(9), 3449-3459.

Douze, E.J., and Sorrels, G.G. Geothermal ground noise surveys. Geophysics, 1972, 37, 813-824.

Dutcher, L.C., Hardt, W.F., and Moyle, W.R., Jr. Preliminary appraisal of ground water in storage with reference to geothermal resources in the Imperial Valley area, California. U.S. Geological Survey Circular 649, 1972, 57 pp.

Elder, J.W., Steady free convectinn in a porous medium heated from below. J. Fluid Mech, 1967a, 27, 29-48.

Elder, J.W., Transient convection in a porous medium. J. Fluid Mech., 1967b, 27(3), 609-623.

Elders, W.A., and Bird, D.K., Investigations of the Dunes geothermal anomaly, Imperial Valley, California, Part 2. University of California, Riverside. IGPP, 1974.

Elders, W.A., Rex, R.W., Meidav, T. Robinson, P.T., and Biehler, S. Crustal spreading in southern California. Science, 1972, 178, 15-24.

Goforth, T.T., Douze, E.J., and Sorrels, G.G. Seismic noise measurements in a geothermal area. Geophys. Prosp., 1972, 20, 76-82.

Grindley, G.W. The geology, structure, and exploitation of the Wairakei geothermal field, Taupo, New Zealand, 1965, 131 pp.

Grindley, G.W. Subsurface structures and relation to steam production in the Broadlands Geothermal Field, New Zealand. Proceedings of the United Nations Symposium on the Development and Utilization of Geothermal Resources. Geothermics, 1970, 2(1), (special issue 2), 248-261.

Helgeson, H.C. Geologic and thermodynamic characteristics of the Salton Sea geothermal system. Am. J. Sci., 1968, 266, 129-166.

Horton, C.W., and Rogers, F.T., Jr. Convective currents in a porous medium. J. Appl. Phys., 1945, 16, 367-370.

Kassoy, D.R., and Zebib, A. Convection fluid dynamics in a model of a fault zone in the earth's crust. J. Fluid Mech., 1978, 88, 769-802.

Kassoy, D.R., and Zebib, A. Variable viscosity effects on the onset of convection in porous media. The Physics of Fluids, December 1975, 18(12), 1649-1651.

Katto, Y., and Masuoka, T. Criterion for the onset of convective flow in a fluid in a porous medium. Int. J. Heat Mass Transfer, 1967, 10, 297-309.

Ketter, Paul and Carel Otte, Geothermal Energy, Stanford University Press, p. 360, 1973.

Kruger, P., and Otte, C. Geothermal energy. Stanford: Stanford University Press, 1973, 360 p.

Lau, K.H., and Cheng, P.. The effect of dike intrusion on free convection in conduction dominated geothermal reservoirs. Int. J. Heat Mass Transfer, 1977, 20, 1205-1210.

Lapwood, E.R. Convection of a fluid in a porous medium. Proc. Cambridge Phil. Soc., 1948, 44, 508-521.

Loeltz, O.J., Ireland, B., Robinson, J.H., and Olmestead, F.H. Geohydrologic reconnaissance of the Imperial Valley, California. U.S. Geological Survey Professional Paper 486-K, 1975, 54.p.

Meidav, T., and Furgerson, R.B. Electrical resistivity for geothermal exploration in the Imperial Valley. In Cooperative geological-geophysical-geochemical investigations of geothermal resources in the Imperial Valley, UCR-IGPP Report, 1971, 43-83.

Minkowycz, W.J., and Cheng, P., Free convection about a vertical cylinder embedded in a porous medium. Int. J. Heat Mass Transfer, 1976, 19, 805-813.

Morland, L.W., Zebib, A., and Kassoy, D.R. Effects of temperature dependent viscosity and expansion coefficient on the onset of convection in an elastic porous matrix. CUMER 76-4, Department of Mechanical Engineering, University of Colorado, Boulder, 1976, p. 16.

Norton, D. Porphyry pluton environments: Fluid rock interactions predicted from theoretical models of heat and mass transfer. Geol. Soc. America, 1975, 7(7), 1215 p.

Rex, R.W. Cooperative geological-geophysical-geochemical investigations of geothermal resources in the Imperial Valley. UCR-IGPP Report, 1971, 153 pp.

Rex, R.W. Origin of the salt of the Imperial Valley and surrounding watershed areas. In Cooperative investigations of geothermal resources in the Imperial Valley area and their potential value for desalting of water and other purposes, IGPP-UCR 72-33, 1972, F1-F38.

Rinehart, C.D., and Ross, D.C. Geology and mineral deposits of the Mt. Morrison quadrangle, Sierra Nevada, California. U.S. Geological Survey Professional Paper No. 385, 1964, 106 pp.

Straus, J.M., and Schubert, G. Thermal convection of water in a porous medium: Effects of temperature and pressure dependent thermodynamic and transport properties. 4 July 1976. (To appear in the Journal of Geophysical Research)

Swanberg, C.A. Heat flow and geothermal potential of the East Mesa KGRA, Imperial Valley, California. In Proceedings of Conference on Research for the Development of Geothermal Energy Resources, Jet Prop. Lab., California Institute of Technology, Pasadena, Calif. 1974, 85-97.

Swanberg, Chandler A., The Mesa Geothermal Anomaly, Imperial Valley, California: A Comparison and Evaluation of Results Obtained from Surface Geophysics and Deep Drilling, Proceedings of the Second United Nations Symposium on the Development and Use of Geothermal Resources, San Francisco, Vol. 2, pp. 1217-1229, 1975.

Ward, P.L., and Jacobs, K.H. Microearthquakes in the Ahuachapan geothermal field, El Salvador, Central America. Science, 1971, 173, 328-330.

Wooding, R.A. Steady state free thermal convection of liquid in a saturated permeable medium. J. Fluid Mechanics, 1957, 2, 273-285.

Wooding, R.A. Rayleigh instability of a thermal boundary layer in flow through a porous medium. J. Fluid Mechanics, 1960, 9, 183-192.

APPENDIX A

Numerical Methods

Basic temperatures in the far field of the aquifer are obtained by integrating the parabolic equation (3.135), which is as follows:

$$\gamma^2 v(z)\theta_{\hat{y}} = d\theta_{zz} \tag{A.1}$$

The Crank Nicolson method (Ketter and Prawel, 1969) is used to develop the following finite difference expression for the above equation.

$$\frac{\gamma^2 v_i}{h}(\theta_{i,j+1} - \theta_{i,j}) = \frac{d}{2h^2}\left[\theta_{i+1,j+1} + \theta_{i-1,j+1} - 2\theta_{i,j+1} + \theta_{i+1,j} + \theta_{i-1,j} - 2\theta_{i,j}\right] \tag{A.2}$$

where

h = step size

i,i+1,... = steps in z direction

j,j+1,... = steps in $\hat{y}$ direction

Upon simplification (A.2) yields

$$A_{i1}\bar{\theta}_{i-1} + A_{i2}\bar{\theta}_i + A_{i3}\bar{\theta}_{i+1} = A_{i4} \tag{A.3}$$

where

$$A_{i1} = -\frac{d}{2h\,\gamma^2\,v_i} \tag{A.4}$$

$$A_{i2} = 1 + \frac{d}{h\,\gamma^2\,v_i} \tag{A.5}$$

$$A_{i3} = A_{i1} \tag{A.6}$$

$$A_{i4} = \frac{d}{2h\,\gamma^2\,v_i}\,\theta_{old}(i-1) + \left(1 - \frac{d}{h\,\gamma^2\,v_i}\right)\theta_{old}(i) + \frac{d}{2h\,\gamma^2\,v_i}\,\theta_{old}(i+1) \tag{A.7}$$

$$\bar{\theta}_{i-1} = \theta_{i-1,j+1},\quad \bar{\theta}_i = \theta_{i,j+1},\quad \bar{\theta}_{i+1} = \theta_{i+1,j+1} \tag{A.8}$$

$$\theta_{old}(i-1) = \theta_{i-1,j},\quad \theta_{old}(i) = \theta_{i,j},\quad \theta_{old}(i+1) = \theta_{i+1,j} \tag{A.9}$$

The range of i determines the number of equations in (A.3) Subroutine 'Band 3' in the code 'CLAYCAP' solves the system of equations (A.3). Code 'CLAYCAP' is given in Appendix B and determines the temperatures and the isotherms in the aquifer and the cap. It also calculates the temperature gradients at the surface. Other programs, used in the Technical Report, are also included in Appendix B.

APPENDIX B

```
                PROGRAM VELPT (INPUT,OUTPUT)
000003          SINH(Z)=(EXP(Z)-EXP(-Z))/2.
000016          COSH(Z)= (EXP(Z)+EXP(-Z))/2.
000030          W(Z)= A1*COSH(Z)+ DD*SINH(Z)-1.
000044          DIMENSION T1(101),T2(101),T3(101)
000044          COMMON P,YE,CO
000044    100   FORMAT(1H ,11F9.6)
000044    101   FORMAT(9F12.8)
000044    105   FORMAT(5F15.6)
000044          DO 6 KK=1,10
000046          READ 105,TF,AM,RA,YE,D
000063          PRINT105,TF,AM,RA,YE,D
000101          DD=1./SQRT(D)
000105          E=EXP(DD)
000107          F=EXP(-DD)
000113          COSH1=(E+F)/2. $ SINH1=(E-F)/2.
000117          PI=4.*ATAN(1.)
000123          SQPI=SQRT(PI)
000125          CO=2./SQRT(PI)
000130          A1= DD*(AM+COSH1)/SINH1
000133          GA=SQRT(RA*YE*YE)
000140          P=SQRT(GA*GA*(A1-1.)+.5)
000146          CC=YE*GA*GA*TF/(6.*SQPI*D*(P**3))
000154          DY=.1 $ DZ=.1
000157          DZ1=.01
000160          DO 2 I=1,11
000162          Y=(I-1)*DY
000166          DO 1 J=1,11
000167          B=-(J-1)*DZ*DD
000174          Z=B/DD
000176          VA=W(B)
000200          PA=D*VA*(1.-Y) -Z*Z/2.
000205          WF=-(A1/DD)*SINH(B)-COSH(B)+1.+Z
000221          VF=Y*VA
000223    1     PRINT 101,Y,Z,AM,VA,PA,WF,VF
000246    2     CONTINUE
000250          DO 5 I=1,101
000252          Z=-(I-1)*DZ1
000256          Z1=Z/YE
000260          Z2=P*Z1
000262          CALL ERF1(Z2,E1)
000264          T1(I)=1.-TF*E1
000270          T2(I)=CC*(1.+E1-(1.+Z2*Z2)*EXP(-Z2*Z2) )
000303    5     T3(I)=T1(I)+T2(I)
000307          PRINT 100, (T1(K),K=1,10)
000315          PRINT 100, (T1(K),K=11,20)
000323          PRINT 100, (T1(K),K=21,101,10)
000335          PRINT 100, (T2(K), K=1,10)
000343          PRINT 100, (T2(K), K=11,20)
000351          PRINT 100, (T2(K), K=21,101,10)
000363          PRINT 100, (T3(K),K=1,10)
000371          PRINT 100, (T3(K),K=11,20)
000377          PRINT 100, (T3(K),K=21,101,10)
000411    6     CONTINUE
000413          END
```

```
                SUBROUTINE ERF1 (Z,E)
000005          DIMENSION DU1(101)
000005          COMMON P,YE,CO
000005          N=100
000006          N1=N+1
000010          H=Z/N
000011          DO 1 I=1,N1
000013          X=(I-1)*H
000017      1   DU1(I)=EXP(-X*X)
000030          E1=0.
000031          DO 2 I=3,N1,2
000032      2   E1=E1+(DU1(I-2)+4.*DU1(I-1)+DU1(I))*(H/3.)
000045          E=CO*E1
000046          RETURN
000047          END
```

```
                PROGRAM INTEGRL (INPUT,OUTPUT)
000003          DIMENSION DU(5000)
000003      100 FORMAT(8F15.6)
000003      105 FORMAT(5F15.6)
000003          DO 8 KK=1,10
000005          READ 105,TF,AM,RA,YE,D
000022          PRINT105,TF,AM,RA,YE,D
000040          DD=1./SQRT(D)
000044          PI=4.*ATAN(1.)
000047          CO=2./SQRT(PI)
000052          E=EXP(DD)
000054          F=EXP(-DD)
000060          COSH1=(E+F)/2.
000063          SINH1=(E-F)/2.
000064          A1=(AM+COSH1)*DD/SINH1
000070          GA=SQRT(RA*YE*YE)
000074          P=GA*GA*(A1-1.)/2.
000100          Y=1.
000101          K=1
000102      6   FE=4.
000104          N=200
000105      5   N1=N+1
000107          H=FE/N
000111          DO 1 I=1,N1
000113          X=(I-1)*H
000117      1   DU(I)= EXP((-X*X/(4.*P))+(P-SQRT(P*P+X*X))*Y-P+SQRT(P*P+X*X))
000150          SUM=0.
000151          DO 2 I=2,N1
000152      2   SUM=SUM+(DU(I)+DU(I-1))*(.5*H)
000163          Q2=2.*TF*SUM/PI
000166          IF(K.EQ. 1) GO TO 3
000170          IF(ABS(Q2-Q1).LT. .00001)GO TO 4
000175      3   K=K+1
000177          Q1=Q2
000200          FE=FE+1.
000202          N=N+50
000204          GO TO 5
000204      4   Q3=TF*SQRT(2.*P/(PI*Y))
000213          Y1=YE*Y
000215          Y2=Y1*YE/D
000217          QUA=Q1/YE
000220          SIM=Q3/YE
000222          PRINT 100,Y,Y1,Y2,FE,Q1,Q3,QUA,SIM
000245          IF(Y.GT. 240.) GO TO 8
000251          Y=Y+1.
000252          GO TO 6
000252      8   CONTINUE
000254          END
```

```
                PROGRAM INTGRL2 (INPUT,OUTPUT)
000003          DIMENSION DU(5000)
000003          COMMON P,CO
000003     100  FORMAT(8F15.6)
000003     105  FORMAT(5F15.6)
000003          READ 105,TF,AM,RA,YE,D
000021          PRINT105,TF,AM,RA,YE,D
000037          DD=1./SQRT(D)
000043          PI=4.*ATAN(1.)
000046          CO=2./SQRT(PI)
000051          E=EXP(DD)
000053          F=EXP(-DD)
000057          COSH1=(E+F)/2.
000062          SINH1=(E-F)/2.
000063          A1=(AM+COSH1)*DD/SINH1
000067          GA=SQRT(RA*YE*YE)
000073          P=GA*GA*(A1-1.)/2.
000077          Y=45.
000100          Y1=YE*Y
000102          Y2=YE*Y1/D
000104          PRINT 100,Y,Y1,Y2
000115     8    Z=0.
000116     6    K=1
000117          FE=4.
000121          N=200
000122     5    N1=N+1
000124          H=FE/N
000126          DU(1)=Z
000130          DO 1 I=2,N1
000131          X=(I-1)*H
000135     1    DU(I)= EXP((-X*X/(4.*P))+(P-SQRT(P*P+X*X))*Y-P+SQRT(P*P+X*X))*SIN
               1(X*Z)/X
000173          SUM=0.
000174          DO 2 I=2,N1
000175     2    SUM=SUM+(DU(I)+DU(I-1))*(.5*H)
000206          Q2=2.*TF*SUM/PI
000211          IF(K.EQ. 1) GO TO 3
000213          IF(ABS(Q2-Q1).LT. .00001)GO TO 4
000220     3    K=K+1
000222          Q1=Q2
000223          FE=FE+1.
000225          N=N+50
000227          GO TO 5
000227     4    T=1.-Q2
000231          Z1=YE*Z
000233          Z2=Z1/SQRT(YE)
000237          IF(Y.GT. 0.)CALL ERF(Y1,Z2,E2)
000243          T1=1.-TF*E2
000246          PRINT 100,Z,Z1,FE,Q2,T,T1
000266          IF(ABS(Z).GE.10.) GO TO 7
000272          Z=Z-.2
000273          GO TO 6
000274     7    IF(Y.GT. 80.) STOP
000301          Y=Y+4.
000303          Y1=YE*Y

000305          Y2=YE*Y1/D
000307          PRINT 100,Y,Y1,Y2
000320          GO TO 8
000321          END
```

```
                      SUBROUTINE ERF(Y,Z,E)
000006                DIMENSION DU1(101)
000006                COMMON P,CO
000006                N=100
000007                N1=N+1
000011                FE=Z*SQRT(P/(2.*Y))
000020                H=FE/N
000022                DO1 I=1,N1
000024                X=(I-1)*H
000030          1     DU1(I)=EXP(-X*X)
000041                E1=0.
000042                DO 2 I=2,N1
000043          2     E1=E1+(DU1(I-1)+DU1(I))*(.5*H)
000054                E=CO*E1
000055                RETURN
000056                END
```

```
                PROGRAM PROFILE (INPUT,OUTPUT)
000003          SINH(ZZ)=(EXP(ZZ)-EXP(-ZZ))/2.
000016          COSH(ZZ)=(EXP(ZZ)+EXP(-ZZ))/2.
000030          W(ZP)=A1*COSH(ZP)+B1*SINH(ZP)-1.
000044          DIMENSION NSCALE(4),LABEL(3),Z(101),TOLD(101),TNEW(101),A(101,4),V
               1(101),T(101,101),X(101),FP(6),YO(1000),ZO(1000)
000044          COMMON M,N,DY
000044    101   FORMAT(1H0,//5X*Y*,5X*TEMPERATURE AT DIFFRENT DEPTHS IN THE AQUIFE
               2R*//)
000044    102   FORMAT(1H0,F5.2,F5.2,11F9.6/)
000044    103   FORMAT(11F9.6/)
000044    104   FORMAT(////4X*THE POINTS(YO,ZO) ON THE ISOTHERM T=*F7.4/(7(3X2F7.4
               1)))
000044    105   FORMAT(5F15.6)
000044    106   FORMAT(4F20.6)
000044    111   FORMAT(F15.5)
000044    112   FORMAT(I6)
          C     R=DY*D/(2.*DZ*DZ*GA*GA)  WHERE GA=SQRT(RA*YE*YE)
000044          DATA YMAX,NFRPR,NFRPL,NPLOTS/1.,10,10,10/
000044          DATA (FP(I),I=1,6)/1.,1.2,1.4,1.6,1.8,1.999/
000044          DY=.01 $ DZ=.01
000047          M=101
000050          N=101
000051          M1=M-1
000053          PI=4.*ATAN(1.)
000056          CO=2./SQRT(PI)
000061          DO 12 I=6,M
000062    12    T(I,1)=1.
000070          DO 107  KK=1,12
000071          READ 105,TF,AM,RA,YE,D
000106          PRINT105,TF,AM,RA,YE,D
000124          DD=1./SQRT(D)
000130          E=EXP(DD)
000132          F=EXP(-DD)
000136          COSH1=(E+F)/2. $ SINH1=(E-F)/2.
000142          GA=SQRT(RA*YE*YE)
000147          R=D /(2.*DZ*GA*GA)
000152          A1=(AM+COSH1)*DD/SINH1
000156          B1=DD
000157          P=SQRT(GA*GA*(A1-1.)*.5)
          C     DEFINE Z(I),V(I),T(I),X(I)
000165          DO 13 I=1,M
000166          ZT=(I-1)*DY
000172    13    X(I)=ZT
000176          DO 1 I=1,M
000177          ZT=-(I-1)*DZ
000203          Z(I)=ZT
000205          ZTT=ZT*DD
000207    1     V(I)=W(ZTT)
000215          PRINT 101
          C     SPECIFY TEMPERATURE AT Y=.05
000220          Y=.01
000222          Y1=Y*D/YE
000224          NDT=1
000225          J=2
```

```
000226          ZT=0.
000227          DO 7 I=1,M
000231          CALL ERF1( D, P,Y,ZT,E1)
000234          TOLD(I)=1.-TF*E1+ (TF*GA*GA*SQRT(.5*Y/D)/(4.*P*P))*((ZT/SQRT(2.*D
                1*Y)) *( 1.+E1)-( P*ZT*ZT/(D*Y*SQRT(PI)))*EXP(-P*P*ZT*ZT/(2.*D*Y)))
000301          IF(I.EQ. 2) DT=(TOLD(2)-TOLD(1))/DZ
000306          T(J,I)=TOLD(I)
000312    7     ZT=ZT-DZ
000316          PRINT 102,Y,Y1,(TOLD(I),I=1,10)
000327          PRINT 102,Y,Y1,(TOLD(I),I=11,M,10)
000346          PRINT 111,DT
          C     CALCULATE TNEW, THE TEMPERATURE AT Y+DY
000354    2     Y=Y+DY
000356          Y1=Y*D/YE
000360          J=J+1
000362          NDT=NDT+1
          C     COMPUTE A(I,J)
000363          DO 3 I=2,M1
000364          A(I,1)=R/V(I)
000366          A(I,2)=-1.-2.*R/V(I)
000373          A(I,3)=A(I,1)
000374    3     A(I,4)=-(R/V(I))*TOLD(I-1)+(2.*R/V(I)-1.)*TOLD(I)-R/(V(I))*TOLD(I+
               31)
          C     MODIFY THE MATRIX A(I,J)
000412          A(2,4)=A(2,4)-A(2,1)
000414          A(2,1)=0.
000415          A(M1,4)=A(M1,4)-A(M1,3)*(1.+TF)
000421          A(M1,3)=0.
000423          CALL BAND3(M1,A,TNEW)
000425          DO 4 I=2,M1
000427          TOLD(I)=TNEW(I)
000431          IF(I.EQ. 2) DT=(TOLD(2)-TOLD(1))/DZ
000436    4     T(J,I)=TOLD(I)
000444          T(J,M)=1.+TF
000450          IF(Y.GT. .1) GO TO 8
000454          PRINT 102,Y,Y1,(TOLD(I),I=1,10)
000465          PRINT 102,Y,Y1,(TOLD(I),I=11,M,10)
000504          PRINT 111,DT
          C     PRINT VELOCITY WHEN NDT=N*NFRPR,N BEING A POSITIVE INTEGER AND PLO
          C     T IT WHEN NDT=N*NFRPL,N=1,2,---,NPLOTS.
000512    8     IF((NDT/NFRPR)*NFRPR.NE.NDT) GO TO 5
000517          PRINT 102,Y,Y1,(TOLD(I),I= 1,M,10)
000535          PRINT 111,DT
000543    5     IF((NDT/NFRPL)*NFRPL.NE.NDT) GO TO 6
000550          IF((NDT/NFRPL).GT. NPLOTS) GO TO 6
000554    6     IF(Y.LT.YMAX .AND. J.LT. 101) GO TO 2
000565          DO 10 I=1,M,10
000566    10    PRINT 103,(T(J,I),J=1,M,10)
000604          DO 11 K=1,6
000605          FA=FP(K)
000607          CALL POINTS(X,Z,T,FA,YO,ZO,KMAXO)
000615          PRINT 104,(FA,((YO(L),ZO(L)),L=1,KMAXO))
000634    11    CONTINUE
000636    107   CONTINUE
000640          END
```

```
                      SUBROUTINE POINTS (X,Y,F,FA,XX,YY, KMAX)
000012                DIMENSION X(101),Y(101),F(101,101),XX(1000),YY(1000)
000012                COMMON M,N,DY
000012                K=0
000013                I=0
000014           1    J=1
000015                I=I+1
000017                IF(I.GT. M) GO TO 7
000022           2    P=F(I,J)-FA
000027                IF(ABS(P).LE. .00001) GO TO 6
000032           3    J=J+1
000034                IF(J.GT. N) GO TO 1
000037                Q=F(I,J)-FA
000043                IF(P*Q) 5,5,4
000045           4    P=Q
000047                GO TO 3
000047           5    K=K+1
000051                XX(K)=X(I)
000054                YY(K)=Y(J)+DY*ABS(Q)/(ABS(P)+ABS(Q))
000067                P=Q
000071                GO TO 3
000071           6    K=K+1
000073                XX(K)=X(I)
000076                YY(K)=Y(J)
000101                J=J+1
000103                IF(J.GT. N) GO TO 1
000106                GO TO 2
000106           7    KMAX=K
000110                RETURN
000111                END

                      SUBROUTINE BAND 3 (N,A,X)
000006                DIMENSION A(101,4),X(101)
000006          106   FORMAT(3F30.10)
000006                M=N-1
000010                M1=M-1
000011                DO 10 I=3,M
000012                A(I,2)=A(I,2)*A(I-1,2)-A(I,1)*A(I-1,3)
000020                A(I,3)=A(I,3)*A(I-1,2)
000023          10    A(I,4)=A(I,4)*A(I-1,2)-A(I,1)*A(I-1,4)
000033                X(N)=(A(N,4)*A(M,2)-A(N,1)*A(M,4))/(A(N,2)*A(M,2)-A(N,1)*A(M,3))
000047                DO 20 K=1,M1
000051                J=N-K
000052          20    X(J)=(A(J,4)-A(J,3)*X(J+1))/A(J,2)
000062                RETURN
000063                END

                      SUBROUTINE ERF1  ( D, P,Y,Z,E)
000010                DIMENSION DU1(101)
000010                PI=4.*ATAN(1.)
000013                CO=2./SQRT(PI)
000016                N=100
000017                N1=N+1
000021                FE=P*Z/ SQRT(2.*D*Y)
000034                H=FE/N
000036                DO1 I=1,N1
000040                X=(I-1)*H
000044           1    DU1(I)=EXP(-X*X)
000057                E1=0.
000060                DO 2 I=3,N1,2
000061           2    E1=E1+(DU1(I-2)+4.*DU1(I-1)+DU1(I))*(H/3.)
000075                E=CO*E1
000076                RETURN
000077                END
```

```
                PROGRAM CAPVELP (INPUT,OUTPUT)
000003          COSH(ZZ)=(EXP(ZZ)+EXP(-ZZ))/2.
000016          SINH(ZZ)=(EXP(ZZ)-EXP(-ZZ))/2.
000030          W(ZP)=A2*COSH(ZP)+B2*SINH(ZP)-C2
000044          WA(ZA)=SQRT(D)*(-A2*SINH(ZA)+B2*(1.-COSH(ZA))+C2*ZA)
000066          DIMENSION VAQ(101),WF(101),VF(11),PF(101),PAQ(101)
000066     101  FORMAT(7F10.4)
000066          M=11
000067          DZ=.1
000071          DY=.1
000072          DO 111 J=1,12
000073          READ 101,D,CAPL,ALEMDA,AM,RA,TF,YE
000114          PRINT101,D,CAPL,ALEMDA,AM,RA,TF,YE
000136          DD=1./SQRT(D)
000142          E=EXP(DD)
000144          F=EXP(-DD)
000150          COSH1=(E+F)/2. $ SINH1=(E-F)/2.
000154          C2= ALEMDA/(ALEMDA+CAPL)
000157          B2= DD*C2
000160          A2= DD*(AM+C2*COSH1)/SINH1
                C     CALCULATE AND PRINT PRESSURE AND VELOCITIES IN THE FAULT.
000165          DO 1 I=1,M
000166          ZT=-(I-1)*DZ
000172          ZTT=DD*ZT
000174          VAQ(I)=W(ZTT)
000200          WF(I)=WA(ZTT)
000204          PF(I)=D*VAQ(I)-(CAPL*CAPL-2.*CAPL*ZT+ALEMDA*ZT*ZT)/(2.*(ALEMDA+
                1CAPL))
000216     1    PRINT 101,VAQ(I),WF(I),PF(I)
000233          Z=-.5*DD
000235          VA=W(Z)
000237          DO 2 I=1,11
000240          YT=(I-1)*DY
000244          VF(I)=VA*YT
000246     2    PRINT 101,YT,VF(I)
                C     CALCULATE AND PRINT PRESSURE IN THE AQUIFER
000257          Y=0.
000260          DO 3 I=1,M,5
000262     4    PAQ(I)=PF(I)-VAQ(I)*Y*D
000267          PRINT 101,Y,PAQ(I)
000277          IF(Y. GE. .98) GO TO 5
000302          Y=Y+.1
000303          GO TO 4
000304     5    Y=0.
000305     3    CONTINUE
000310     111  CONTINUE
000312          END
```

```
                      PROGRAM CPFAULT (INPUT,OUTPUT)
000003                DIMENSION TCAP(51),TAQ(101)
000003          101   FORMAT(7F10.4)
000003          102   FORMAT(1H0,F10.6)
000003                DZ=.01
000005                PI=4.*ATAN(1.)
000010                SQPI=SQRT(PI)
000012                DO 107 KK=1,9
000013                READ 101,D,CAPL,ALEMDA,AM,RA,TF,YE
000034                PRINT101,D,CAPL,ALEMDA,AM,RA,TF,YE
000056                DD=1./SQRT(D)
000062                E=EXP(DD)
000064                F=EXP(-DD)
000070                COSH1=(E+F)/2. $ SINH1=(E-F)/2.
000074                GA=SQRT(RA*YE*YE)
000101                B1= ALEMDA/(ALEMDA+CAPL)
000103                A1=DD*(AM+B1*COSH1)/SINH1
000110                P=SQRT(GA*GA*(A1-B1)*.50)
000115                C1=(YE*SQPI*ALEMDA)/(2.*P*CAPL)
000122                L=CAPL/DZ+1.2
000125                DO 1 I=1,L
000127                ZT=(I-1)*DZ
000133          1     TCAP(I)=1.+TF*(1.-ZT/CAPL)*(1.-C1)
000145                DO 2 I=1,101
000147                ZT=-(I-1)*DZ
000153                CALL ERF (YE,P,ZT,E1)
000156          2     TAQ(I)=1.+TF-C1*TF*(1.+E1)
000166                DO 3 I=1,L
000167          3     PRINT 102,TCAP(I)
000177                DO 4 I=1,31
000200          4     PRINT 102,TAQ(I)
000207                DO 5 I=31,101,10
000211          5     PRINT 102,TAQ(I)
000220          107   CONTINUE
000222                END


                      SUBROUTINE ERF(YE,P,ZT,E)
000007                DIMENSION DU1(101)
000007                N=100
000010                N1=N+1
000012                PI=4.*ATAN(1.)
000015                CO=2./SQRT(PI)
000020                FE=P*ZT/YE
000024                H=FE/N
000026                DO 1 I=1,N1
000030                X=(I-1)*H
000034          1     DU1(I)=EXP(-X*X)
000046                E1=0.
000047                DO 2 I=3,N1,2
000050          2     E1=E1+(DU1(I-2)+4.*DU1(I-1)+DU1(I))*(H/3.)
000064                E=CO*E1
000065                RETURN
000066                END
```

```
                PROGRAM MATCH (INPUT,OUTPUT)
000003      101 FORMAT(7F10.4)
000003          PI=4.*ATAN(1.)
000007          SQPI=SQRT(PI)
000011          READ 101,D,CAPL,ALEMDA,AM,RA,TF,YE
000032          PRINT101,D,CAPL,ALEMDA,AM,RA,TF,YE
000054          DDT=CAPL-.01
000056          DD=1./SQRT(D)
000062          E=EXP(DD)
000064          F=EXP(-DD)
000070          COSH1=(E+F)/2. $ SINH1=(E-F)/2.
000074          GA=SQRT(RA*YE*YE)
000101          B1=ALEMDA/(ALEMDA+CAPL)
000103          A1=DD*(AM+B1*COSH1)/SINH1
000110          P=SQRT(GA*GA*(A1-B1)*.25)
000115          C1=(TF*ALEMDA)/(SQPI*CAPL*P)
000121          Y=0.
000122      7   ETA=0.
000123      6   Z=ETA*SQRT(YE*Y)
000131          CALL ERF(P,ETA,ER)
000133          TAQF=1.+TF-C1*SQRT(Y*YE)*(SQPI*P*ETA*(1.+ER)+EXP(-P*P*ETA*ETA))
000156          PRINT 101,Z,ETA,Y,TAQF
000171          IF(ABS(ETA).GE. 7. ) GO TO 5
000175          ETA=ETA-.5
000176          GO TO 6
000177      5   IF(Y.GT. 1.) GO TO 1
000203          Y=Y+.01
000204          GO TO 7
000204      1   IF(Y.GT. 2.) STOP
000211          Y=Y+.1
000213          GO TO 7
000214          END



                SUBROUTINE ERF(P,ETA,E)
000006          DIMENSION DU1(101)
000006          PI=4.*ATAN(1.)
000011          CO=2./SQRT(PI)
000014          N=100
000015          N1=N+1
000017          FE=P*ETA
000022          H=FE/N
000023          DO 1 I=1,N1
000025          X=(I-1)*H
000031      1   DU1(I)=EXP(-X*X)
000042          E1=0.
000043          DO 2 I=3,N1,2
000044      2   E1=E1+(DU1(I-2)+4.*DU1(I-1)+DU1(I))*(H/3.)
000057          E=CO*E1
000060          RETURN
000061          END
```

```
                PROGRAM REGION6 (INPUT,OUTPUT)
000003          COSH(ZZ)=(EXP(ZZ)+EXP(-ZZ))/2.
000016          SINH(ZZ)=(EXP(ZZ)-EXP(-ZZ))/2.
000030          DIMENSION DU1(10000), T(41,26)
000030     101  FORMAT(7F10.4)
000030     102  FORMAT(I6)
000030     103  FORMAT(1H0,10F12.6)
000030     104  FORMAT(7F15.8)
000030          PI=4.*ATAN(1.)
000034          SQPI=SQRT(PI)
000036          DO 107 KK=1,9
000037          READ 101,D,CAPL,ALEMDA,AM,RA,TF,YE
000060          PRINT101,D,CAPL,ALEMDA,AM,RA,TF,YE
000102          SQYE=SQRT(YE)
000105          DD=1./SQRT(D)
000110          E=EXP(DD)
000112          F=EXP(-DD)
000116          COSH1=(E+F)/2. $ SINH1=(E-F)/2.
000122          B1= ALEMDA/(ALEMDA+CAPL)
000125          GA=SQRT(RA*YE*YE)
000131          A1=(AM+B1*COSH1)*DD/SINH1
000135          P=SQRT(GA*GA*(A1-B1)*.25)
000143          B2=TF*ALEMDA*SQYE/(P*CAPL*SQPI)
000150          PRINT 104,B1,GA,A1,P,B2
000165          L=7
000166          DZ1=.05
000170          DZ2=.02
000171          IF(CAPL.GE. .49) L=10
000175          IF(CAPL.GE. .49) DZ1=.1
000201          DY1=.02
000203          DY2=.1
000204          M=41
000205          L1=L-1
000207          DO 12 I=1.M
000211          YT=(I-1)*DY1
000215          IF(I.GT. 26) YT=(I-26)*DY2+.5
000223     12   T(I,1)=1.+TF-B2*SQRT(YT)
000234          Z1=CAPL-.01
000236          DO 14 J=1,M
000240          DO 14II=2,L
000241          Y=(J-1)*DY1
000245          IF(J.GT. 26) Y=(J-26)*DY2+.5
000254          Z=(II-1)*DZ1
000260          IF(II.GT. 5) Z= (II-5)*DZ2+4.*DZ1
000267          N=200
000270          A=PI*(1.-Z/CAPL)
000274          FE=4.
000276          K=1
000277     5    H=FE/N
000302          N1=N+1
000304          DO 1 I=1,N1
000305          X=(I-1)*H
000311          C=PI*ABS(Y-X)/CAPL
000315          D1=PI*(Y+X)/CAPL
000317     1    DU1(I)=( SQRT(X)*SIN(A)) *(1./(COSH(C)+COS(A))-1./(COSH(D1)+COS(A)
```

```
                1))
000351              E1=0.
000352              DO 2 I=3,N1,2
000353        2     E1=E1+(DU1(I-2)+4.*DU1(I-1)+DU1(I))*(H/3.)
000366              E3=-E1/(2.*CAPL)
000371              IF(K.EQ. 1) GO TO 3
000373              IF(ABS(E3-E33).LT. .001    ) GO TO 4
000377        3     K=K+1
000401              E33=E3
000402              FE=FE+1.
000404              N=N+20
000406              GO TO 5
000406        4     T(J,II)= 1.+TF*(1.-Z/CAPL)+B2*E3
000420        14    CONTINUE
000425              DO 10 I=1,M
000427              DT=(T(I,L1)-1.)/DZ2
000435        10    PRINT 101,DT
000445              DO 11 I=1,L
000446        11    PRINT 103,(T(J,I),J=1,10)
000464              DO 16 I=1,L
000465        16    PRINT 103,(T(J,I),J=11,M,10)
000504        107   CONTINUE
000506              END
```

```
                PROGRAM CLAYCAP (INPUT,OUTPUT)
000003          COSH(ZZ)=(EXP(ZZ)+EXP(-ZZ))/2.
000016          SINH(ZZ)=(EXP(ZZ)-EXP(-ZZ))/2.
000030          W(ZP)=A1*COSH(ZP)+B2* SINH(ZP)-B1
000044          DIMENSION Z(151),TOLD(101),TNEW(101),A(101,4),V(101),X(101),
               1TCOMB(101,151)      ,FP(6),YO(1000),ZO(1000),DT(101),Y1(101)
000044          COMMON P,M,N,DY
000044     101  FORMAT(7F10.4)
000044     102  FORMAT(1H0,F5.2,F5.2,11F9.6/)
000044     103  FORMAT(1H0,10F12.6)
000044     104  FORMAT(////4X*THE POINTS(YO,ZO) ON THE ISOTHERM T=*F7.4/(7(3X2F7.4
               1)))
000044     105  FORMAT(1H0,//5X*Y*,5X*TEMPERATURE AT DIFFRENT DEPTHS IN THE AQUIFE
               2R AND CLAY CAP*//)
000044     106  FORMAT(I6,4F16.5)
000044     111  FORMAT(F15.5)
000044     112  FORMAT(I6)
           C    R=DY*D/(2.*DZ*DZ*GA*GA)  WHERE GA=SQRT(RA*YE*YE)
000044          DATA YMAX,NFRPR,NFRPL,NPLOTS/1.,10,10,10/
000044          DATA (FP(I),I=1,6)/1.,1.2,1.3,1.4,1.5,1.599/
000044          DY=.01 $ DZ=.01
000047          M=101
000050          PI=4.*ATAN(1.)
000053          DO 107 KK=1,23
000054          READ 101,D,CAPL,ALEMDA,AM,RA,TF,YE
000075          PRINT101,D,CAPL,ALEMDA,AM,RA,TF,YE
000117          DD=1./SQRT(D)
000123          E=EXP(DD)
000125          F=EXP(-DD)
000131          COSH1=(E+F)/2. $ SINH1=(E-F)/2.
000135          GA=SQRT(RA*YE*YE)
000142          B1= ALEMDA/(ALEMDA+CAPL)
000144          R=D /(2.*DZ*GA*GA)
000150          B2=DD*B1
000152          A1=(AM+B1*COSH1)*DD/SINH1
000155          P=SQRT(GA*GA*(A1-B1)*.25)
000163          M1=M-1
000165          L=CAPL/DZ+1.2
000170          L2=4
000171          L1=L2+1
000172          IMAX=L+M-1
000174          N=IMAX
000175          NDT=1
000176          J=2
           C    DEFINE X(I) WHICH IS SAME AS Y(I)
000177          Y=.01
000200          DO 13 I=1,M
000202          ZT=(I-1)*DY
000206          Y1(I)=ZT*D/YE
000211     13   X(I)=ZT
           C    DEFINE V(I)
000215          DO 9 I=1,M
000216          ZT=-(I-1)*DZ*DD
000223     9    V(I)=W(ZT)
           C    DEFINE Z(I)
```

```
000232          DO 20 I=1,IMAX
000233     20   Z(I)=CAPL-DZ*(I-1)
           C    CALCULATE TEMPERATURE AT Z=0. AND FOR DIFFRENT VALUES OF Y KEEPING
           C    HEAT TRANSFER AND TEMPERATURE CONTINUOUS AT Z=0.
           C    CALCULATE AND PRINT THE TEMPERATURES IN THE CLAY CAP
           C    SPECIFY THE TEMPERATURE AT Y=.01
000243          DO 14 I=1,L
000244          ZT=CAPL-DZ*(I-1)
000251     14   TCOMB(2,I)=1.+(1.-ZT/CAPL)*TF*(1.-ALEMDA*SQRT(Y*D/PI)/(CAPL*P))
000276          DT(2)=-(TCOMB(2,2)-TCOMB(2,1))/DZ
000301          PRINT 105
000304          DO 1 I=2,M
000306          LL=L+I-1
000310          ZT=-(I-1)*DZ
000313          ETA=ZT/SQRT(Y*D)
000321          CALL ERF1(ETA,E1)
000323          TOLD(I)=1.+TF-(ALEMDA*TF*SQRT(Y*D/PI)/(CAPL*P))*(SQRT(PI)*P*ETA*(1
               1.+E1)+EXP(-P*P*ETA*ETA))
000354     1    TCOMB(2,LL)=TOLD(I)
000362          TOLD(1)=TCOMB(2,L)
           C    SPECIFY TEMPERATURE IN THE AQUIFER AT Y=0.01
           C    CALCULATE TNEW, THE TEMPERATURE AT Y+DY
000365     2    Y=Y+DY
000367          J=J+1
000371          NDT=NDT+1
000372          TCOR1=TOLD(1)
           C    COMPUTE A(I,J)
000373     18   DO 3 I=2,M1
000375          A(I,1)=R/V(I)
000377          A(I,2)=-1.-2.*R/V(I)
000404          A(I,3)=A(I,1)
000405     3    A(I,4)=-(R/V(I))*TOLD(I-1)+(2.*R/V(I)-1.)*TOLD(I)-R/(V(I))*TOLD(I+
               31)
           C    MODIFY THE MATRIX A(I,J)
000423          A(2,4)=A(2,4)-A(2,1) *TCOR1
000426          A(2,1)=0.
000427          A(M1,4)=A(M1,4)-A(M1,3)*(1.+TF)
000433          A(M1,3)=0.
000435          CALL BAND3(M1,A,TNEW)
000437          TCOR=((TNEW(2))/DZ+ALEMDA/CAPL)/(1./DZ+ALEMDA/CAPL)
000447          IF(ABS(TCOR-TCOR1  ) .LT. .000001) GO TO 17
000453          TCOR1=TCOR
000454          GO TO 18
000454     17   TOLD(1)=TCOR
000456          DO 4 I=2,M1
000457          LL=L+I-1
000461          TOLD(I)=TNEW(I)
000463     4    TCOMB(J,LL)=TOLD(I)
000471          TCOMB(J,N)=1.+TF
000475          DO 19 I=1,L
000477          ZT=CAPL-DZ*(I-1)
000504     19   TCOMB(J,I)=(1.-TOLD(1))*ZT/CAPL+TOLD(1)
000515          DT(J)=(1.-TOLD(1))/CAPL
           C    PRINT VELOCITY WHEN NDT=N*NFRPR,N BEING A POSITIVE INTEGER AND PLO
           C    T IT WHEN NDT=N*NFRPL,N=1,2,---,NPLOTS.
000521     8    IF((NDT/NFRPR)*NFRPR.NE.NDT) GO TO 5
```

```
000526     5    IF((NDT/NFRPL)*NFRPL.NE.NDT) GO TO 6
000533          IF((NDT/NFRPL).GT. NPLOTS) GO TO 6
000537     6    IF(Y.LT.YMAX .AND. J.LT. 101) GO TO 2
000550          DO 28 J=2,M
000551     28   PRINT 103,X(J),Y1(J),DT(J)
000565          DO7 I=1,L2
000566     7    PRINT 103,(TCOMB(J,I),J=2,10)
000603          DO 10 I=L1,L,10
000605     10   PRINT 103,(TCOMB(J,I),J=2,10)
000622          DO 12 I=L,IMAX,10
000623     12   PRINT 103,(TCOMB(J,I),J=2,10)
000640          DO 11 I=1,L2
000641     11   PRINT 103,(TCOMB(J,I),J=11,M,10)
000657          DO 15 I=L1,L,10
000661     15   PRINT 103,(TCOMB(J,I),J=11,M,10)
000677          DO 27 I=L,IMAX,10
000700     27   PRINT 103,(TCOMB(J,I),J=11,M,10)
000716          DO 22 K=1,6
000717          FA=FP(K)
000721          CALL POINTS (X,Z,TCOMB,FA,YO,ZO,KMAXO)
000727          PRINT 104,(FA,((YO(L),ZO(L)),L=1,KMAXO))
000746     22   CONTINUE
000750     107  CONTINUE
000752          END

                SUBROUTINE POINTS (X,Y,F,FA,XX,YY, KMAX)
000012          DIMENSION X(101),Y(151),F(101,151),XX(1000),YY(1000)
000012          COMMON DUMMY(1),M,N,DY
000012          K=0
000013          I=0
000014     1    J=1
000015          I=I+1
000017          IF(I.GT. M) GO TO 7
000022     2    P=F(I,J)-FA
000027          IF(ABS(P).LE. .00001) GO TO 6
000032     3    J=J+1
000034          IF(J.GT. N) GO TO 1
000037          Q=F(I,J)-FA
000043          IF(P*Q) 5,5,4
000045     4    P=Q
000047          GO TO 3
000047     5    K=K+1
000051          XX(K)=X(I)
000054          YY(K)=Y(J)+DY*ABS(Q)/(ABS(P)+ABS(Q))
000067          P=Q
000071          GO TO 3
000071     6    K=K+1
000073          XX(K)=X(I)
000076          YY(K)=Y(J)
000101          J=J+1
000103          IF(J.GT. N) GO TO 1
000106          GO TO 2
000106     7    KMAX=K
000110          RETURN
000111          END
```

```
                      SUBROUTINE ERF1(Z,E)
000005                DIMENSION DU1(101)
000005                COMMON P
000005                N=100
000006                N1=N+1
000010                PI=4.*ATAN(1.)
000013                CO=2./SQRT(PI)
000016                FE=P*Z
000021                H=FE/N
000023                DO 1 I=1,N1
000025                X=(I-1)*H
000031           1    DU1(I)=EXP(-X*X)
000042                E1=0.
000043                DO 2 I=3,N1,2
000044           2    E1=E1+(DU1(I-2)+4.*DU1(I-1)+DU1(I))*(H/3.)
000057                E=CO*E1
000060                RETURN
000061                END


                      SUBROUTINE BAND 3 (N,A,X)
000006                DIMENSION A(101,4),X(101)
000006                M=N-1
000010                M1=M-1
000011                DO 10 I=3,M
000012                A(I,2)=A(I,2)*A(I-1,2)-A(I,1)*A(I-1,3)
000020                A(I,3)=A(I,3)*A(I-1,2)
000023           10   A(I,4)=A(I,4)*A(I-1,2)-A(I,1)*A(I-1,4)
000033                X(N)=(A(N,4)*A(M,2)-A(N,1)*A(M,4))/(A(N,2)*A(M,2)-A(N,1)*A(M,3))
000047                DO 20 K=1,M1
000051                J=N-K
000052           20   X(J)=(A(J,4)-A(J,3)*X(J+1))/A(J,2)
000062                RETURN
000063                END
```